SPATIOTEMPORAL CONTROL OF TGFβ SIGNALING WITH LIGHT

D i s s e r t a t i o n

zur Erlangung des akademischen Grades

doctor rerum naturalium

(Dr. *rer. nat.)*

im Fach

Biophysik

eingereicht an der

Lebenswissenschaftlichen Fakultät

der

Humboldt-Universität zu Berlin

von

Yuchao Li, M.Sc.

Präsidentin der Humboldt-Universität zu Berlin

Prof. Dr.-Ing. Dr. Sabine Kunst

Dekan der Lebenswissenschaftlichen Fakultät

Prof. Dr. Bernhard Grimm

Gutachter/innen: Prof. Dr. Dr. h.c. Edda Klipp

Prof. Dr. Nils Blüthgen

Dr. Zhike Zi

Tag der mündlichen Prüfung: 17. 04. 2019

Abstract

Cells employ signaling pathways to make decisions in response to changes in their immediate environment. Transforming Growth Factor β (TGFβ) signaling pathway plays pivotal roles in regulating many cellular processes, including cell proliferation, differentiation and migrations. Although the principal components of TGFβ signaling have been identified and explored in recent decades, understanding its dynamic behavior is limited by the lack of tools that allow the control of TGFβ signaling at high spatiotemporal resolution. In this thesis, we developed an optogenetic system (the optoTGFβ system), in which light is used to control TGFβ signaling precisely in time and space. First, we validated the functionality of the optoTGFβ system by comparing it with the endogenous TGFβ signaling system. Second, by simultaneously monitoring the subcellular translocation of the receptors and Smad proteins using live cell imaging, we showed that TGFβ signaling can be specifically activated in single cells through modulating the light stimulations. Third, in combination with mathematical modeling, we quantitatively characterized the dynamics of TGFβ signaling in the optoTGFβ system. The spatial and temporal precision of optical control makes the optoTGFβ system a novel and powerful tool for quantitative analyses and manipulation of TGFβ signaling at the single cell level.

Keywords:

optogenetics, signaling transduction, TGFβ, spatiotemporal precision, mathematical model

Zusammenfassung

Zellen benutzen Signalwege ein, um auf Änderungen in ihrer unmittelbaren Umgebung zu reagieren. Der Signalweg des transformierenden Wachstumsfaktors β (TGFβ) spielt eine entscheidende Rolle bei der Regulierung vieler zellulärer Prozesse, einschließlich Zellproliferation, Differenzierung und Migration. Obwohl die Hauptkomponenten der TGFβ-Signalgebung in den letzten Jahrzehnten identifiziert und erforscht wurden, ist das Verständnis ihres dynamischen Verhaltens durch das Fehlen von Methoden eingeschränkt, die die Steuerung der TGFβ-Signalgebung mit hoher räumlicher und zeitlicher Auflösung ermöglichen. In dieser Arbeit wurde ein optogenetisches System (das optoTGFβ-System) entwickelt, bei dem Licht dazu verwendet wird, die TGFβ-Signalgebung zeitlich und räumlich präzise zu steuern. Erstens wurde die Funktionalität des optoTGFβ-Systems durch Vergleich mit dem endogenen TGFβ-Signalsystem überprüft. Zweitens wurde durch das gleichzeitige Überwachen der subzellulären Translokation der Rezeptoren und der Smad-Proteine mittels „Live Cell Imaging“ gezeigt, dass die TGFβ-Signalgebung durch Modulation der Lichtstimulationen in einzelnen Zellen spezifisch aktiviert werden kann. Drittens wurde in Kombination mit der mathematischen Modellierung die Dynamik der TGFβ-Signalgebung im optoTGFβ-System quantitativ bestimmt. Die räumliche und zeitliche Präzision der optischen Kontrolle machen das optoTGFβ-System zu einem neuartigen und leistungsfähigen Methode für die quantitative Analyse und Manipulation von TGFβ-Signalen auf Einzelzellebene.

Schlagwörter:

optogenetik, Signaltransduktion, TGFβ, raumzeitliche Präzision, Mathematische Modellierung

Contents

1

Introduction

Life, as an amazing existence that feeds on negative entropy in a universe with unavoidably increasing entropy, has to communicate with its environment constantly. As the basic building blocks of life, cell has to perceive, make sense and respond to its environment, which is implemented by a variety of signaling pathways. Among them, TGFβ signaling is one of the highly conserved and crucial signaling pathways for various cellular processes such as cell proliferation and migration.

As the ultimate source of energy for life, light is not only powering biological processes, but could also modulate them via a series of photosensitive proteins. With the development of synthetic biology and optogenetics, researchers harnessed these light-modulated proteins to create artificial photosensitive proteins for modulating a wider range of cellular processes. Due to its convenience and high spatiotemporal resolution, optogenetics is a powerful approach to study and control cellular activities.

In this chapter, I first introduced the general principles of signaling pathways. Then focusing on the TGFβ signaling, I introduced its major components, core molecular mechanisms, and some other properties. Later on, I introduced two sets of optogenetic toolkits: one is for modulating membrane voltage potential; the other is for modulating cell signaling. We mainly focused on the later one, from which we would select proper tools for manipulating TGFβ signaling in the following chapters.

1.1 Signaling transduction

Cells are the basic element for most organisms. On the one hand, cells have to perceive and respond to the surrounding signals correctly for successful survival. On the other hand, an organic body, or a microbial community has to employ multiple signals to govern and coordinate the corresponding cells efficiently for its proper development. Defects or deviation in signal perception or information processing are related to common diseases such as heart disease, cancer, diabetes and Alzheimer's disease.

At the molecular level, there exists a series of biochemical processes that transmit the signal from the starting point of signal perceiving, to the end point of cellular response. Commonly we call this series of molecular events as signaling transduction or signaling pathway. There are mainly three stages (**Figure 1.1.1**) in the signaling transduction in which various molecular components are involved in specific biochemical reactions: signal perception, intracellular signal transmission and cellular response.

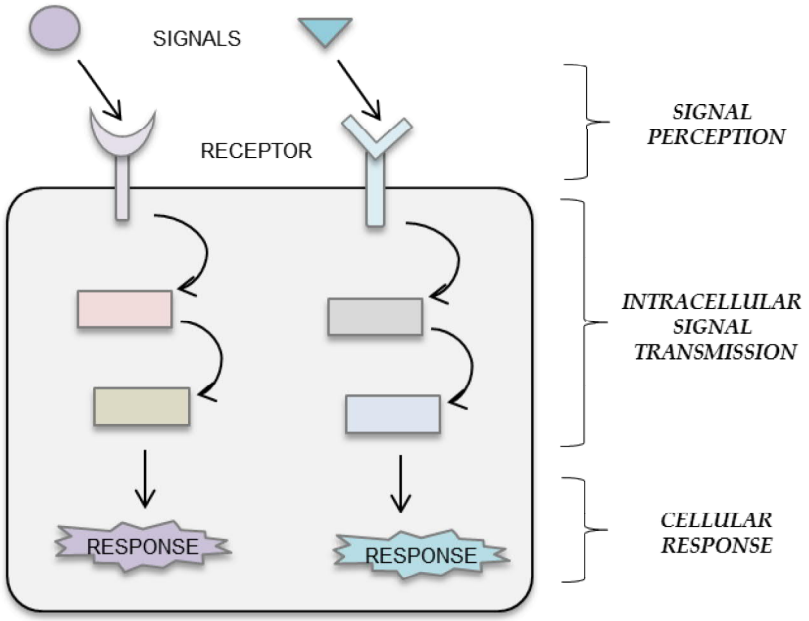

Figure 1.1.1 Signaling transduction. The three main stages in signaling transduction: signal perception by receptors, which translates the signal into a biochemical signal; intracellular signal transmission by a series of molecular events that relay the signal; cellar response such as gene expression, or metabolism alternation.

The signal perception stage involves the detection of a specific stimulus, and translates it into a biochemical signal. The stimuli could range from physical signals (e.g. mechanical forces[1], osmolarity[2], temperature[3], light[4]) to chemical signals, commonly known as ligands, which constitute the majority of the stimuli. The second stage of signaling transduction consists of a series of molecular

events that relay or process the signal, including protein translocation, allosteric regulation, protein phosphorylation, other posttranslational modifications (methylation, acetylation) and so on. The last stage of signaling transduction is the cellular response such as gene expression[5], protein degradation[6] or metabolism alteration[7].

Cell signaling involves multiple processes in which various regulators and effectors participate and form networks. Therefore, traditional approaches in biological researches focusing on individual parts of the signaling pathways are not sufficient to fully understand them. Systems biology provides us with a theoretical tool to analyze the underlying structure as well as the spatiotemporal dynamics of the cell signaling networks. Through combining experimental approaches with theoretical analysis, we could not only better characterize the cell signaling, but also modulate it effectively for therapeutic purposes.

There are numerous signaling pathways in the cells (**Figure 1.1.2**), for instance, MAPK/ERK signaling pathway is well-known for its regulation on cell cycle entry and proliferation[8], PI3K/Akt/mTOR signaling pathway for its modulation on cell proliferation and differentiation[9], JAK-STAT signaling pathway for its regulation on immunity and development[10], etc.

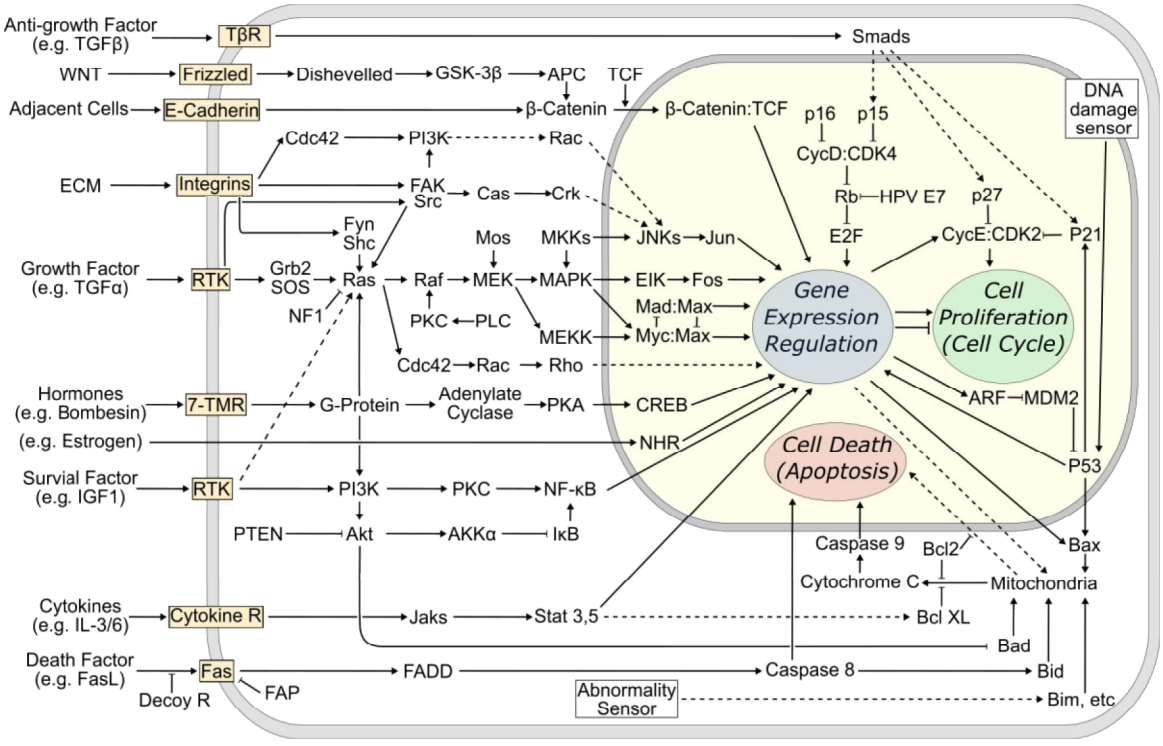

Figure 1.1.2 Signaling pathways. Numerous cell signaling pathways exist in the cells. These signaling circuits transmit extracellular signals as well as intracellular signals to regulate cellular activities and cell fate. This figure is adapted, modified from Hanahan *et al.* (2000)[11].

1.2 TGFβ signaling pathway

Among the diverse signaling pathways, the transforming growth factor beta (TGFβ) signaling pathway plays an important role in various cellular processes including cell proliferation, differentiation and migration (**Figure 1.2.1**)[12]. Accordingly, malfunctions of TGFβ signaling have been connected to a variety of disease such as atherosclerosis, cancer, developmental defects [13], reproductive disorders, and connective tissue diseases[14].

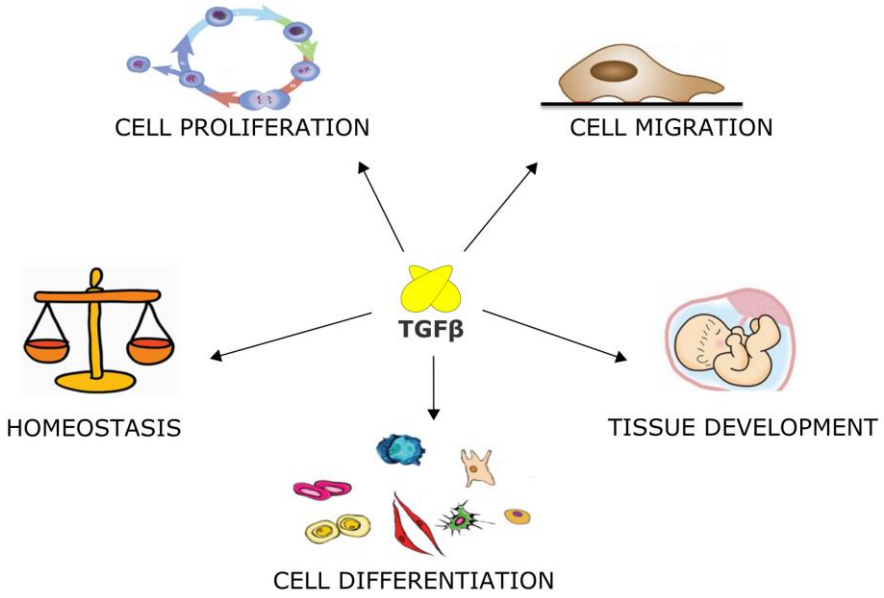

Figure 1.2.1 Functions of TGFβ signaling. TGFβ signaling plays a crucial role in multiple cellular processes such as cell proliferation, cell differentiation, tissue development, cell migration and homeostasis.

Although the functions of TGFβ signaling are versatile, the core molecular mechanism of the canonical signaling transduction is relatively simple (**Figure 1.2.2**). Briefly, a dimeric ligand (the active form)[15] induces the assembly of two type I receptors and two type II receptors to form a symmetric 2:2:2 complex (ligand-receptor-complex, LRC). The oligomerization of the receptors promotes activation of the type I receptor through transphosphorylation, catalyzed by the constitutively active kinase of the type II receptor[16]. In the canonical TGFβ signaling, the activated kinase domain of the type I receptor phosphorylates the receptor-regulated Smad proteins (R-Smads, i.e., Smad2 and Smad3 for TGFβ-like signaling pathway; Smad1, Smad5 and Smad8 for BMP-like signaling pathway) [17]. The R-Smads then bind to the common mediator Smad4 (co-Smad) and translocate into the nucleus[18]. There, these phosphorylated R-Smads/co-Smad complexes bind to DNA in conjunction with other transcription factors/cofactors, regulating the transcription of various target genes[19,20].

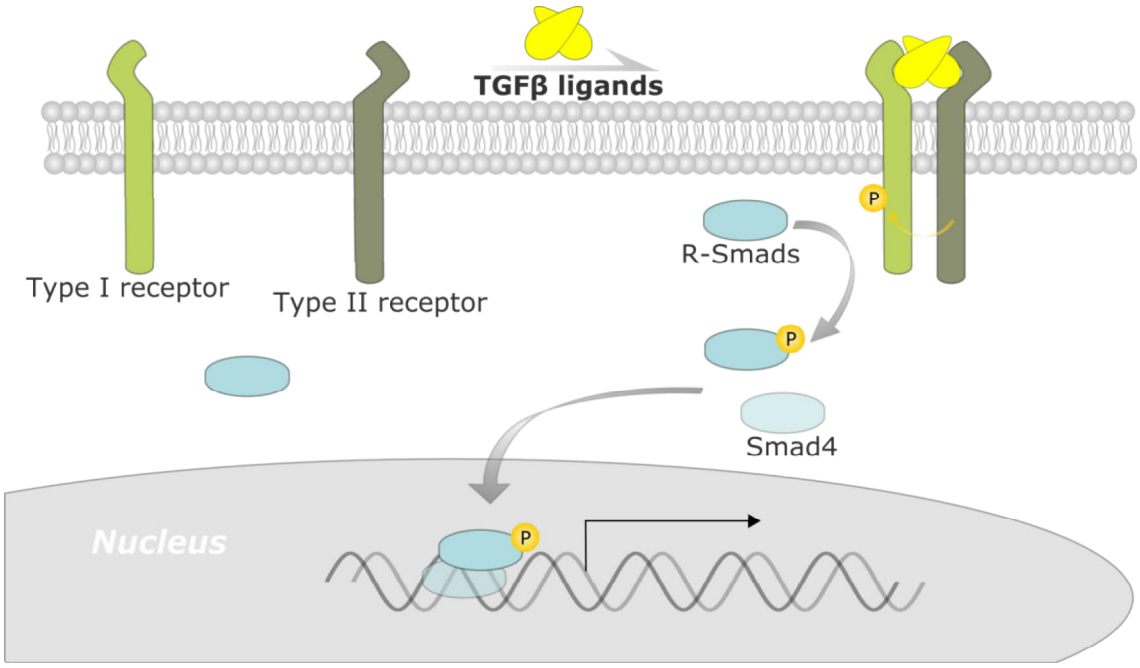

Figure 1.2.2 Molecular mechanism of TGFβ signaling. A pair of TGFβ ligands form a dimer and bind to the extracellular domains of a pair of type II receptors, which then recruit and phosphorylate a pair of type I receptors. The activated type I receptors then phosphorylate the R-Smads (receptor-regulated Smads), which together with the co-Smad (Smad4) translocate into the nucleus and regulate the transcription of multiple target genes.

The TGFβ superfamily is a large group of structurally-related growth factors which is conserved and developed throughout metazoan evolution. According to their sequence similarity as well as functionality, these cytokines are divided into two major groups: TGFβ-like group and BMP (Bone Morphogenetic Proteins)-like group. The TGFβ-like group includes TGFβs, Nodals, Activins and a few GDFs (Growth and Differentiation Factors). The BMP-like group contains BMPs, AMH (Anti-Müllerian hormone) and most GDFs[21]. The TGFβ family signaling pathways emerged at the onset of metazoan life and evolved rapidly to higher degrees of complexity[22]. *Caenorhabditis elegans* express five TGFβ related ligands, including the BMP-like DBL-1, the TGFβ-like DAF-7 and three yet unexplored ligands: UNC-129, TIG-2 and TIG-3. *Drosophila melanogaster* expresses seven TGFβ family ligands, including BMP-like Dpp (Decapentaplegic), Scw (Screw) and Gbb (Glass bottom boat), regulating patterning and differentiation; TGFβ-like dActivin and Daw (Dawdle), regulating tissue-specific events; and other less understood members. *Xenopus laevis* expresses TGFβs, Activins, Nodals, Activins, GDFs and BMPs[23] as well as some unique members such as XNR1-6[24] and Derrière[25]. Consistent with the increasing anatomical complexity and new functionality, mammalian genomes encode over 30 TGFβ family ligands for various fundamental cellular processes.

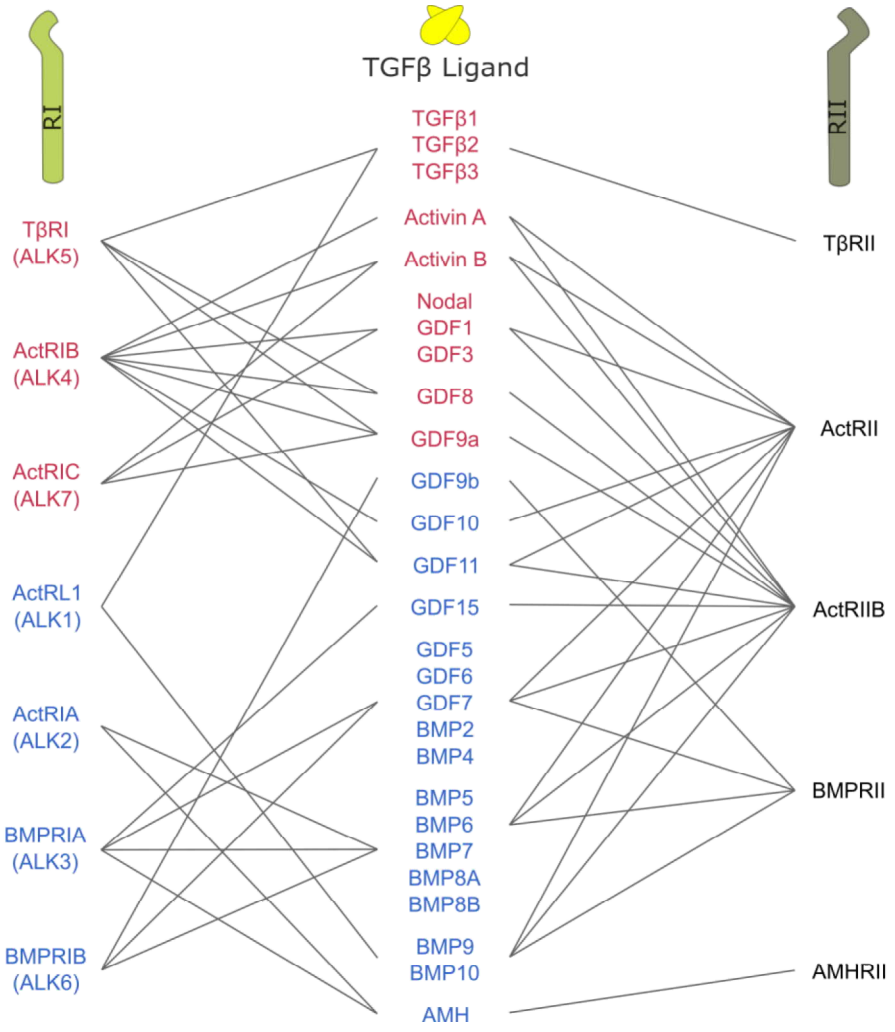

Figure 1.2.3 Schematic illustration of the specific binding between TGFβ ligands and TGFβ receptors. RI, type I receptor; RII, type II receptor. In red color, TGFβ-like pathway members; in blue color, BMP-like pathway members. This figure is adapted, modified from Heldin *et al*. (2016)[26].

In accordance with the TGFβ ligand family, there is a TGFβ receptor family. However, in contrast to the large family of TGFβ ligands, the TGFβ receptor family is relatively small, with only 12 members in mammals, including seven type I receptors and five type II receptors in human. The TGFβ signaling is initiated by the assembly of a LRC comprised of one pair of TGFβ ligand binding to a pair of type I receptors and a pair of type II receptors. Each TGFβ ligand family member binds to specific combinations of type I and type II receptors, and each receptor is shared by several TGFβ ligand family members (**Figure 1.2.3**). Receptors in this family are dual specificity kinases, and have structural characteristics similar to both tyrosine kinases and serine/threonine kinase[27]. Generally, the type II TGFβ receptors have higher affinities for the ligands than

the type I TGFβ receptors[28], whereas type I BMP receptors have higher affinities for the ligands than the type II BMP receptors[29].

Among the members of the TGFβ superfamily, TGFβ1 is the first identified one. Later on, TGFβ2 and TGFβ3 have been identified as another two isoforms. Members of this TGFβ subfamily and their receptors have been better characterized compared with other subfamilies. In this study, we zoom in and focus on the TGFβ subfamily signaling.

1.2.1 Characteristics of the TGFβ signaling pathway components

1.2.1.1 TGFβ Ligands

The biologically active form of TGFβ ligand is characterized by a homodimer that is stabilized by hydrophobic interactions and a covalent disulfide bond. In each monomer, three highly conserved intra-molecular disulfide bonds form a tight structure termed the 'cystine knot', interlocking the extended beta strands in the ligands[30]. The mature and dimeric form of TGFβ ligand is released from a precursor protein, which contains a large amino-terminus prodomain for correct folding[31].

The activity of TGFβ ligands is determined by several aspects. Firstly, different ligand isoforms differ in their affinities to the receptors. For instance, TGFβ2 shows lower affinity than TGFβ1 and TGFβ3 to TβRII[32]. Secondly, various extracellular ligand-binding proteins regulate the TGFβ ligands access to the receptors. For instance, ligand-trapping proteins such as LAP (latency-associated polypeptide) and α2-macroglobulin, sequester the ligands from their corresponding receptors[33,34]; mediators such as LTBP1 (latent TGFβ-binding protein 1) could mediate interactions with integrin receptors to release the mature ligands from the traps[35,36]

1.2.1.2 TGFβ Receptors

The TGFβ receptors comprise a small cysteine-rich extracellular domain, a transmembrane domain, a juxta-membrane domain and a kinase domain. Compared with BMP type II receptor and most tyrosine kinase receptors, the carboxyl-terminus of their kinase domains are relatively shorter. The extracellular domains of the TGFβ receptors are responsible for the recognition of the ligands, which facilitates formation of LRC and initiates the signaling. Glycosylation on the extracellular domains regulates TGFβ receptor activity through determining its sensitivity to the ligands, and affecting internalization and cell-surface transportation of the receptors [37-39].

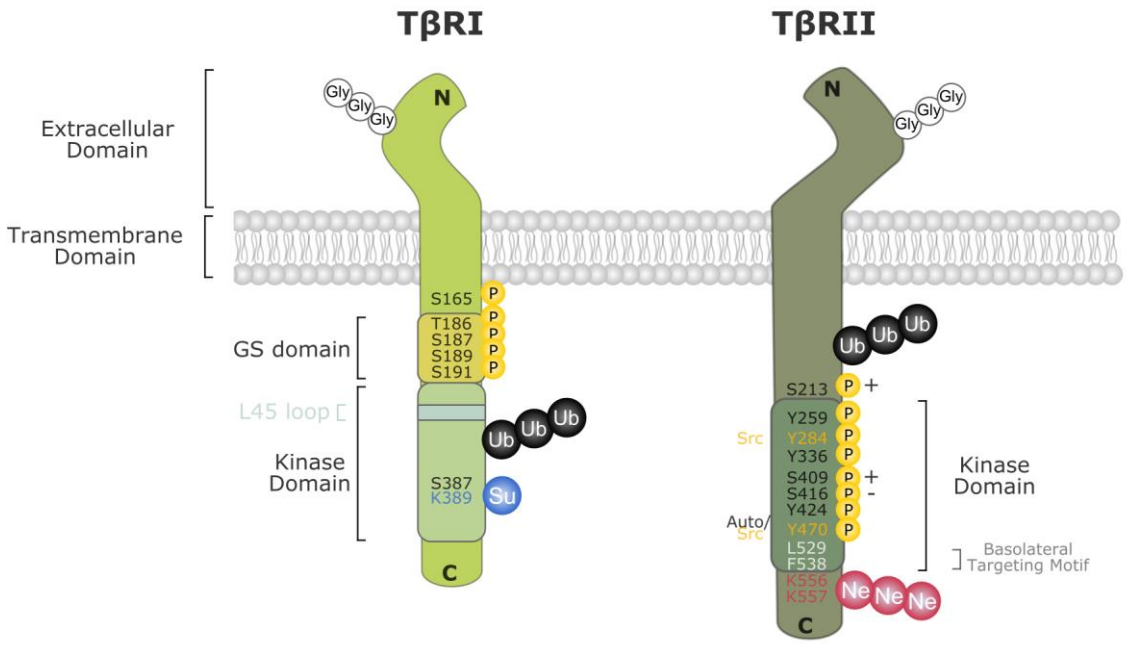

Figure 1.2.4 Schematic diagram of the structural/functional characteristics of TβRI and TβRII. The TGFβ receptors are composed of four major structural motifs: an extracellular domain, a transmembrane domain, a juxta-membrane domain and a kinase domain. The L45 loop on TβRI is the epitope for its specific recognition of Smads. The motif between L529 and F538 in TβRII is responsible for its delivery to the basolateral side of the polarized epithelial cells. Phosphorylation sites, post-translationally modifies residues and functional motifs are indicated. White circles with 'Gly', N-linked glycosylations; yellow circles with 'P', phosphorylation sites; black circles with 'Ub', ubiquitins; blue circles with 'Su', SUMO groups; red circles with 'Ne', NEDD8 moleculrs. '+' and '-' beside the phosphorylation sites indicate positive and negative impact of phosphorylation on the kinase activity. 'Src' beside the Y284 and Y470, the sites phosphorylated by Src, in contrast to other auto-phosphorylation sites on TβRII. 'Auto' beside Y470, indicating it could be also auto-phosphorylated. N, amino terminus; C, carboxyl-terminus. This figure is adapted, modified from Heldin *et al*. (2016)[26].

The activity of the TGFβ receptors is mainly regulated by phosphorylation, post-translationally modification and other functional motifs in their cytoplasmic region (**Figure 1.2.4**).

TβRII is constitutively active and its kinase activity is regulated by auto-phosphorylation at several serine and tyrosine residues, including Ser213, Ser409, Ser416, Tyr259, Tyr336, Tyr424 and Tyr470[40,41]. Among them, phosphorylation at Ser213 or Ser409 promotes its kinase activity, while phosphorylation at Ser416 inhibits its activity[40]. In addition, TβRII can also be phosphorylated by Src at Tyr284 and Tyr470 for regulation of various responses[42,43]. TCPTP (the T cell protein tyrosine phosphatase) has been shown to dephosphorylate TβRII tail tyrosine residues, inhibiting TβRs dependent fibrotic signaling[44].

The activity of TβRI is mainly regulated by phosphorylation of the residues in its GS domain, which is promoted by the ligand-induced approximation between the homodimers of TβRI and TβRII. The phosphorylation of TβRI on the one hand results in a conformational transformation, which relieves the kinase from the binding of the inhibitor FKBP12 (FK506-binding protein), and on the other hand, facilitates its interaction with the R-Smads[45-47]. Residues in the GS domain that are phosphorylated by TβRII include Ser187, Ser189, Ser191 and Thr186, which reside just upstream of the kinase domain[48]. Although none of these residues is crucial for TβRI kinase activation, phosphorylation level in this region needs to reach a certain threshold for the activation. Besides the phosphorylation in the GS domain, TGFβ signaling could also be modulated by phosphorylation at Ser165 in the juxamembrane area[49]. Phosphatase such as PP1 (protein phosphatase 1) could dephosphorylate TβRI by binding to Smad7 and thus being recruited to the receptor[50]. Another phosphatase PP2A (protein phosphatase 2A) regulates the receptors reciprocally through the two isoforms of its regulatory subunit B: while Bα (PPP2R2A) stabilizes the TβRI and enhances signaling, Bδ (PPP2R2D) restricts the receptor activity[51,52].

Besides phosphorylation, other layers of regulation exist for TGFβ receptors, which are implemented by ubiquitylation, deubiquitylation, sumoylation and neddylation. The stability of the TGFβ receptors is controlled by the balance between polyubiquitylation and deubibiquitylation, although the exact residues that are modified haven't been identified yet. The E3 ligases of the Smurf (Smad ubiquitination related factor) family have been shown to enhance the turnover of TβRI through Smad7, which plays as a negative feedback for tightly regulating the TGFβ signaling[53,54]. Several deubiquitylases such as USP4 (ubiquitin specific protease), USP15 and USP11 have been identified for deubiquitylating TβRI and thus promoting the TGFβ signaling[55-57].

The amino acid residue Lys389 in the kinase domain of TβRI participates in signaling by sumoylation, which promotes Smads phosphorylation. The sumoylation process is further regulated by a nearby residue Ser387[58,59]. Two residues (Lys556 and Lys567) downstream of the kinase domain of TβRII could be modified by NEDD8 (neural precursor cell expressed, developmentally down-regulated 8), which is an ubiquitin-like molecule. This inhibits the degradation of TβRII through preventing its endocytosis to caveolin-positive compartments, while promoting its endocytosis to early endosomes[60]. In addition, an LTAxxVAxxF motif at the end of the TβRII kinase domain ensures its proper delivery to the basolateral membrane[61].

1.2.1.3 Smads

Smad family proteins mediate TGFβ signaling from the trans-membrane receptors to the nucleus. According to their structural and functional characteristics, members of the Smad family are divided into three classes: R-Smad (Receptor-regulated Smad), Co-Smad (Common mediator Smad) and I-Smad (Inhibitory Smad). R-Smads directly associate with and are activated by type I receptors. The activated R-Smads then form heteromeric complexes with Co-Smads and shuttle into the nucleus to regulate target gene transcription. I-Smads are transcriptionally induced by TGFβ ligands and negatively regulate TGFβ signaling via a variety of mechanisms. For example, through binding to the type I receptors, I-Smads not only block the association and phosphorylation of R-Smads, but also recruit PP1 (protein phosphatase 1) or Smurfs to dephosphorylate or degrade the receptors, respectively. Moreover, I-Smads also disrupt the formation of Smads-DNA complex, and engage HDACs (Histone deacetylases) to repress transcription in the nucleus[50,62-64].

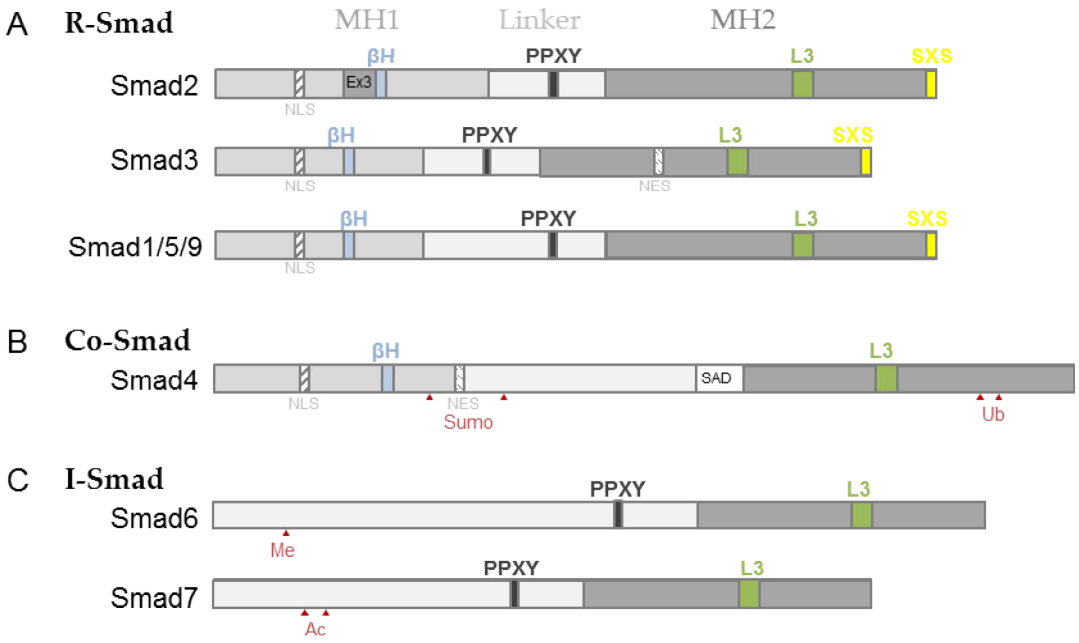

Figure 1.2.5 Schematic illustration of the Smads architecture. The three functional classes of the Smad family: R-Smads, direct phosphorylation target of activated type I receptors (A); Co-Smad, the common mediator, could bind to various R-Smads (B); I-Smads, negative regulators of the TGFβ signaling (C). βH, the β-hairpin domain. PPXY, the proline-tyrosine motif. L3, the L3 loop. SXS, the C-terminus SXS motif. NLS, nuclear localization signal. NES, nuclear export signal. Ex3, the exon 3 of Smad2. SAD, the Smad4 activation domain. 'Sumo' with red triangle, sumoylation site. 'Ub' with red triangle, ubiquitylation site. 'Me' with red triangle, methylation site. 'Ac' with red triangle, acetylation site. This figure is adapted, modified from Moustakas et al. (2009)[65].

The architectures of all the R-Smads and Co-Smads are similar: a conserved MH1 (Mad Homology 1) domain at the N-terminus, a conserved MH2 domain at the C-ternimus, and a linker domain connecting them (**Figure 1.2.5** A, B). The MH1 is a DNA binding domain which carries the NLS (nuclear localization signal) and mediates specific DNA binding through the βH (β-hairpin) structure[66]. The additional exon (Ex3) of Smad2 interferes with its direct DNA binding[67]. MH2 is important for Smads oligomerization, and their specific interaction with TβRI or DNA binding partners. The SXS motif in MH2 at the C-terminus of R-Smads is the target of activated TβRI. The L3 loop within MH2 is responsible for specific association between Smads and the L45 loop of TβRI [68,69]. The linker area between MH1 and MH2 domains is unstructured and divergent. It is rich in serines and prolines that are targeted by diverse kinases, which promotes its interaction with various modulatory proteins, and thus facilitates cross-talk of TGFβ signaling with other signaling cascades. For example, the PPXY motif within the linker region is responsible for interactions with WW domain proteins (e.g. Smurfs, TAZ/YAP) for suppressing TGFβ signaling[70,71]. In Smad4, a SAD (Smad4 activation domain) exists instead of the PPXY motif, which determines the transcriptional activation of the Smads complex[72]. In I-Smads (**Figure 1.2.5** C), the MH2 domain is conserved, which enables them to interact with the type I receptors, but the MH1 domain is absent.

Besides phosphorylation, activity of Smads is subjected to post-translational modifications. R-Smads are negatively regulated by ubiquitination for proteasomal degradation[73], and are positively influenced by acetylation[74,75]. Smad4 could be mono- or ploy-ubiquitinated to promote Smads oligomerization or Smad4 degradation, respectively[76]. Smad4 was also found to be modified by SUMO-1[77]. Moreover, I-Smads have been shown to be subject to acetylation, ubiquitination and methylation[78,79].

1.2.2 Non-Smad signaling

In addition to the canonical TGFβ signaling through intracellular Smads pathway, diverse cellular signaling transmitted through other mediators also occur upon TGFβ stimulation, which complements the Smad dependent actions. Examples of the non-Smad signaling are MAPK (mitogen-activated protein kinase) pathways, small GTPases, and translocation of the cleaved TβRI-ICD (intracellular domain of TβRI) (**Figure 1.2.6**).

Recruitment of tyrosine kinases is related to TGFβ mediated MAPK signaling activation. On the one hand, TβRI has been found to be tyrosine phosphorylated upon TGFβ stimulation, the activated TβRI recruits and directly phosphorylates tyrosine and serine of ShcA proteins, which then recruit Grb2 and SOS to initiate

the Ras-Raf-MEK-Erk MAPK signaling cascade[80]. This leads to regulation of cell proliferation or cell migration. On the other hand, TβRII has been found to be phosphorylated on Tyr284 by Src. This is facilitated by TGFβ induced αvβ3 integrin upregulation, which enables β3 integrin to physically interact with TβRII[81,82]. The phosphorylated Tyr284 then coordinates the selectively docking of the SH2 domains of Grb2 (growth factor receptor binding protein 2) and Shc (Src homology 2 domain containing) to TβRII, thereby couples TGFβ to p38 MAPK signaling activation[42]. This Src-dependent TGFβ signaling is related to breast cancer progression[81]. Furthermore, activated TβRI in LRC could recruit the ubiquitin ligase TRAF6 (TNF (Tumor necrosis factor) receptor associated factor 6) and enhance the auto-ubiquitination of it. TRAF6 then activates the catalytic function of the TAK1 (TGFβ activated kinase 1) by Lys63-linked polyubiquitylation, which in turn results in activation of the p38/JNK (c-Jun N-terminal kinase) MAPK cascades. This MAPK signaling activation regulates apoptosis and EMT[83,84].

TβRII could regulate small GTPases, which plays an important role in TGFβ induced EMT (epithelial-to-mesenchymal transition). Briefly, TβRII is shown to phosphorylate the polarity protein Par6 (Partitioning defective 6 homolog), which then recruits the E3 ligase Smurf1 to ubiquitinate the small GTPase RhoA for localized degradation. Because the RhoA controls the assembly of tight junctions, loss of RhoA promotes dissolution of tight junctions and EMT, which plays important roles in early development, wound healing and disease like cancer[85-87]. Although Smad-dependent TGFβ signaling is indispensable for complete TGFβ-induced EMT, various studies demonstrate the importance of this non-Smad signaling in metastasis[88].

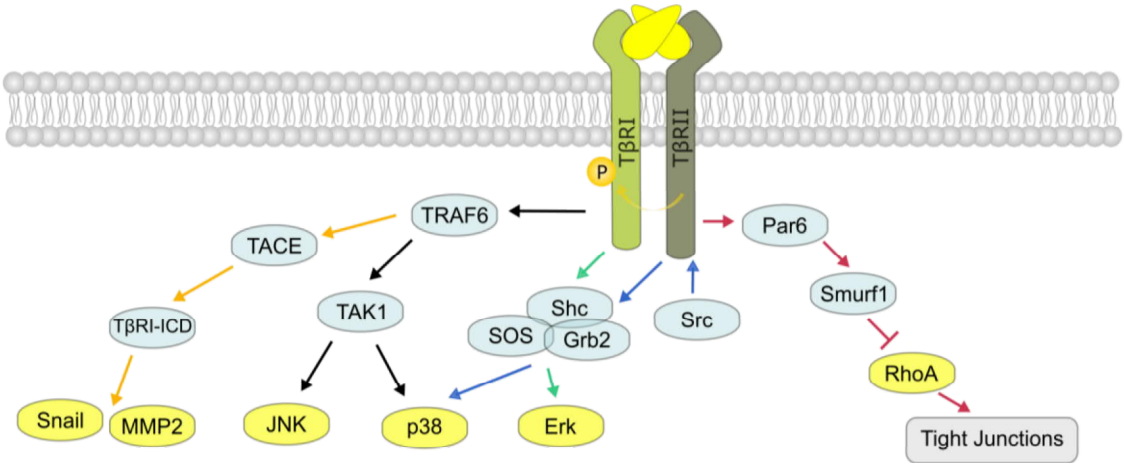

Figure 1.2.6 Examples of non-canonical TGFβ signaling. TGFβ receptors can signal independently of the Smads, to induce context dependent responses through activating various signaling pathways such as MAPK signaling, small GTPases, or direct transcriptional regulation by the cleaved TβRI-ICD. Different pathways are distinguished by different colors of arrows.

TGFβ could also induce cleavage of TβRI at Gly120 by TACE (TNF-alpha converting enzyme). The cleavage liberates the ICD of TβRI, and it is promoted via TRAF6 mediated polyubiquitination on TβRI[89]. The released TβRI-ICD translocates into nucleus and associates with p300 to transcriptionally regulate target genes involved in tumor invasiveness, such as MMP2 and Snail.

1.2.3 Membrane trafficking in TGFβ signaling

Consistent with many other cell surface receptors, TGFβ receptors undergo constitutive endocytosis and recycling, independent of ligand stimulation[90]. Therefore, aside from the presence of TGFβ receptors on the cell surface, there exists an intracellular pool of TGFβ receptors. There are two distinct ways of receptor internalization, clathrin-dependent and caveolin-dependent endocytosis, which have been regarded to positively facilitate and negatively regulate TGFβ signaling (**Figure 1.2.7**).

The clathrin-dependent endocytosis on the one hand negatively regulates signaling transduction by decreasing the potent receptors on the cell surface and mediating receptor degradation; but on the other hand, it increases the proximity between the activated receptors and their downstream substrates or other signaling regulators in the cytoplasm, thereby enhancing TGFβ signaling. The clathrin-dependent internalization occurs through formation of clathrin-coated vesicles, which is dependent on the interaction between the intracellular domain of the receptors and the N-terminal trunk domain of the β2 adaptin subunit of AP2 (clathrin-associated adaptor protein complex) [91]. Once LRC is internalized, TGFβ signaling is promoted by several positive regulators localized in the EEA1 positive early endosomes, which are important signaling centers for signaling transduction. SARA (Smad anchor for receptor activation), Hrs/Hgs (hepatocyte growth factor-regulated tyrosine kinase substrate) and endofin are three typical positive regulators that reside in early endosome through their FYVE (Fab1, YOTB/ZK632.12, Vac1 and EEA1) domain[92,93]. SARA promotes R-Smads phosphorylation by functioning as a scaffold protein and facilitating the presentation of the R-Smads[94]. Hrs functions by binding to Smad2 and cooperating with SARA[95]. Endofin facilitates TGFβ signaling by interacting with Smad4[96]. Besides, SARA also cooperates with the tumor suppressor protein cPML (cytoplasmic promeylocytic leukemia) and the adaptor protein DAB2 (disabled-2) for linking the receptors to Smads and stabilizing the complex, thus facilitating TGFβ signaling[97,98]. Due to the importance of the early endosomes for TGFβ signaling, the small GTPase Rab5, which regulates the early endosome dynamics, plays a crucial role in modulating TGFβ signaling [99,100].

A portion of the internalized TGFβ receptors will recycle back to the plasma membrane (PM), probably in the absence of ligand[101]. Recycling of the internalized receptors is dependent on Rab11, which marks the perinuclear recycling endosomes[102,103]. Besides, various regulators exist in controlling the recycling processes, such as CIN85 and DAB2/ Vps26 (retromer vacuolar protein sorting protein 26) for promoting TβRI and TβRII recycling, respectively[104-106].

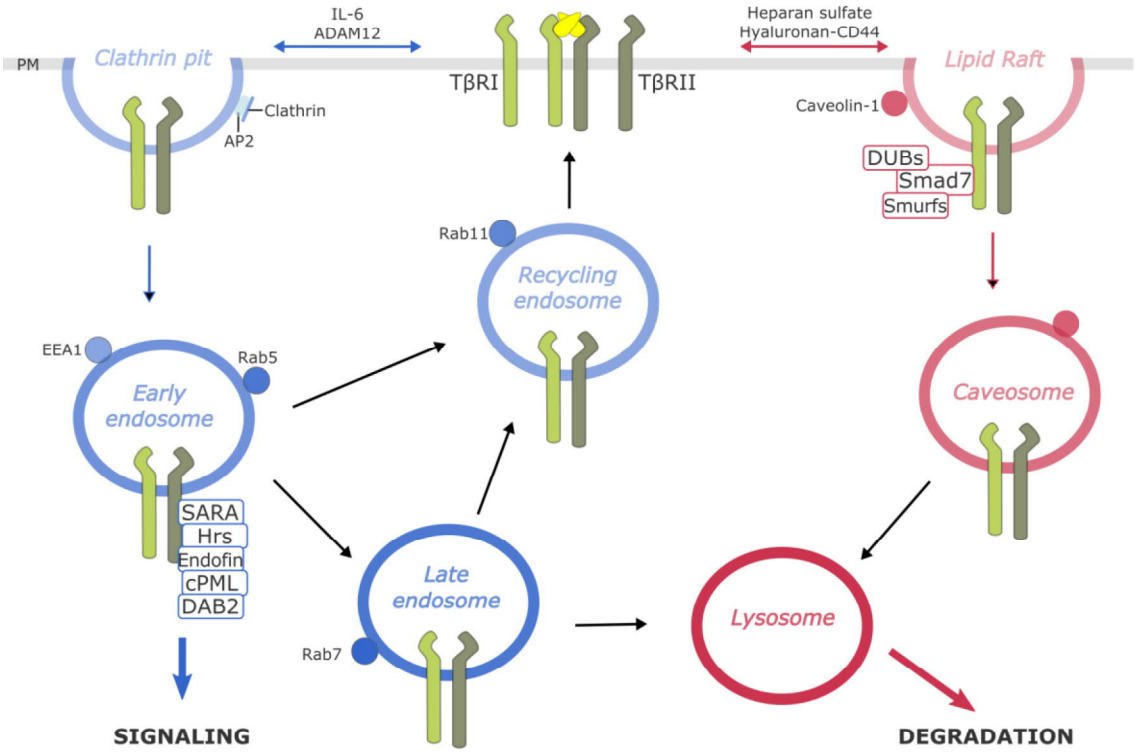

Figure 1.2.7 Membrane trafficking of TGFβ receptors. TGFβ receptors undergo constitutive internalization and intracellular sorting through two distinct pathways: clathrin-dependent and caveolin-dependent pathways, to enhance and turn off signaling, respectively. In the clathrin-dependent pathway (blue), receptors are internalized via clathrin-coated pits. SARA, Hrs, Endofin, cPML and DAB2 cooperate to promote Smads signaling in the EEA1-rich early endosome. From there, a portion of the receptors can recycle back to the cell surface via the Rab11-positive recycling endosome; others are sorted to the Rab7-labeled late endosome, and then either enter the recycling procedure or continue to the lysosome to be degraded. In the caveolin-dependent pathway (red), receptors are internalized via caveolin-positive lipid rafts and enter the caveolin-positive endosome, then eventually reach the lysosome where the final protein degradation takes place. The caveolin-1 associates with TβRI and facilitates its interaction with Smad7, which carries ubiquitin ligase (e.g., Smurfs) and deubiquitylase (e.g., DUBs) to regulate the ubiquitination of the receptors as well as Smad7 itself. The distribution of TGFβ receptors on the plasma membrane is regulated by IL-6, ADAM12 and heparin sulfate, hyaluronan-CD44 for shifting the receptors to the clathrin pits and lipid raft, respectively. This figure is adapted, modified from Heldin *et al*. (2016)[26].

Caveolin-dependent endocytosis occurs through cholesterol-rich lipid rafts/caveolin-coated vesicles and acts to turn off the TGFβ signaling by promoting receptors degradation. Through this pathway, caveolin-1 associates with TβRI and facilitates its degradation in proteasomes or lysosomes through interaction with Smad7/Smurf complex [107,108]. Besides the negative effects on TGFβ signaling, lipid rafts participate in several non-canonical TGFβ signaling pathways. For instance, caveolin-1 promotes TGFβ induced upregulation of type I procollagen via PI3K/Akt/mTOR signaling pathway[109]; cholesterol-rich lipid rafts mediate TGFβ induced MAPK activation[110]; eNOS (endothelial nitric oxide synthase) activation in lipid rafts is facilitated by its association with TGFβ receptors, which is inhibited by TGFβ stimulation[111]. Moreover, caveolin-1 interacts with ALK1 and facilitates its signaling through Smad1/5[112].

TGFβ signaling is elaborately regulated by the balance between the two branches of internalization (i.e., clathrin and caveolin dependent endocytosis). IL-6 (Interleukin-6) and AMAM12 (a disintegrin and metalloproteinase 12) could enhance the signaling through promoting trafficking of the receptors to the non-raft pools[113,114]. While heparin sulfate and CD44 facilitate partition of the receptors to the lipid-rafts, resulting in attenuation of the signaling[93]. In addition, the regulation of N-glycan processing on the receptors also influences the TGFβ signaling through balancing their surface retention with internalization[38]. Interestingly, the rates of internalization and recycling are not affected by ligand binding[102], while a decrease in ligand binding was shown upon ligand induced receptors oligomerization[115].

1.2.4 TGFβ signaling in context

As mentioned above, the function of TGFβ is versatile and even seemingly paradoxical: it can regulate different genes in different tissues; it can help ES cells maintain pluripotency, but also promote differentiation; it suppresses tumor progression in pre-malignant cells, but enhances metastasis in carcinoma cells. The contrast between the multi-functionality of TGFβ signaling and the simple central engine of the Smad signaling suggests that the cellular context rather than the cytokine itself dictates the specific responses[12]. Here, we list several examples of context-dependent specific TGFβ signaling.

Cell-type-specific master transcription factors recruits TGFβ induced R-Smads to specific sites in the genome for orchestrating cell-type-specific regulation by TGFβ. For instance, Smad3 is recruited by Oct4 in ES (embryonic stem) cells for maintaining hES cell identity, by MYOD1 (myoblast determination protein 1) in mesenchymal progenitors for myogenic process, and by PU.1 in pro-B cells for regulation of cell differentiation fate[116].

Besides, TGFβ is also a master of T cell trades, therefore a crucial player in immune or inflammatory functions by regulating T cell development, homeostasis, tolerance and differentiation, depending on specific cell types as well as environmental cues[117].

In hepatic and breast epithelial cells, or during palate fusion, heart development and renal fibrosis, with WNT providing the proper context, TGFβ could trigger EMT via two complementary pathways: first, a pathway of TβRI-Smads-Snail/TWIST1 (TWIST-related protein 1) to repress the expression of a key epithelial cell junction gene, CDH1; second, a pathway of TβRII-Par6-Smurf-RhoA to dissolve tight junctions[12,88,118].

In epithelial cells, neural and hematopoietic cells, the anti-proliferation effect of TGFβ is mainly mediated by activating the CDK (cyclin-dependent kinase) inhibitors and repressing the Myc. Specifically, in skin keratinocytes, the TGFβ-induced Smads complex cooperates with FOXO (Forkhead box O) factors, ETS1 (E26 transformation-specific proto-Oncogene 1) and AP2 to promote transcription of CDKN1A and CDNK2B. At the same time, the activated Smads complex interacts with E2Fs to inhibit Myc expression[12].

In premalignant cells where an oncogenic driver mutation appears, TGFβ triggers apoptosis and thus suppresses tumor progression. However, these cells tend to eliminate the tumor suppressive effects of TGFβ by accumulating more driver mutations on upstream signaling transducers such as TGFβ receptors and Smads (mainly happens in pancreatic and gastrointestinal carcinomas), or downstream effectors such as CDK4 inhibitor p15-INK4b (frequently happens in breast carcinomas, melanomas and gliomas). As a result, tumor cells withstand and even create a TGFβ-rich microenvironment which is profitable for tumor progression and metastasis[12].

1.2.5 Approaches to investigate or manipulate TGFβ signaling

The principal components, the related regulators, as well as numerous target genes of TGFβ signaling were identified decades ago. Crystal structures of these components were gradually resolved[28,47,119-128], and disease-causing mutations were also discovered to provide implications for medical applications[129]. With the development of the systems biology, mathematical models have been developed to aid the comprehension of signal processing dynamics in the TGFβ signaling pathway[130-136]. However, due to the vagueness or the poor resolution of the current available biological experimental methods, it is still very far away from quantitatively understanding the wring of the TGFβ regulated molecular network in different context, as well as the dynamics of TGFβ signaling under

various perturbations. Ergo, precise control of TGFβ signaling is urgently demanded for practical applications, especially at the single cell level.

Several efforts have been made to manipulate the canonical TGFβ signaling. At the level of controlling TGFβ receptors, synthetic surfaces presenting ligand peptides to TGFβ receptors have been generated to preorganize these receptors and potentiate local TGFβ signaling, sensitizing bound cells to subpicomolar concentrations of TGFβ, therefore precise spatial control could be achieved[137]. Chimeric receptors that could be activated by chemically-induced dimerization have also been constructed for isolating and interrogating the characteristics of specific receptors[138-140]. Small molecular inhibitors have been screened or developed to inhibit the kinase activity of the TGFβ receptors[141-143]. At the level of controlling TGFβ ligands, antisense oligonucleotides/RNAs and antibodies have been designed to modulate the activity of the TGFβ ligands[144-147].

All of these strategies depend on the preparation and administering of small chemicals or even antibodies to stimulate the cells. The recent development of the field of optogenetics provides us with an alternative option to activate cells: shining light on cells. Light stimulation is superior to the traditional ligand stimulation on several aspects (**Table 1.2-1**). Firstly, light is much more convenient to manipulate. With light sources (of certain wavelengths) and a coupled electric controller, any patterns of stimulation could be realized by coding in the software. Secondly, with light, spatiotemporal control could be easily achieved at the subcellular resolution, just as structures of subcellular objects could be accessed under a modern microscope. In addition, the procedure of medium change (which is necessary for ligand stimulation) might play as a stimulus, and thus might interfere with the results. Light stimulation avoids this interference by avoiding the necessity of medium change.

Table 1.2-1 Comparison of light and ligand for perturbing cell signaling

	Light	Ligand
Manipulation	Convenient	Inconvenient
Spatiotemporal control	Precise	Poor
Need Medium Change	No	Yes

1.3 Optogenetics

Optogenetics is a recently developed field of study, which involves using light to control the activities of proteins or cellular functions in living cells by introducing light-sensitive proteins. At the beginning, optogenetic tools were mainly developed on light-sensitive ion channels for modulating membrane voltage potential, which has transformed the neurosciences. Later on, another set of optogenetic tools have emerged and quickly been developed to allow control of molecular interactions and signaling cascades. Due to the convenience and precision of manipulating light stimulation, optogenetics is a powerful tool to achieve high spatiotemporal resolution, which is not only beneficial for scientific research, but also a potent approach for therapeutic application.

1.3.1 Optogenetic tools for modulating membrane voltage potential

Neuronal communication is based on the 'switch' between the activation of transient electrical signals (spiking) by membrane depolarization, and the inhibition of these signals by membrane hyperpolarization. To study the functional relationships among the various neurons, and their individual contribution to the network functions or certain behaviors, it is necessary to precisely target and control the electrical activities in specific neurons.

Nowadays, a toolbox of light-activated neuronal switches is available for precisely operating the currents in neurons, by converting light into electricity (**Figure 1.3.1**). They were borrowed and developed from the natural world, in which photo-sensory or photosynthetic molecules prevail throughout the kingdom of life. By exogenously expressing these light-sensitive tools in certain neurons, we could turn them on or off by shining light on them. Therefore, light could be converted to electricity, and thus be used as an on-off switch to control the membrane potential in these cells.

ChR2 (Channelrhodopsin-2) is among the first ones in this toolbox. In response to blue light activation, it acts as a nonselective cation channel and triggers a spike to depolarize the neuron[148]. Another protein, VChR1 (*Volvox* channelrhodopsin-1) was also identified to induce spiking, in response to red-shifted light[149]. Besides activating the neuronal signaling, tools for hyperpolarizing neurons (thus inhibiting the signaling) were also identified and developed. For example, NpHR (halorhodopsin) works as a chloride pump under yellow light irradiation to block signaling by hyperpolarizing the neuron[150]; Arch (archaerhodopsin-3)[151], fungal opsins Mac[152], GtR3 (rhodopsin-3)[153], and BR (bacteriorhodopsin)[154] all work as light-sensitive proton pumps, which could be applied to inhibit spikes through hyperpolarizing neurons.

The toolbox is also expanded by reengineering the existing naturally occurring genes. For example, ChETA[155] and SFO[156] mutants derived from ChR2, are faster and slower versions of ChR2, respectively; eNpHR (enhanced halorhodopsin) mutants from NpHR, show improved membrane targeting property[157]; and eBR is a mutant of BR with enhanced performance in cultured neurons [153].

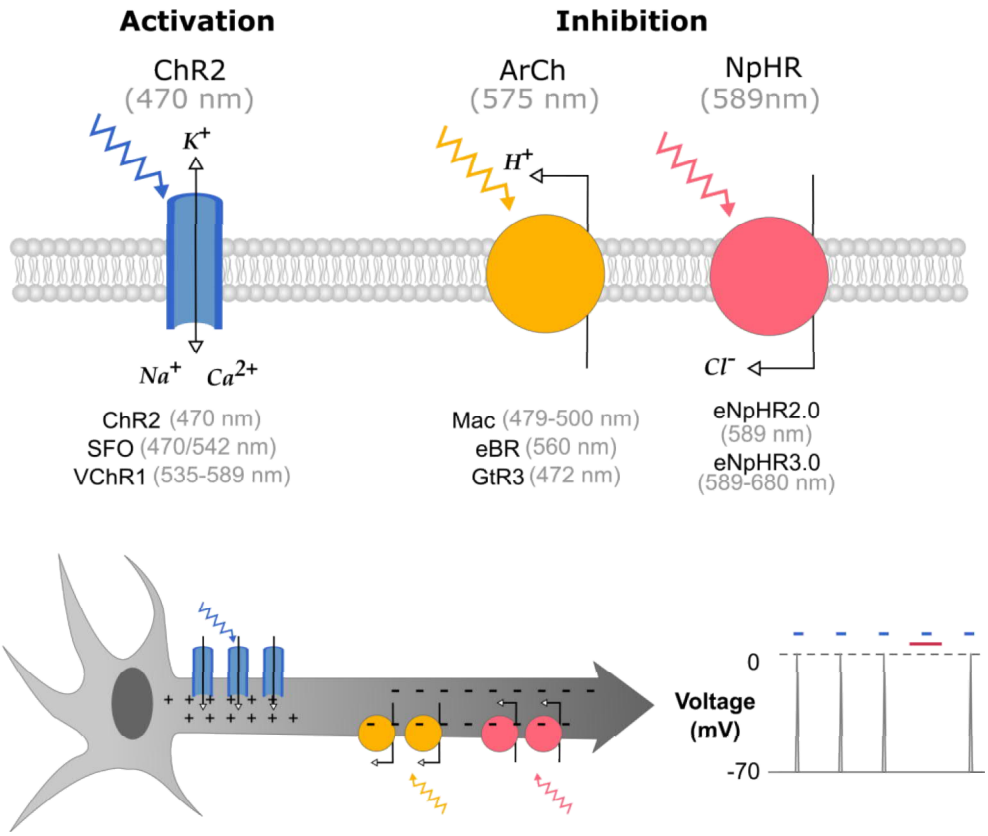

Figure 1.3.1 Optogenetic tool box for modulating membrane voltage potential[158]. ChR2 and its derivatives could activate transient electrical signals by membrane depolarization; NpHR (woking as a chloride pump), Arch (functioning as a proton pump) and their derivatives could inhibit signals through different ways. This figure is adapted, modified from Pastrana (2011)[158].

Since its advent, optogenetics has revolutionized the landscape of neuroscience by providing a set of tools enabling us to efficiently probe the specific neural circuit components. It has been successfully employed to promote our understanding of not only the neural circuits mediating normal behavior, but also its aberration underlying the dysfunctional behavior or psychiatric diseases, including addiction, mood disorders, obsessive compulsive disorder, and Parkinson's disease, among others[159].

1.3.2 Optogenetic tools for modulating cell signaling

Recent years, the field of optogenetics has moved beyond the toolbox of light-gated ion channels, another toolbox is also quickly developed, for modulating cell signaling. In this toolbox, photosensitive proteins undergo reversible conformational changes in response to specific light wavelength, which alters their binding affinities, resulting in diverse light-induced activities. Therefore, when fusing a signaling domain to the light-sensitive protein or its partner, it is easy to achieve inducible protein association, gene regulation, clustering-based activation/inhibition, or conformational change[160-163] (**Figure 1.3.2**).

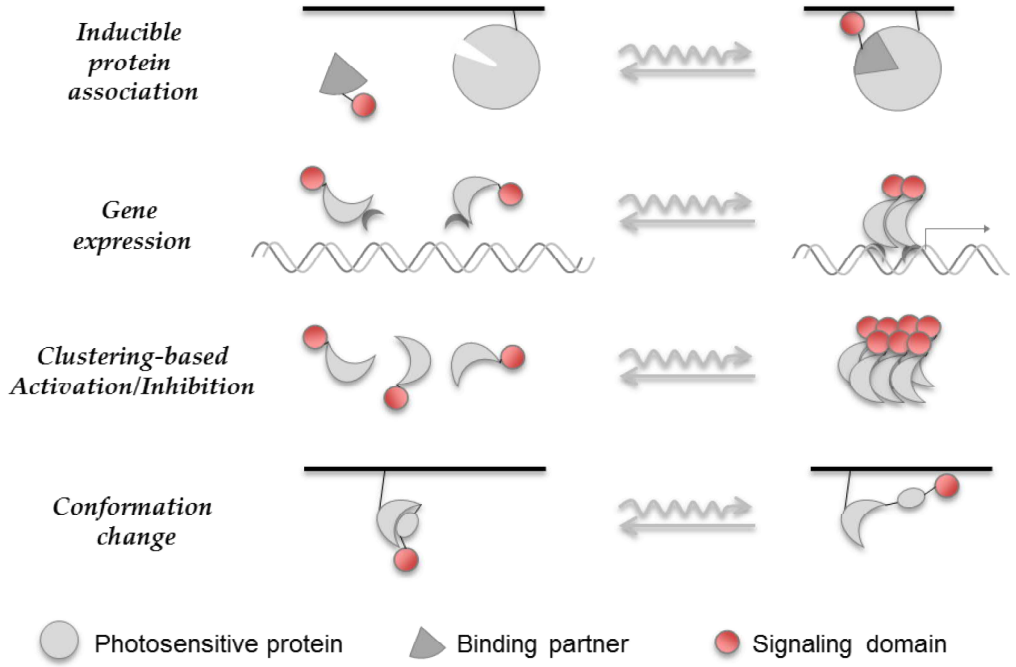

Figure 1.3.2 Strategies for controlling cell signaling optogenetically. The optogenetic tools could be applied to modulate cell signaling through various approaches. When fusing the signaling domain to a light-sensitive protein or its partner, we could achieve inducible protein association by heterodimerization; gene expression by recruiting transcription activators; clustering-based activation or inhibition through regulating the densities of the signaling domains or being sequestered, respectively; and conformational change to conceal or relieve a signaling domain. Waved arrows indicate the response to light stimulation. Straight arrows in the opposite direction indicate reversion in dark or in response to an alternative light wavelength. This figure is adapted, modified from Tischer *et al*. (2014)[164].

Currently available photosensitive modules in this toolbox spread throughout the spectrum between UV (Ultraviolet) and infrared (infra-red) wavelengths (**Figure 1.3.3**). They vary not only in absorption spectrum, but also in size and turn-on/turn-off kinetics (**Table 1.3-1**). Some of them need us to supply the cells with exogenous chromophores (e.g. PCB), but others employ chromophores that

are endogenous in mammalian cells (e.g. flavin). It is of prime importance to compare these properties and then select proper optogenetic modules for developing the light-controllable cell signaling system. The best appropriate module is also dependent on the properties of the cell signaling to be controlled, as well as the compatibility of the fluorescent proteins. By taking the advantage of the diversity of optogenetic modules, multi-chromatic control of cellular activity is also possible for achieving more layers of manipulation[165].

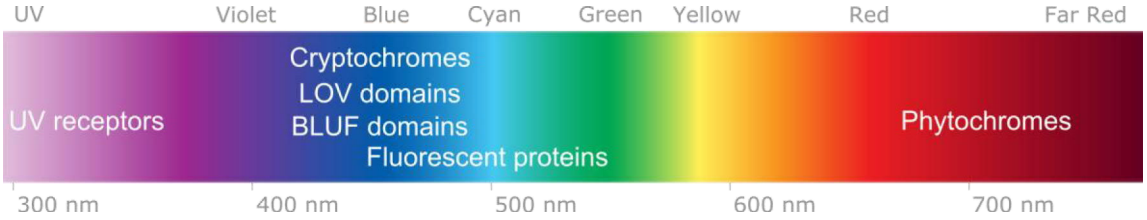

Figure 1.3.3 A diversity of photosensitive modules. The localization of each module on the spectrum indicates the color of its activation light.

1.3.2.1 Optogenetic modules

Optogenetic modules for manipulating cellular signaling are derived from photosensitive modules of organisms throughout the kingdom of life, including bacteria, fungi, plants and mammals. A variety of biological phenomena are induced by light stimulation, including visual perception, flowering, phototropism and phototaxis. Upon specific light absorption, the chromophore of the photo-sensory module is excited and transformed by photochemical reactions, which induces the amino acid backbone of the photosensitive protein to undergo rearrangement. This conformational alternation then activates the photosensitive module through undocking or affecting their protein-protein interactions [166]. In addition to the natural occurring photo-sensors, the toolbox for modulating cell signaling is also expanded by artificial ones which are developed through mutations.

Phytochromes

Phytochromes are a set of photoreceptors at the far-red end of the spectrum in the toolbox. Bacterial BphP1 (bathy phytochrome1) is activated by infrared light and binds to its natural partner PpsR2; PhyB (phytochrome B) from *Arabidopsis thaliana* is activated by red light irradiation and binds to its cofactor PIF3 or PIF6 (phytochrome interacting factor); while Cph1 (cyanobacterial phytochrome 1) undergoes homodimerization in response to red light stimulation. Notably, all these activation processes could be efficiently reversed by another wavelength. This dual optical controllability could benefit higher level of quantitative perturbation and regulation of the biological activity. PhyB-PIF3/PIF6

heterodimerization has been applied to study Rho GTPase and MAPK signaling pathways, and also has been used to control the nuclear shuttling of proteins. In addition, bilin molecules are needed as the chromophores of the phytochromes: PΦB (phytochromobilin), PCB (phytococyanobilin) and BV (biliverdin IXα) are for plant, cyanobacterial and bacterial/fungal phytochromes, respectively. Among them, BV is endogenously expressed in all cells and thus not necessary to be supplied externally.

Fluorescent proteins

Fluorescent proteins could also be modified and developed to be optogenetic tools. Dronpa is a monomer GFP (green fluorescent protein) that undergoes reversible transitions between dark and fluorescent states by cyan and violet light stimulation, respectively. The substitution of K145N generates a light-switchable module, Dronpa145N, which forms tetramers at the micro-molar concentration in the dark, or upon violet light irradiation, and forms monomerizes upon blue light stimulation[167]. The light-switchable tetramerization/monomerization of Dronpa145N has mainly been applied to uncage and thus activate proteins such as the Cdc42 GEF (guanine nucleotide exchange factor) ITSN (intersectin), or the NS3-4A protease[167].

Cryptochromes

Cryptochromes are probably the most widely used photoreceptors across the evolutionary lineages of bacteria, plants and animals[168]. They respond to blue light irradiation, and implement diverse crucial biological functions such as magneto-reception, plant development and circadian rhythms[169]. The chromophore incorporated by cryptochromes is a single molecule of FAD (flavin adenine dinucleotide), which non-covalently binds to the PHR (photolyase homology region) domain of the cryptochromes. Upon blue light irradiation, the FAD is reduced, which induces conformational changes of the PHR domain into the biological active form. The activated cryptochromes could recover to the original state when blue light is off. Among the cryptochromes, CRY2 (cryptochrome 2) of *Arabidopsis thaliana* is widely adopted to optogenetically control protein homodimerization or heterodimerization. The activated CRY2 forms homooligomers, or forms heterodimers with CIB1 (cryptochromes-interacting basic helix-loop-helix 1). The photoactivation occurs in microseconds upon blue light irradiation, and the activated CRY2 resets to its dark state within minutes, followed by the complex dissociation[170]. A CRY2 mutant, CRY2olig with an E490G mutation in the PHR domain, shows enhanced oligomerization ability, and could be used as an efficient optogenetic tool for clustering-based activation or sequestration[171]. The photocycle kinetics of the CRY2-CIB1 dimerization module have also been further optimized, through perturbing the α13-α14 turn

motif of CRY2[172]. Currently, a truncated version of the CRY2-CIB1 module, CRY2PHR (amino acids 1-498)-CIBN (amino acids 1-170) is more commonly used due to the smaller size and low basal activity[173]. The oligomerization ability of CRY2 has been applied to proteins that require oligomerization or dimerization for activation, such as LRP6, FGFR, hROS1, FGFR, Raf and Trk (tropomyosin-related kinase) receptors[166]. The heterodimerization of the CRY2-CIB1 module has been applied to study apoptosis, small GTPases, kinesin motor KIF5A, dynein adaptor protein BICDN, MAPK or PI3K/AKT signaling pathways[174].

LOV domains

LOV (light-oxygen-voltage) sensing domains are another category of blue light sensitive units, which incorporate flavin chromophores, including FMN (flavin mononucleotide) and FAD. The LOV domain family exists in prokaryotes, fungi and plants, and all of the LOV domains contain a conserved PAS (Per-Arnt-Sim) core flanked by helical elements. Blue light could activate the flavin chromophores, which then form an adduct with a cysteine residue in the PAS core, resulting in conformational changes of the LOV domain. The adduct is gradually hydrolyzed in the dark, and the LOV domain reverts to its initial state.

Three kinds of LOV domains are commonly used in optogenetics: FKF1 (flacin-binding, Kelch repeat, F-box protein), AsLOV2 (*Avena sativa* LOV domain 2) and VVD (vivid). Upon photoexcitation, FKF1 undergoes dimerization with its binding partner GI (GIGANTEA) within minutes, and the association is stable for hours after turning off the light. The FKF1-GI system has been applied for RAC1 activation through plasma membrane (PM) recruitment of a constitutively active RAC1 mutant lacking the CAAX motif[175]. AsLOV2 is from the phototropin 1 of *Avena sativa*, its PAS core is flanked by two α-helix, A'α and Jα which unfold and detach from the core within seconds upon light-induced conformational change of the core[176]. This light induced dissociation of Jα from the LOV2 core makes it an efficient optogenetic uncaging approach, and has been applied for uncaging of Caspase7, Rac1, Cdc42, mDia1, and uncaging of PKI (protein kinase inhibitory) peptides for inhibition of PKA (protein kinase A). VVD is the smallest homodimerization tool in the optogenetic toolkit, which reversibly forms homodimer via its Ncap (N-terminal Cap) in response to blue light.

Variants of these LOV domains have been engineered to expand the optogenetic toolbox. A variety of AsLOV2 mutants improve the dynamic range of the LOV-Jα system. AsLOV2 based LINuS (light-inducible nuclear localization signal), LEXY (light-inducible nuclear export system) and LANS (light-activated nuclear shuttle) systems have been developed to control nuclear shuttling of proteins [177-179]. Two other AsLOV2 based systems, iLID (improved light inducible dimer) and TULIPs (tunable, light-controlled interacting protein tags), provide photoinducible heterodimerization tools, which have been applied for recruiting

specific proteins to target sites in various studies[174,180-182]. Magnets pair of pMag-nMag is derived from VVD for strict heterodimerization, through exchanging the neutral amino acids at the homodimer interface of wildtype VVD with positively or negatively charged ones [183].

UV receptors

UVR8 (UV-B resistance 8) as an optogenetic tool resides at the ultra-violet end of the spectrum. The default state of UVR8 in the dark is in the form of homodimer, mediated by salt bridges at the interface. No incorporated chromophore is needed for UVR8 activation. Instead, the intrinsic tryptophan residues clusters around the homodimer interface could be excited by UV-B and destabilize the salt bridges, resulting in rapid dissociation of the homodimer into monomers, which can interact with its binding partners such as COP1 (constitutive photomorphogenesis protein 1). Compared with the fast dissociation upon light irradiation, interaction of UVR8-COP1 is stable for hours in the dark[166]. Therefore, this optogenetic system has mainly been applied for recruiting transcription activation domain to induce gene expression, or triggering protein secretion[166].

BLUF domains

BLUF (blue light utilizing FAD) domains are mostly found in proteins of bacteria and algae. They employ FAD as chromophore and undergo conformational changes triggered by blue light activated FAD reduction. In contrast to other optogenetic systems which affect cell signaling through modulating protein interactions, BLUF domain-based optogenetic systems have a predefined function of photo-inducible adenylyl cyclase activity, regulating cAMP production. euPAC and bPAC, derived from *Euglena gracilis* and *Beggiatoa* respectively, are two commonly used BLUF domains in optogenetics[166]. A novel light-inducible guanylyl cyclase is engineered by replacing the amino acid residues at the substrate binding pocket of bPAC, resulting in its substrate specificity for guanosine instead of adenosine[184].

The optogenetic toolboxes are continuously expanding, evolving and being optimized. Novel photo-sensitive proteins are being discovered and added to the toolboxes. The currently available tools are being optimized on every aspect, including the light-induced activation/recovery kinetics, the affinities, and the wavelength for photo-switching. Because most of these tools are adapted from photo-sensors from other kingdoms such as plants or bacteria, they are orthogonal to the endogenous cell signaling cascades in mammalian cells, which could improve the predictability of the signaling. However, codon optimization for mammalian expression is necessary to be done to improve their expression efficiency, as well as their proper functionality in the target cells.

Table 1.3-1 Examples of available optogenetic tools for manipulating cell signaling

Photo-sensitive protein	Turn-on/ Turn-off ($t_{1/2}$) speed [a]	Size (kDa)	Cofactor	Mechanism	Chromophore requirement [b]	λ_{on} [c] (nm)	λ_{off} [d] (nm)	Ref
BphP1	s / s	80	Q-PAS1/ PpsR2	Heterodimerization, Dissociation	Biliverdin[e]	750	650	185
BphG1	NA	110	-	Conformational change	Biliverdin[e]	700	750	186
PhyB	s / s (hr in dark)	130	PIF3/6	Heterodimerization, Dissociation	PΦB [f]	650	750	163,187
CPH1	ms / ms	60	-	Homodimerization	PCB [f]	650	750	188
Dronpa145N	s / s	30	-	Tetramerization, Dissociation	None	500	400	167
CRY2	s / m	70	CIB1	Heterodimerization, Oligomerization	FAD [e]	450	NA	161,170
CRY2olig	s / m	60	-	Oligomerization	FAD [e]	450	NA	171
FKF1	m / hr	70	GIGANTEA	Heterodimerization, Dissociation	FMN [e]	450	NA	189
AsLOV2	s / s	17	Zdk (dark)	Conformational change, Dissociation	FMN [e]	450	NA	176
RsLOV	NA / m	20	-	Homodimerization, Dissociation	FMN [e]	450	NA	190
VVD	s / hr	17	-	Homodimerization	FMN [e]	450	NA	191
Magnets	s / hr	17	-	Heterodimerization	FMN [e]	450	NA	183

Table 1.3-1 Examples of available optogenetic tools for manipulating cell signaling (continued)

Photo-sensitive protein	Turn-on/ Turn-off ($t_{1/2}$) speed [a]	Size (kDa)	Cofactor	Mechanism	Chromophore requirement [b]	λ_{on} [c] (nm)	λ_{off} [d] (nm)	Ref
AU1	s / m	16	-	Homodimerization	FMN [e]	450	NA	192
El222	s / s	25	-	Homodimerization, DNA binding	FMN [e]	450	NA	193
YtvA	m / hr	30	-	Conformational change	FMN [e]	450	NA	194,195
euPAC	s / s	110,90	-	cAMP production	FAD [e]	450	NA	196
bPAC	s / s	40	-	cAMP, cGMP production	FAD [e]	450	NA	197
UVR8	s / hr	50	COP1	Heterodimerization, Dissociation	None	300	NA	198,199
optoXRs(opsin/ GPCR)	ms / s	80	-	G-protein activation	11-cis retinal [g]	various	NA	200-202

a) Turn-on speed: the speed with which the system activates when illuminated by the stimulatory light (λon); Turn-off speed: the speed with which the system resets when illuminated by inhibitory light (λoff) or in the dark.
b) Small molecules, if needed, to make the protein photo-sensitive.
c) The light wavelength that is most effective to activate the system. Other wavelengths may still work but require higher intensities/ longer exposures.
d) The light wavelength, if any, that resets the system.
e) Endogenous in mammalian cells.
f) Exogenous, needs to be supplied.
g) Endogenous in mammalian cells, but only produced in the photoreceptor organs, thus needs to be supplied for cultured cells[203].

1.3.2.2 Advantages of optogenetic control

Besides its non-invasive way to act on cells, light has great advantages as a stimulus, because it could be manipulated conveniently, in terms of intensity, specific space and time. Therefore, optogenetic approaches benefit biological analysis or signaling manipulation through isolating distinct sub-circuits, quantitatively analyzing responses to specific stimulations, controlling cellular signaling in space, and controlling cellular signaling in time (**Figure 1.3.4**).

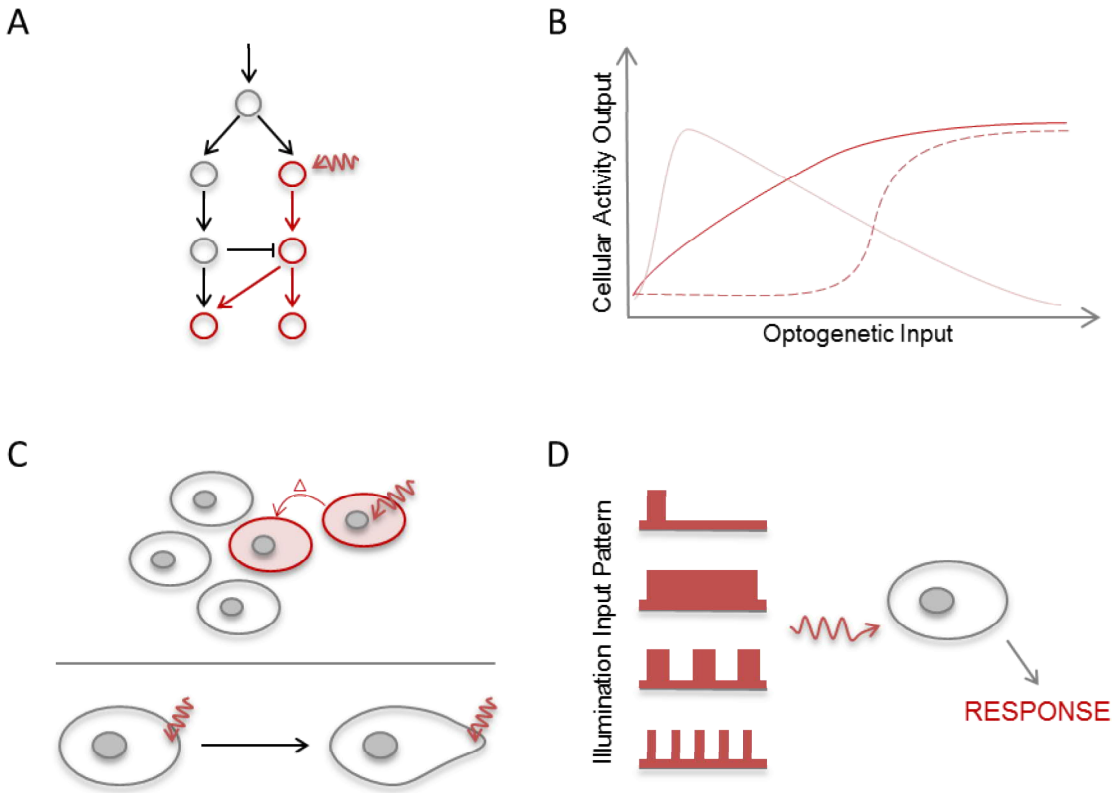

Figure 1.3.4 Schematics depicting the advantages of optogenetic control. (A) Optogenetics enable isolating specific sub-circuits with precise and defined inputs control. (B) Optogenetics facilitates analyzing the input-output behavior quantitatively. (C) Optogenetic regulation of signaling in space, for both multicellular signaling (upper panel) and subcellular signaling (lower panel). (D) Optogenetic regulation of signaling in time, specific illumination pattern could elicit specific response. Wavy arrows denote light input.

Isolation of distinct sub-circuits

Cellular signaling networks often display a complex, interconnected architecture with cross-talks and feedback regulations, which makes it challenging to disentangle specific sub-circuits by the traditional chemical perturbation experiments. Chemicals, especially ligands, could induce various branches of a signaling cascade, and other side-effects such as off-target are often unavoidable. This often complicates the biological analysis by affecting the topology of the signaling network. In contrast, in optogenetic studies or applications, only the proteins containing the light-sensitive modules would response to perturbations of specific optical stimulation. Consequently, through dissecting a signaling pathway and uncoupling specific signaling arms from it, optogenetic modules provide efficient tools to study the specific sub-circuits within the full complex signaling network.

Growth factors activate both PI3K/Akt and Ras/Erk signaling with possible crosstalks between them, Toettcher *et al.* built an optogenetic system to selectively activate the Ras/Erk branch and follow the information flow in it[204]. In another example, the PI3K and Akt signaling was selectively activated in time and space to reveal their distinct roles in adipocyte insulin action[205]. More and more other studies apply optogenetic controls to access distinct nodes in the physiological signaling network.

Quantitative control and analysis of signaling responses

The quantitative control of light input makes optogenetics an efficient way to interrogate how upstream signaling is quantitatively transmitted to the specific downstream responses. Optogenetics facilitates quantitative analysis of cell signaling through precisely controlling optical stimulations, then quantitatively measuring cellular responses to specific stimulations, and finally determining the logic of the signaling information flow. For example, by applying various illumination patters to a photo-activable Akt system, and recording the corresponding time course data of Akt activation, Katsura *et al.* developed a computational model, which enables quantitatively control the Akt activity[206].

Besides the direct assignment of light input pattern, it is also possible to deploy a closed-loop in-silico feedback module to maintain a certain response level. In this optogenetic strategy, live-cell response readout is monitored in real time, and is compared with a target response level. A proper light input that would minimize the deviation between them is then calculated in silico and applied to the cells[207,208]. This could robustly clamp the desired response levels, despite the inevitable biological fluctuations and modeling inaccuracies.

In addition, properties of biological systems such as gradient sensing, frequency response or fold change detection could be studied more conveniently by optogenetic approaches[209-211].

Control of signaling in space

Spatial regulation of cell signaling is important at levels of both organismal biology and cellular processes coordination. Therefore, optogenetics provides excellent tools for manipulating signaling in space, to understand spatial regulation of multicellular signaling, as well as subcellular signaling.

Cell-to-cell communication is crucial for biological processes such as development and signal gradient interpretation. In contrast to chemical treatment, which is hard to target specific cells in a population due to the inherent diffusion property, light stimulation could spatially restrict activation to certain light-sensitive cells. For example, propagation of signaling between adjacent cells is found in STAT3 signaling and ERK activity pulses [204,212]. Lateral inhibition is a rational way to sharpen signal interpretation in the eyes and other multicellular contexts [164,213]. These are only possible to be investigated by precisely controlling the inputs in space.

At the subcellular level, optogenetic systems enable studies on coordinated cellular processes, such as cell polarization or cellular movement *in vivo*. By using AsLOV2 to control Rac1, Wu *et al.* demonstrated conditional lamellipodia formation only at illuminated subcellular sites[162]. As another example, in one study on individual neutrophil migration in zebrafish, Rac was photo-activated locally at the leading edge, resulting in protrusion but not polarization. This demonstrates a two-tiered PI3K-mediated cell motility regulation paradigm[214]. In a third study, optical control of MAPK signaling by locally recruiting Cdc24 resulted in light-directed polarized growth[181]. Combining mathematical models that incorporate spatial information of each signaling node, cellular signaling activity could be better characterized[215].

Control of signaling in time

Biological information is not only encoded in the current level of signaling, but also encoded in the dynamics of signaling over time (**Figure 4.3.2**), which largely extends the complexity of biological information flow[216]. For example, transient or sustained Erk signaling induced by EGF (Epidermal growth factor) or NGF (Nerve growth factor), results in cell proliferation or differentiation, respectively; oscillated or sustained level of nuclear NF-κB induced by TNFα or LPS, triggers inflammatory response genes or adaptive immune response genes, respectively; repeated small pulses or a single larger pulse of p53 induced by γ-radiation or UV radiation, are associated with cell cycle arrest or apoptosis, respectively[217].

Therefore, manipulating and decoding the timing of signaling are of crucial importance for investigating and controlling the specific cellular functions.

Optogenetics approaches have shown their power in manipulation of temporal signaling pattern. By applying the PhyB-PIF module to recruit RasGEF to the plasma membrane, researchers could activate Ras by illuminating specific cells in various patterns. This work elucidates how the Ras/Erk module can specify distinct physiological outcomes[204]. In a recent study, the optogenetic platform was applied to isolate Raf/Erk or Akt signaling pathway and implement precise time-variant input, demonstrating the precise timing of Raf/Erk and Akt activation is crucial in protecting the PC12 cells against oxidative injury[218]. Temporal effects of Raf/Mek/Erk or Akt on other cellular functions or in other cell types have also been revealed[206,219]. In another study, optogenetic manipulation of the duration of Nodal signaling showed that extended Nodal signaling within the organizer suppresses endoderm differentiation, while it promotes prechordal plate specification. This suggests the temporal pattern of Nodal signaling determines cell fate specification during gastrulation[220].

2

Development of the optoTGFβ System

Due to the various advantages of using optogenetic approaches to interrogate signaling pathways, we attempted to apply optogenetic tools to manipulate TGFβ signaling. First, we questioned how likely it would be successful to build a synthetic TGFβ system. By referring to the literature, we found that TGFβ signaling could be triggered by association between the two types of TGFβ receptors. Since optogenetic modules could be applied to control protein association, it is feasible to build a light-controllable TGFβ signaling system. Second, to decide the best-fit photosensitive module for manipulating TGFβ signaling, we compared different properties of the diverse modules in the optogenetic toolkit. PHR-CIBN, which is a simplified version of a phytochromes module, turned out to be a promising one. Third, we tried to design a chimeric light-controllable TGFβ system (optoTGFβ) by considering the details, such as the subcellular localization of the chimeric proteins, and the fluorescent protein usage. The final design of the optoTGFβ system consists of a pair of optoTβRs (optoTβRI: Myr-cytoTβRI-CIBN; optoTβRII: cytoTβRII-CRY2PHR-tdTomato) and a TGFβ signaling readout (iRFP-Smad2). By molecular cloning and stable transfection, we established cell lines that stably expressing the optoTGFβ system, and confirmed the synthetic protein expression by western blotting experiments.

2.1 Feasibility of using optogenetic tools to manipulate TGFβ signaling

The first step of TGFβ signaling following ligand binding is the recruitment of TβRI by TβRII. Therefore, the most intuitive way to control TGFβ signaling is through manipulating the association between the receptors. The first question would be: is it possible to trigger TGFβ signaling by simply bringing the receptors together?

Referring to the literature, researchers have tried to construct chimeric TGFβ receptors by fusing the cytoplasmic region of the TGFβ receptors to chemical-binding proteins (e.g., EPOR)[138] or other ligand-binding proteins (e.g., FKBP12 and FRB)[139], and successfully activated TGFβ signaling with the corresponding chemicals or ligand (**Figure 2.1.1**). These studies demonstrate that, neither the extracellular domains nor the transmembrane regions of the receptors is indispensable for TGFβ signaling activation, as long as the cytoplasmic region of TβRI could be taken closely enough to TβRII, by any means. Therefore, we concluded that it is feasible to activate TGFβ signaling by applying optogenetic tools, through the inducible protein association strategy (**Figure 1.3.2**).

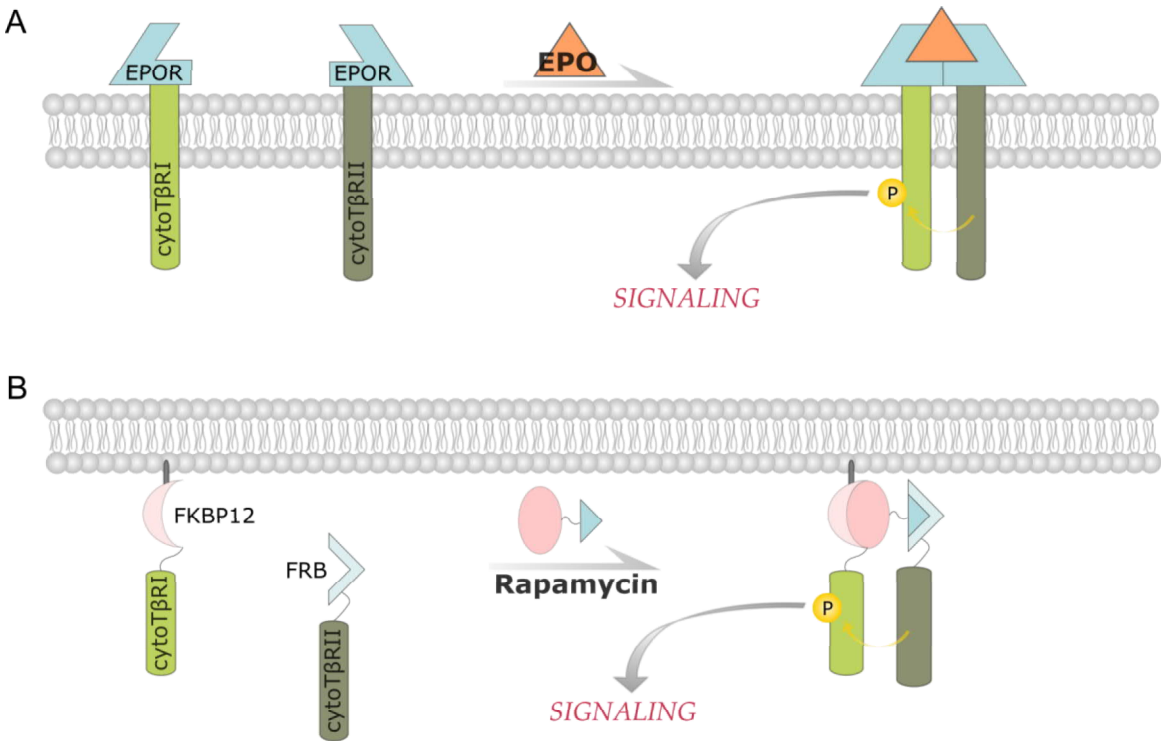

Figure 2.1.1 TGFβ signaling by other ligands or chemicals. (A) EPO could induce TGFβ signaling by replacing the extracellular domains of the TGFβ receptors with the extracellular domain of the EPO receptor[138]. (B) TGFβ signaling could be activated by small chemicals when fusing the TGFβ receptors to the corresponding chemical binding proteins[139]. 'cyto' denotes the cytoplasmic region.

2.2 Choose the proper optogenetic tools

In the optogenetic toolbox, lots of photosensitive modules could be used to induce protein association. To choose the best one, we should inspect and compare the properties of different optogenetic modules. Firstly, the shorter the wavelength, the more toxic the light is to the living cells, thus it would be safer to use longer wavelength for activation/deactivation in experiments. Secondly, in order to control and monitor activities of each type of TGFβ receptor independently, it would be better to use the hetero-dimerization strategy, i.e., fuse the light-sensitive protein or its binding partner to TβRI or TβRII respectively. Thirdly, the speed of activation/deactivation should be considered. Fast turn-on/turn-off rates are more preferred. Fourthly, size and conformation of the optogenetic modules should also be taken in to account. Fifthly, regarding the chromophore usage, every coin has two sides: on the one hand, modules requiring exogenous chromophore (e.g. PCB) need to be supplied with chromophore for activation, which is not as convenient as those modules requiring endogenous chromophore (e.g. flavin). However, on the other hand, this also means that when handling the cells (e.g., during the cell culturing or FACS sorting), it is not necessary to avoid light of the corresponding wavelength, which might accidently activate the signaling.

By considering these various aspects, we decided to start with the CRY2-CIB1 module. This module has been successfully used to control the activity of receptors of another signaling pathway (**Figure 2.2.1**) [221], which also makes the CRY2-CIB1 module a promising tool to manipulate TGFβ signaling. As the PHR domain of CRY2 and the N-terminal region of CIB1 have the full function of light-inducible association, we would use this simplified version, PHR-CIBN in this study[170].

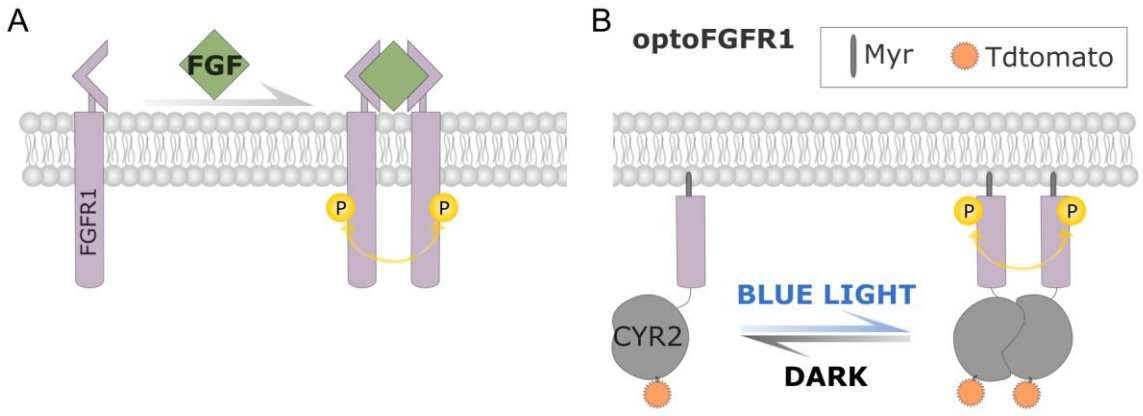

Figure 2.2.1 Schematic representation of wild-type (WT) FGFR1 (A) and optoFGFR1 (B). (A) FGF ligand induces homodimerization of the FGFR1 receptors on the plasma membrane, followed by transphosphorylation and downstream signaling. (B) Dimerization and activation of the FGFR1 is induced by CRY2 clustering upon blue light stimulation. Myr, the myristoylation sequence.

2.3 Design the constructs of the light-controllable TGFβ system

Up to now, we have considered a pair of TGFβ receptors, and a photo-inducible heterodimerization module (PHR-CIBN), to achieve the light-controllable TGFβ signaling activation. To report the activation of the TGFβ signaling, we need readout. Since the nuclear translocation of Smad2 is a core step in TGFβ signaling, we decided to make use of this property. By tagging Smad2 with a fluorescent protein, the activity of Smad2 could be easily monitored under the microscopy. In addition, it would be better to follow the activity of the receptors by tagging them with fluorescent proteins as well. Furthermore, the localization of the chimeric receptors hasn't been determined, i.e., is it necessary to attach the receptors on the plasma membrane (PM), or better to leave them in the cytosol? Therefore, we have a pool of spare parts (**Figure 2.3.1**), from which there are various possible combinations to construct a light-controllable TGFβ signaling system.

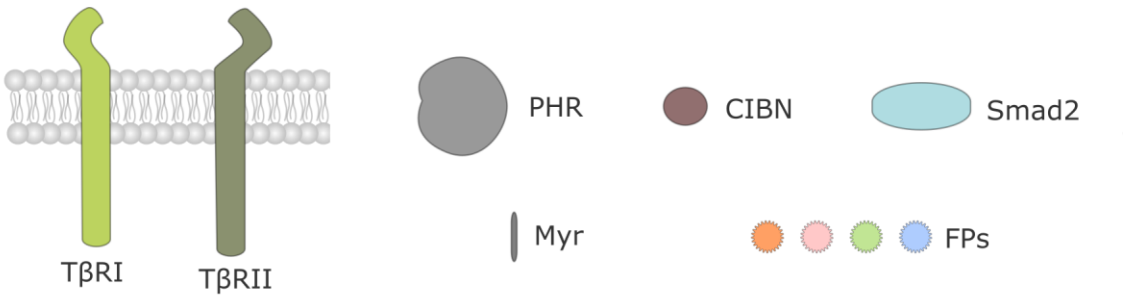

Figure 2.3.1 The spare parts for constructing a light-controllable TGFβ signaling system. PHR, the PHR (photolyase homology region) domain of CRY2; CIBN, the N-terminal region of CIB1; Myr, the myristoylation sequence for membrane targeting; FPs, fluorescent proteins.

First of all, concerning the subcellular localization of the chimeric receptors, we decided to fix one of the receptors to the plasma membrane, leave the other one free in the cytosol, and tag the cytoplasmic one with a fluorescent protein. This design has two advantages: (1) it could separate the two receptors physically to avoid high basal activation, in the situation of no stimulation; (2) it would allow us to monitor the activities of the TGFβ receptors through tracking their localization and the association between the two TGFβ receptors.

Second of all, the usage of fluorescent proteins (FPs) should be carefully considered. Although there are various available FPs spread through the spectrum, as the PHR-CIBN system could be activated by blue light (~480 nm), FPs around the yellow, green and blue light spectrum should be avoided. This is to make sure that the PHR-CIBN system would not be activated when observing and exciting the FPs under the microscopy. Thus it doesn't leave us too many

options: we could only choose FPs in the orange to far-red spectrum, and the selected FPs should be compatible, i.e., their excitation or emission wavelengths should not overlap. In the end, we chose tdTomato and iRFP682 considering that they are bright enough and compatible with each other (**Table 2.3-1**).

Table 2.3-1 Properties of tdTomato and iRFP682

FP	Ex [a] (nm)	Em [b] (nm)	EC [c]	MB [d]	Matura-tion [e]	Photo-stability [f]	Oligomer-ization	Ref
tdTomato	554	581	69,000	48,000	1h	64	dimer	[222]
iRFP682	670	682	90,000	12,600	4.5h	490	dimer	[223]

a) Excitation wavelength (nm).

b) Emission wavelength (nm).

c) Extinction coefficient, capacity for light absorption at the main peak ($(M*cm)^{-1}$).

d) Molecular brightness, product of molar extinction coefficient and quantum yield ($(M*cm)^{-1}$).

e) half-times (t 1/2) for combined folding and chromophore formation at 37 °C.

f) Time for bleaching (t 1/2) from an initial emission rate of 1,000 photons/s down to 500 photons/s (sec).

Taking into account the above aspects, we tested different combinations of Myr, TGFβ receptors, PHR/CIBN and FPs. Some combinations didn't respond to the blue light stimulation at all. Some others did respond but the basal activity is very high (i.e., a high level of nuclear Smad2 was observed even without light stimulation). Finally, we selected one combination with correct response to light activation, and with low basal activity.

In summary, we designed a light controllable TGFβ signaling system, the optoTGFβ system, by introducing the light-sensitive module, PHR-CIBN, which can interact with each other rapidly and reversibly upon blue light irradiation. TGFβ signaling can therefore be trigged ON and OFF at the single cell level by manipulating the illumination pattern. This system is composed of a pair of chimeric receptors which could initiate TGFβ signaling in response to blue light stimulation, and a TGFβ signaling reporter which facilitates monitoring the signaling activity.

2.4 Constructing the optoTGFβ system

2.4.1 The design of the optoTGFβ system

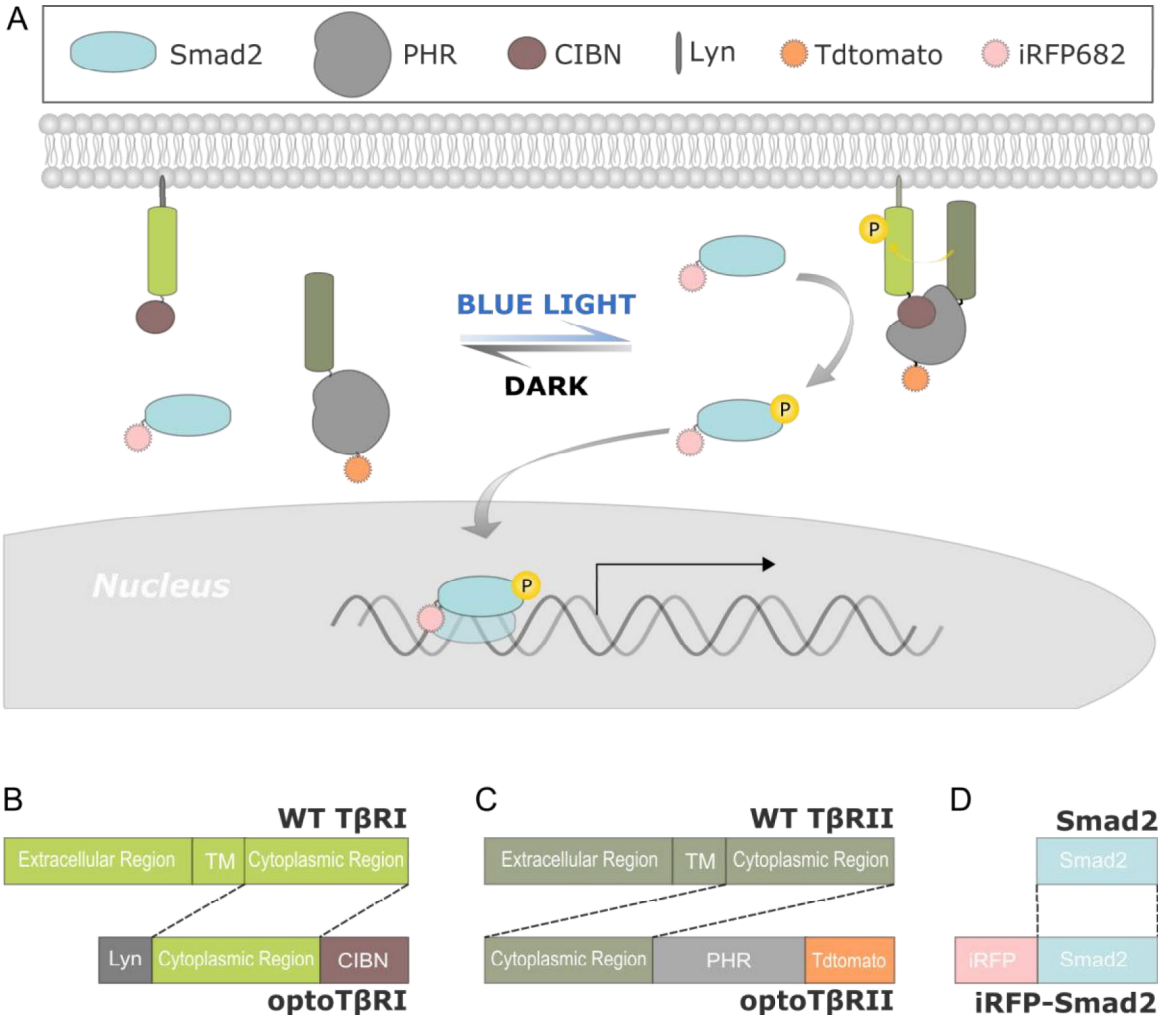

Figure 2.4.1 The development of the optoTGFβ system. (A) Schematic representation of the optoTGFβ system. (B-D) The design of the optoTGFβ constructs. optoTβRI, the cytoplasmic region of TβRI was inserted between the myristoylation signal peptide (Myr) and CIBN (B). optoTβRII, the PHR domain of CRY2 was fused to the cytoplasmic region of TβRII, and tagged with tdTomato (C). Far-red fluorescent protein iRFP682 was tagged at the N-terminal of Smad2 (D). TM, transmembrane region.

The final design of the optoTGFβ system is shown in Figure 2.4.1. Each protein of the light-sensitive module, PHR-CIBN, is fused to cytoplasmic regions of each of the TGFβ receptor pair, TβRII-TβRI, generating optoTβRII (cytoTβRII-CRY2PHR-tdTomato) and optoTβRI (Myr-cytoTβRI-CIBN) (Figure 2.4.1 B-C), respectively. In addition, optoTβRI is attached to the plasma membrane, but optoTβRII is left floating around in the cytosol, and is tagged by an orange

fluorescent protein, tdTomato. This design could on the one hand, separate the chimeric receptors physically to avoid high level of basal TGFβ signaling activity, and on the other hand allow us to follow the association between the two chimeric receptors. Furthermore, Smad2 is tagged by a far-red fluorescent protein iRFP682, to report the activation of the TGFβ signaling (**Figure 2.4.1** D).

Theoretically, in the dark, both optoTβRII and the fluorescence labeled Smad2 are in the cytoplasmic region of the cells. Upon blue light stimulation, the association between the PHR-CIBN pair will bring optoTβRII to optoTβRI, which localizes on the plasma membrane. This will result in the translocation of optoTβRII from the cytoplasm to the plasma membrane, which could be observed under the microscopy via monitoring its FP tag. The association between the chimeric receptors facilitates the phosphorylation and activation of optoTβRI by optoTβRII. This will in turn initiate the TGFβ signaling transduction, indicated by the nuclear translocation of the FP-tagged Smad2. The active Smad2 then binds to target sites of the genome to regulate specific transcriptional activities.

This light induced activation is reversible. Once the blue light is turned off, the active PHR will reset to its inactive form in minutes and leave CIBN, resulting in optoTβRII returning to the cytoplasm, which is followed by the recovery of Smad2.

2.4.2 The establishment of cell lines expressing the optoTGFβ system

After classical molecular cloning and stable transfection of the plasmid encoding the chimeric receptor pair, pLNCX2-optoTβRs, most of the stably transduced cells showed membrane localization of optoTβRII even without light stimulation (**Figure 2.4.2** A). This might be due to the failure of separation at the P2A element of the constructed sequence. In the plasmid of pLNCX2-optoTβRs, a P2A element is inserted between the sequences of the optoTβRI and optoTβRII. Theoretically, optoTβRI and optoTβRII are transcribed to the same mRNA, which is translated before being cleaved at the P2A site into two individual proteins. However, failure of separation at the P2A element will lead to a consistent association between optoTβRI and optoTβRII, so that optoTβRII is always attached to the plasma membrane. Fortunately, there were a few colonies showing cytoplasmic localization of optoTβRII (**Figure 2.4.2** B). When irradiated by a short pulse of blue light (488nm), optoTβRII in these cells translocated to the plasma membrane immediately (**Figure 2.4.2** C). These cells, with the expected localizations of optoTβRII, were further transfected by the plasmid encoding the iRFP682-Smad2 protein.

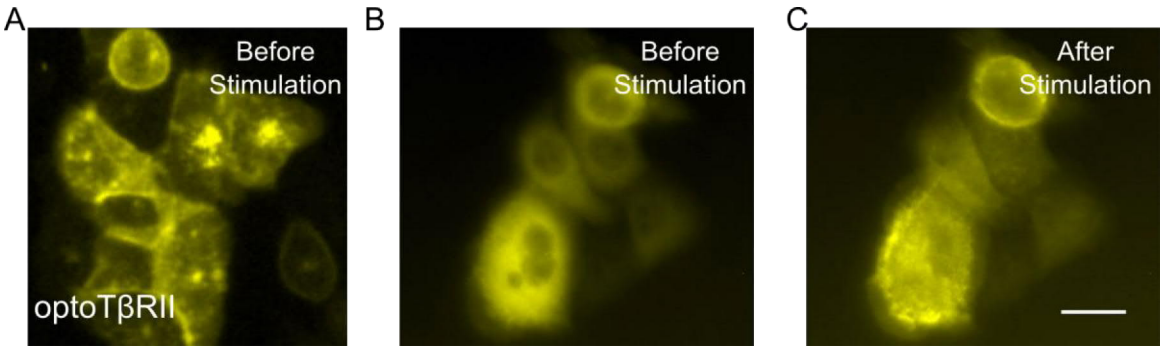

Figure 2.4.2 Different optoTβRII localization in cells stably transfected with the plasmid pLNCX2-optoTβRs. Scale bar: 25 μm. (A) Most cells transduced with pLNCX2-optoTβRs showed membrane localization of optoTβRII (shown as yellow) even without light stimulation. (B-C) A single colony showed cytoplasmic localization of optoTβRII before stimulation (B), and optoTβRII translocation to the plasma membrane in response to a short pulse of blue light stimulation (C).

In the end, we successfully established Hela and HaCaT cell lines that stably express the optoTGFβ system (optoHela and optoHaCaT, respectively). The expression of optoTβRI, optoTβRII and iRFP-Smad2 proteins in these cell lines were validated by immunoblotting experiments (**Figure 2.4.3**). The expression level of iRFP-Smad2 is consistent with the expression level of the endogenous Smad2. The expression level of optoTβRI is not as high as the endogenous TβRI (around half of the endogenous TβRI); however the optoTβRII is much more than the endogenous TβRII (around 4 fold of its endogenous counterpart). The inconsistence of expression levels between the light controllable chimeric TGFβ receptors and the endogenous TGFβ receptors might come from two factors: (1) the abundances of the endogenous TGFβ receptors in Hela cells differ widely (**Table 5.3-1**), which is also confirmed by some preliminary results in our lab; (2) according to the design of the plasmid pLNCX2-optoTβRs, the transcription of both optoTβRI and optoTβRII share the same mRNA and are linked by a P2A bicistronic linker sequence, therefore the mRNA ratio of optoTβRI and optoTβRII should be around 1:1. However, due to the longer sequence (thus harder to be translated) and larger conformation (thus harder to fold correctly) of the PHR domain, the expression level of optoTβRII is usually much lower than that of the optoTβRI[224]. Taken together, the expression difference between the chimeric optoTβRs pair is smaller than that of the endogenous receptor pair.

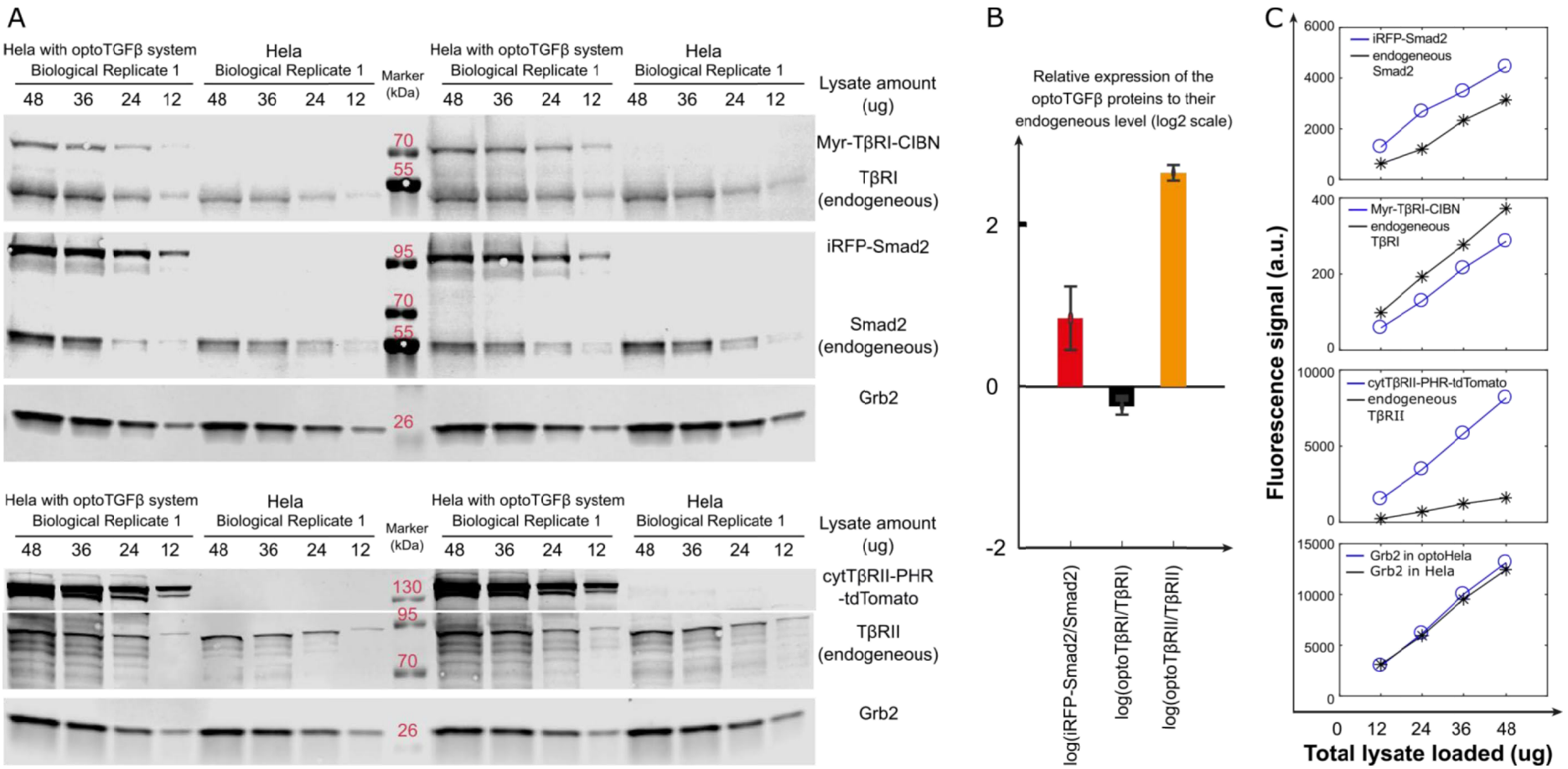

Figure 2.4.3 The expression of iRFP-Smad2, optoTβRI and optoTβRII proteins in the optoHela cells.

(A) Cell lysates were loaded in various amounts to optimize the range where antibody signal is linear. (B) The relative expression levels of iRFP-Smad2, optoTβRI and optoTβRII to the endogenous Smad2, TβRI and TβRII, respectively, were estimated from the averages of two biological replicates. (C) Linear relationships between the antibodies' fluorescence signal and the amount of lysate loaded, when measured with the LI-COR odyssey CLx imaging system.

3

Validation of the optoTGFβ System

After constructing the optoTGFβ system, we tried to characterize it in various aspects. First, we would like to make sure that TGFβ signaling in the optoTGFβ system could be triggered by light stimulation. As expected, upon blue light irradiation, plasma membrane translocation of optoTβRII and nuclear accumulation of Smad2 could be observed. In addition, the optoTGFβ system could also be activated by two-photon irradiation, which implies its deep-tissue application. Second, we would like to test if the light-induced TGFβ signaling could be blocked by receptor inhibitors. Since we didn't modify the components of the endogenous TGFβ signaling pathway, we'd like to check if the endogenous TGFβ signaling is intact. As expected, the light-induced Smad2 activation can be specifically blocked by the TGFβ receptor inhibitor LY364947, and TGFβ ligand could induce Smad2 activation in the light-sensitive cells. Third, besides the subcellular translocation property of the proteins, we also want to test if the light-activated Smad2 is indeed phosphorylated, and if the downstream target gene expression is also triggered by photoactivation. Moreover, we demonstrated that the blue light intensities we used in this study are not toxic to the cells.

3.1 The optoTGFβ system in response to blue light activation

To verify the functionality of the optoTGFβ system, we employed time-lapse microscopy to monitor the optoTGFβ system activation upon blue light stimulation. As expected, when illuminated with a short pulse of blue light (488 nm, 12.4 μW), optoHela cells showed plasma membrane or nuclear translocation of optoTβRII or iRFP-Smad2, respectively (**Figure 3.1.1** A). Quantification of the fluorescent signals in each channels was consistent with the observation (**Figure 3.1.1** B, C). This result confirms that blue light could activate the canonical TGFβ signaling in the optoTGFβ system.

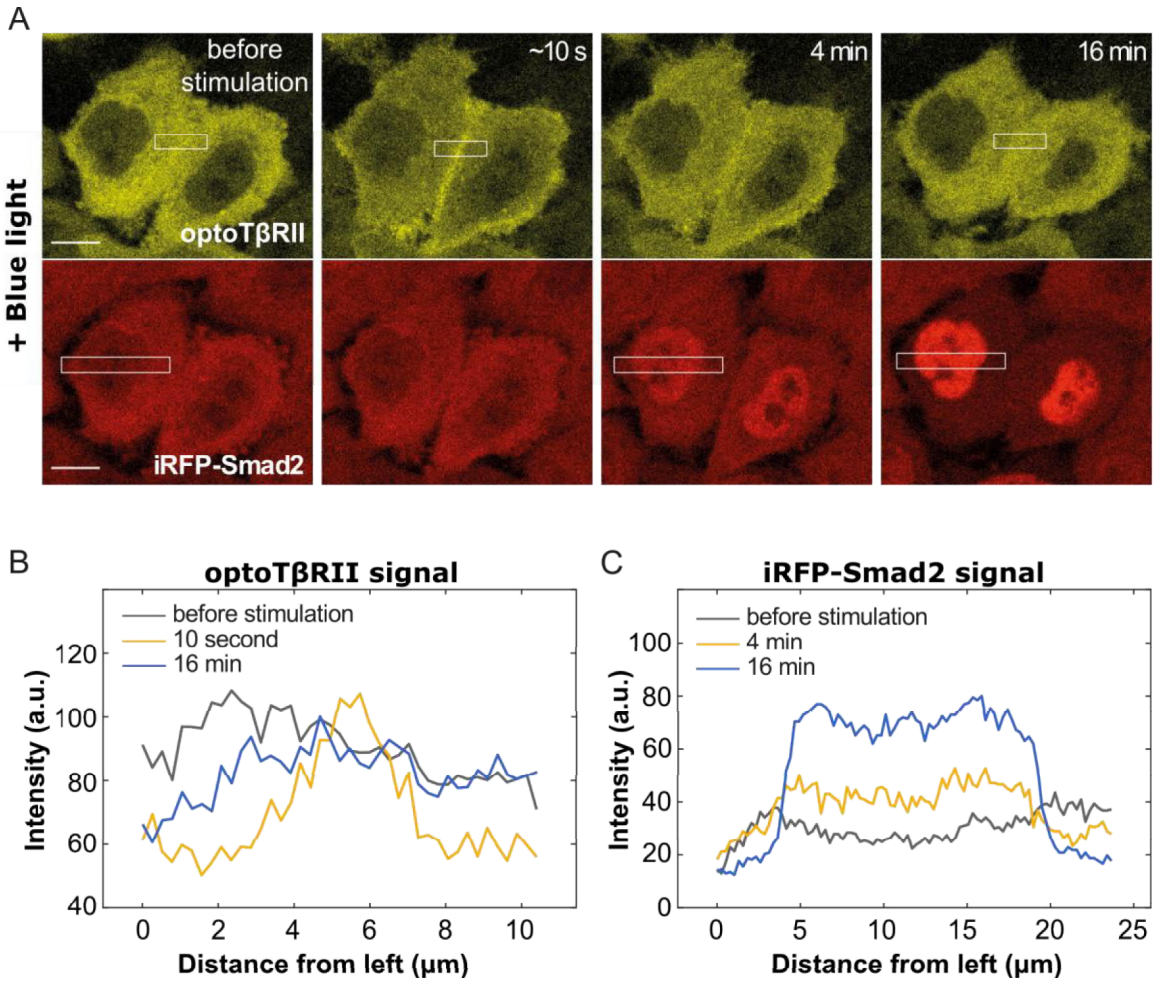

Figure 3.1.1 The optoTGFβs system: a light inducible switch to drive TGFβ/Smad signaling. (A) Representative fluorescent images of optoTβRII (cytoTβRII-PHR-tdTomato, yellow) and iRFP-Smad2 (red) in optoHela cells, stimulated by a short pulse of blue light (488nm; pixel dwell time, 6.3 μs). Scale bar: 10 μm. (B-C) The mean intensity level of optoTβRII (B) or iRPF-Smad2 (C) fluorescence signal within the respective white squares marked in panel A.

Upon a short pulse of blue light stimulation, most optoTβRII arrived at the plasma membrane in 10 seconds, and gradually recovered in 10 minutes in the dark. The observed fast turn-on and relatively slow turn-off kinetics of the optoTGFβ system are consistent with the association and dissociation rates of the PHR-CIBN system[170,215]. As the photon excitation on the confocal laser scanning microscopy could reach the scale of subcellular level, these results suggest that the optoTGFβ system allows us to control and investigate TGFβ signaling at the single cell level.

3.2 The optoTGFβ system in response to two-photon activation

The tissue penetration ability of blue light is poor, therefore it is very hard to access deep layer of cells in the tissue or thick specimens. This limits the use of blue light in experiments or applications that require deep penetration into living tissues or intact animal specimens. Multiphoton could overcome this limitation by using near-infrared excitation light to minimize scattering in the tissue, which enables not only dense living tissue penetration up to about one millimeter in depth, but also highly precise three-dimensional cell targeting. In addition, the lower-energy photons used in multiphoton experiments are less toxic, especially for those cells outside the focal volume[225-227].

Inspired by the work in which the PHR-CIBN module could be successfully activated by multi-photon stimulation[170], we tried to test if our optoTGFβ system could also respond to multi-photon activation or not. Using a chameleon laser with a power of 5.0 %, we found that Smad2 signaling could be triggered by several pulses of two-photon excitation at 860 nm (**Figure 3.2.1**). Compared with the blue light activation, the efficiency of multi-photon activation is much lower, as it needs longer illumination time for the same extent of Smad2 translocation. This is reasonable, as two-photon excitation only activates the light-sensitive proteins at the focal point or focal plane, the amount of proteins being activated during the multi-photon laser scanning process is far less than that by blue light stimulation.

The above experiments of multi-photon microscopy indicate that TGFβ signaling can be activated by two-photon excitation in the optoTGFβ system. This suggests that it is possible to precisely control TGFβ signaling in living organisms with the optoTGFβ system, which further implies its potential medical applications.

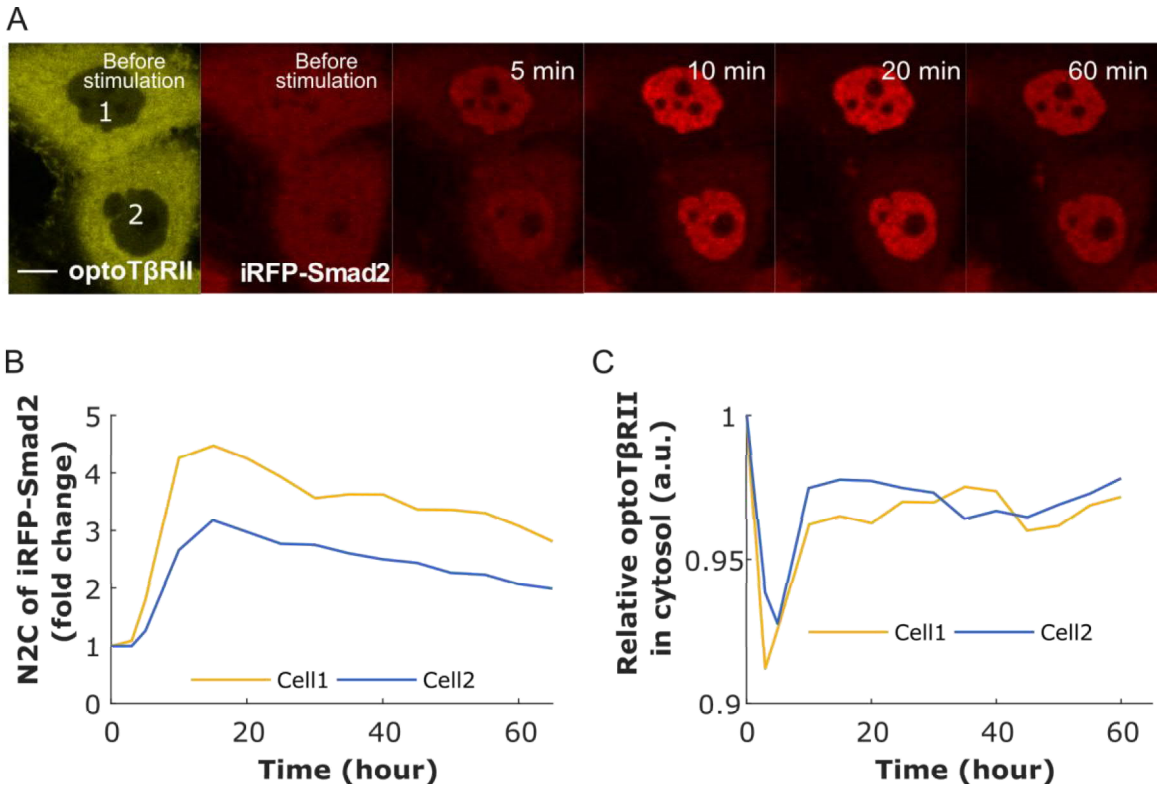

Figure 3.2.1 The optoTGFβs system can be activated by two-photon excitation. (A) Representative fluorescent images of optoTβRII (yellow) and iRFP-Smad2 (red) in optoHela cells, excited by two-photon irradiation (860 nm). Nuclear translocation of iRFP-Smad2 was observed. Scale bar: 10 μm. (B) Quantification of the nuclear iRFP-Smad2 (red signal) signaling dynamics in the two cells labeled in panel A. (C) Quantification of the redistribution dynamics of the corresponding optoTβRII signal.

The successful activation by both blue light and two-photon stimulation indicates that the optoTGFβ system allows us to manipulate and study the TGFβ signaling at the single cell level, and even potentially in vivo.

3.3 The optoTGFβ system activity could be affected by inhibitors and TGFβ ligand

LY364947 is a selective ATP-competitive, cell permeable inhibitor that blocks the kinase activity of both TβRI and TβRII[228]. As the cytoplasmic regions of both types of TGFβ receptors are retained in the optoTGFβ system, LY364947 should be able to inhibit the activity of both optoTβRI and optoTβRII. Indeed, when optoHela cells were cultured in the presence of LY364947, although blue light stimulation could still recruit optoTβRII to the plasma membrane through activating the PHR-CIBN module, iRFP-Smad2 did not translocate into the nucleus (**Figure 3.3.1** A). This is because the kinase activity of the chimeric

receptors was inhibited by LY364947 despite the receptor association, the receptors thus could no longer phosphorylate and activate Smad2. Therefore, the light-induced Smad2 activation of the optoTGFβ system can be specifically blocked by the selective inhibitor of TGFβ receptors (LY364947).

Because we left the endogenous TGFβ signaling components unchanged, the endogenous TGFβ receptors are intact in optoHela or optoHaCaT cells. Moreover, the endogenous and chimeric TGFβ receptors are independent of each other. Therefore, TGFβ ligand should be able to induce iRFP-Smad2 activation in these cells via the endogenous TGFβ receptors. Indeed, when optoHela cells were treated with TGFβ1 in the dark, iRFP-Smad2 was activated and translocated into the nucleus, in the absence of the membrane recruitment of optoTβRII (**Figure 3.3.1** B).

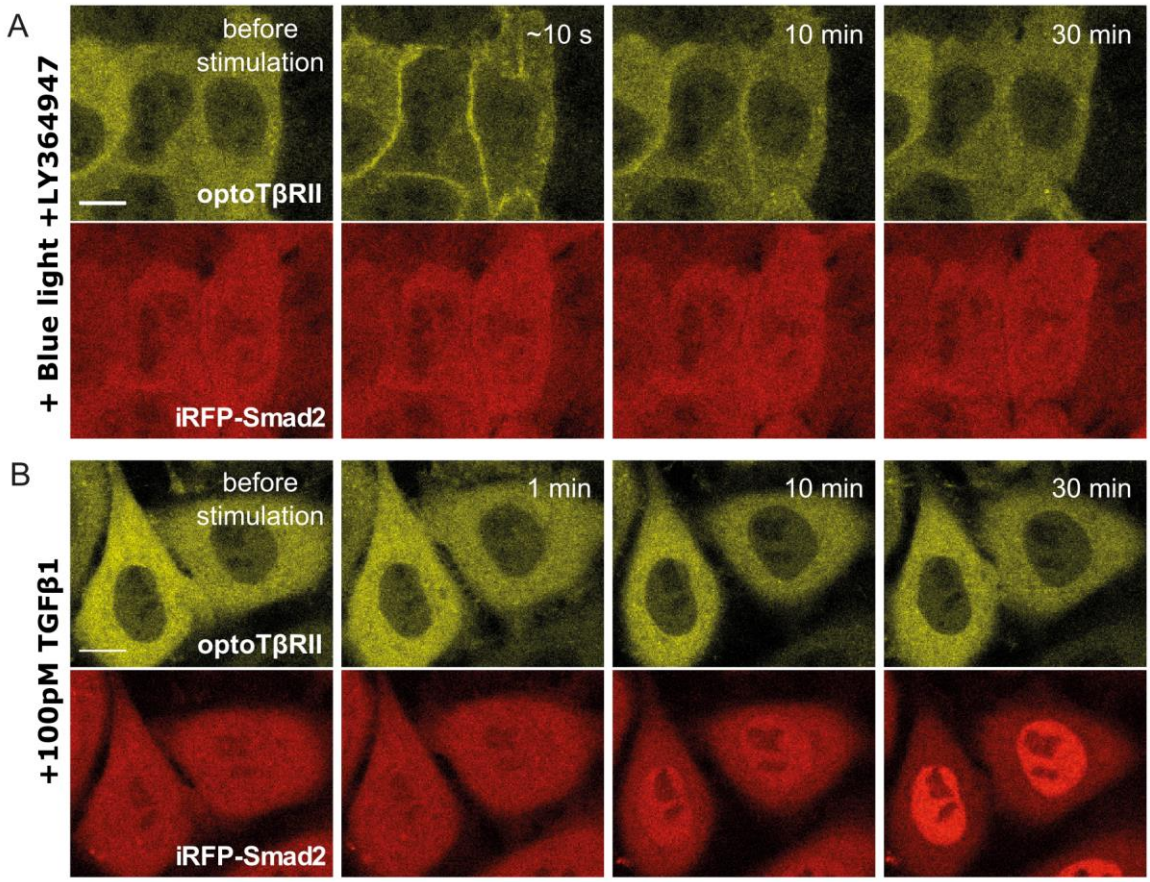

Figure 3.3.1 The responses of the optoTGFβ system to TGFβ receptor inhibitor and TGFβ ligand. Representative fluorescent images of optoTβRII (yellow) and iRFP-Smad2 (red) in optoHela cells. (A) In the presence of TGFβ receptor kinase inhibitor LY364947, Smad2 didn't translocate into nucleus, in spite of optoTβRII translocation induced by a short pulse of blue light (pixel dwell time, 6.3 μs). (B) Smad2 nuclear translocation in response to 100 pM TGFβ1 ligand stimulation, independent of optoTβRII activation. Scale bars: 10 μm.

3.4 Blue light stimulations used in this study are not phototoxic

Blue light could be phototoxic when used at high intensities. Therefore, it is necessary to make sure the blue light intensity for optoTGFβ activation is low enough not to interfere with other cellular processes than the controllable TGFβ signaling activation.

We employ both trypan blue staining and MTT assay to implement cell viability tests (**Figure 3.4.1**). In this experiment, both the un-transduced parental Hela cells and optoHela cells were irradiated in the 488nm LEDs illumination box (at the intensity of 0.8 mW/cm^2) for 24 hours. In parallel, a same set of cells were kept in the dark, which were used as controls. The p-values calculated through a two-sample t-test indicated that, there is no significant difference of cell viability between the cells under 488nm illumination and the control cells in the dark. As the light intensities used to stimulate the optoTGFβ system in this project are always below 0.8 mW/cm2 (the intensity used in these cell viability assays), we could conclude that the blue light stimulations used in this study are not phototoxic to cells either expressing or not expressing the optoTGFβ system.

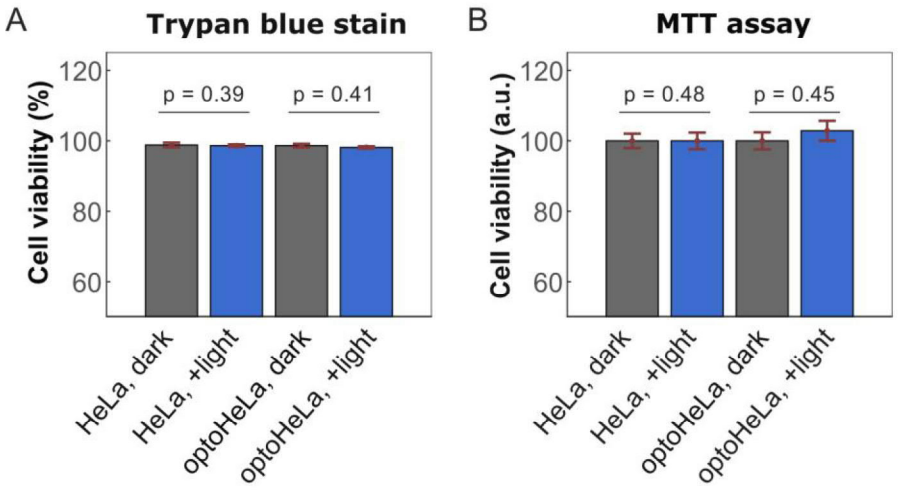

Figure 3.4.1 Cell viability assays for parental Hela cells and optoHela cells after 24 hours of blue light stimulation (488 nm, 0.8 mW/cm2). (A) results of the trypan blue stain assay, (B) results of the MTT cell viability assay. Error bars in (A) and (B) show the SEM (standard errors of the mean) from 6 and 16 replicates, respectively. The p-values were calculated using a 2-sample t-test.

3.5 Blue light induces Smad2 phosphorylation in the optoTGFβ system

In the results above, we observed the nuclear translocation of iRFP-Smad2 upon blue light stimulation, which implies the phosphorylation and activation of iRFP-Smad2 by the activated optoTβRs. To further confirm the functionality of the optoTGFβ system, we measured the phosphorylation levels of both the endogenous Smad2 and the transduced iRFP-Smad2 by western blotting experiments.

Upon 100pM of TGFβ1 ligand stimulation, the phosphorylation level of the endogenous Smad2 increases immediately, and reaches the maximum level in one hour, then gradually decreases. The time course of the endogenous Smad2 phosphorylation in optoHela cells is similar to that in the parental Hela cells (**Figure 3.5.1** A). This is confirmed by quantifying the relative P-Smad2 (phosphorylated Smad2) level on the western blotting images (**Figure 3.5.1** C). However, the phosphorylation dynamics of the chimeric iRFP-Smad2 lags slightly behind the endogenous one – while the endogenous P-Smad2 peaks at around one hour after adding TGFβ ligand, P-iRFP-Smad2 needs around two hours to reach its maximal level. The lower speed of iRFP-Smad2 phosphorylation could be explained by the decreased phosphorylation efficiency, which might be due to the conformational change of Smad2 by the fluorescent tag, or simply due to the larger molecular construction of the iRFP-Smad2 protein. It could also be explained merely by the effect of iRFP-Smad2 overexpression.

However, upon blue light stimulation, phosphorylation dynamics of iRFP-Smad2 and the endogenous Smad2 are similar and consistent. The phosphorylation levels are increased and sustained upon blue light activation, although the phosphorylation of iRFP-Smad2 peaks slightly later than that of the endogenous Smad2 (**Figure 3.5.1** B). Compared with the obvious difference between the endogenous Smad2 and iRFP-Smad2 dynamics in response to ligand stimulation, the smaller difference in the light stimulation experiments could be explained by the higher efficiency of light activation than ligand activation.

Moreover, concerning the long-term TGFβ signaling behavior, the phosphorylation levels of both Smad2s sustain at the maximal levels even after eight hours of illumination (**Figure 3.5.1** D), whereas they falls to around 50% of their maximal levels after eight hours of TGFβ ligand stimulation (**Figure 3.5.1** C). This might be related to the negative regulations that are not functional in the optoTGFβ system. For example, the conformations of the chimeric optoTβRs are different from that of their endogenous counterparts, which help the optoTβRs evade the negative regulation. All these observations of Smad2 phosphorylation are consistent with the dynamics of iRFP-Smad2 nuclear translocation recorded by time-lapse live cell imaging.

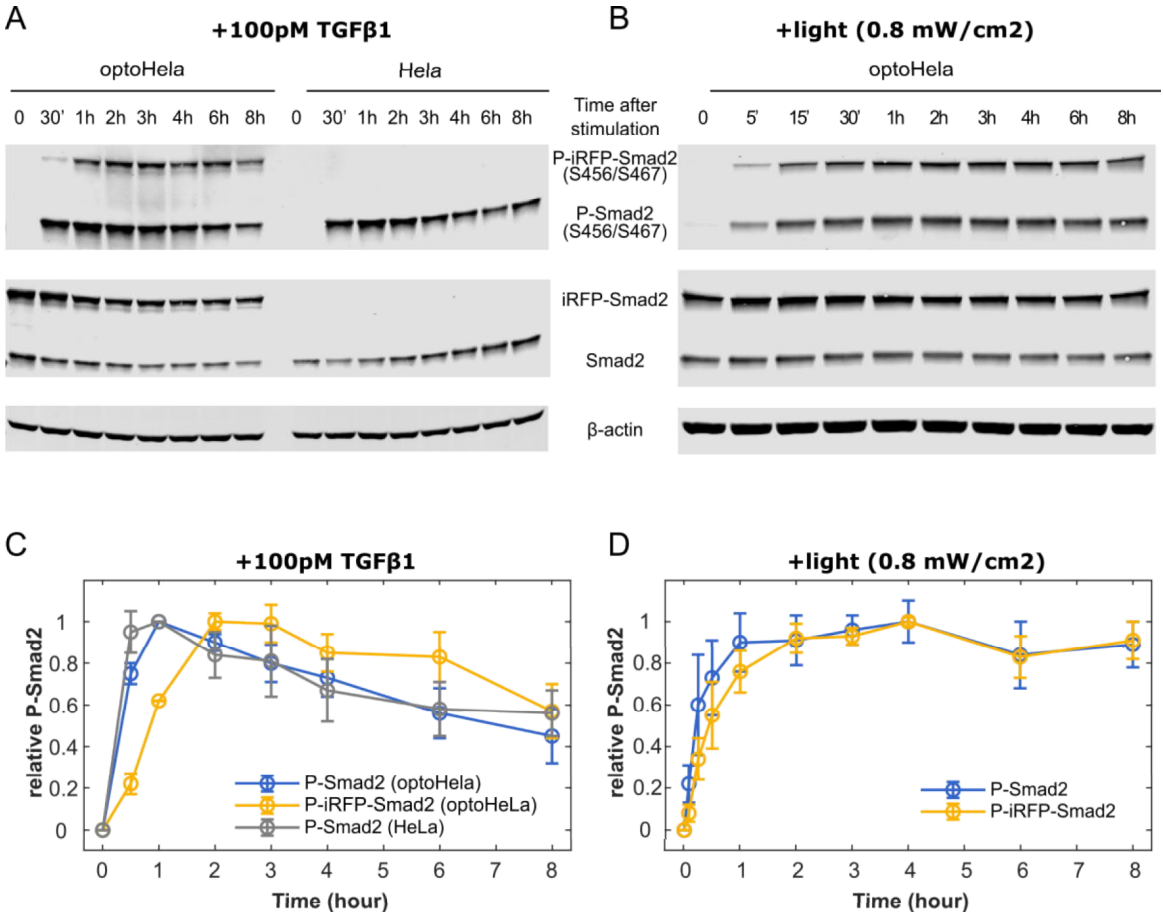

Figure 3.5.1 Time course data of Smad2 phosphorylation dynamics in response to ligand or light activation. (A) Representative western blots of P-Smad2 (phosphorylated Smad2) time course in response to 100 pM TGFβ1 ligand stimulation, in optoHela and Hela cells. (B) Representative western blots of P-Smad2 time course in response to continuous blue light irradiation (488 nm, 0.8 Mw/cm2) in optoHela cells. (C) Quantification of the bands shown in panel A. (D) Quantification of the bands shown in panel B. Relative P-Smad2 level was calculated as the ratio of P-Smad2 to the corresponding Smad2 signal. All the data were normalized by the maximal signal of each time course. Error bars show the standard deviations from three replicates.

In addition, phosphorylation of Smad2 upon various intensities of blue light stimulation is also tested. After setting the blue light of the LEDs illumination box to a specific intensity, optoHela cells were illuminated for 45 minutes before being subjected to immunoblotting analysis. Results showed that the phosphorylation levels of both the endogenous Smad2 and iRFP-Smad2 are consistent: they both increase gradually along with the increasing blue light intensity, but reach a plateau from the intensity of around 2 mW/cm2 (**Figure 3.5.2**). These results suggest that, with the optoTGFβ system, the amplitude of Smad2 activation could be fine-tuned by modulating the power of illumination.

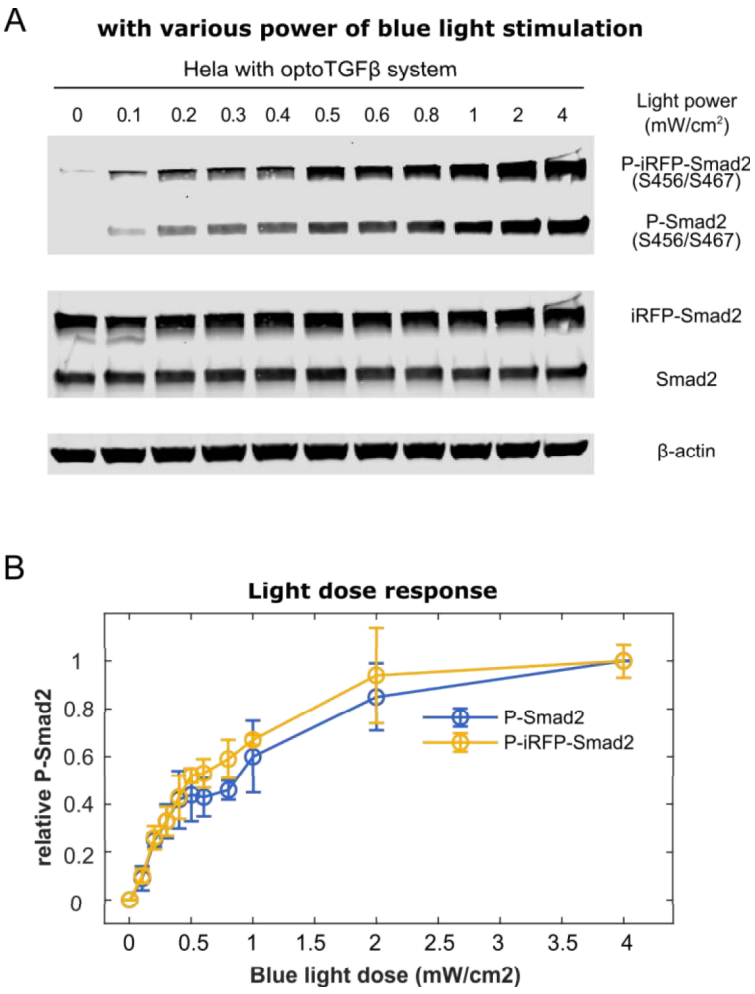

Figure 3.5.2 P-Smad2 responses upon various powers of blue light stimulations. (A) Representative western blots for Smad2 signals in optoHela cells upon various intensities of blue light (488nm) irradiation, samples were collected at 45 minutes after stimulation. (B) Quantification of the bands shown in panel A. Relative P-Smad2 level was calculated as the ratio of P-Smad2 to the corresponding Smad2 signal. All the data were normalized by the maximal signal of each time course. Error bars show the standard deviations from three replicates.

3.6 Blue light induces expression of downstream TGFβ responsive genes

Although the upstream TGFβ signaling (Smad2 phosphorylation and nuclear translocation) of the optoTGFβ system has been confirmed, its downstream gene expression activities still need to be evaluated. Here we chose Smad7[229], TMEPAI (Prostate Transmembrane Protein, Androgen Induced 1)[230], and PAI1 (Serpin Family E Member 1)[231] as representatives. We implemented qPCR (quantitative PCR) experiments to check their respective mRNA levels at various time-points after blue light stimulation (**Figure 3.6.1**). For both Hela and HaCaT cells expressing the optoTGFβ system, blue light can efficiently induce the expression of the three downstream TGFβ responsive genes.

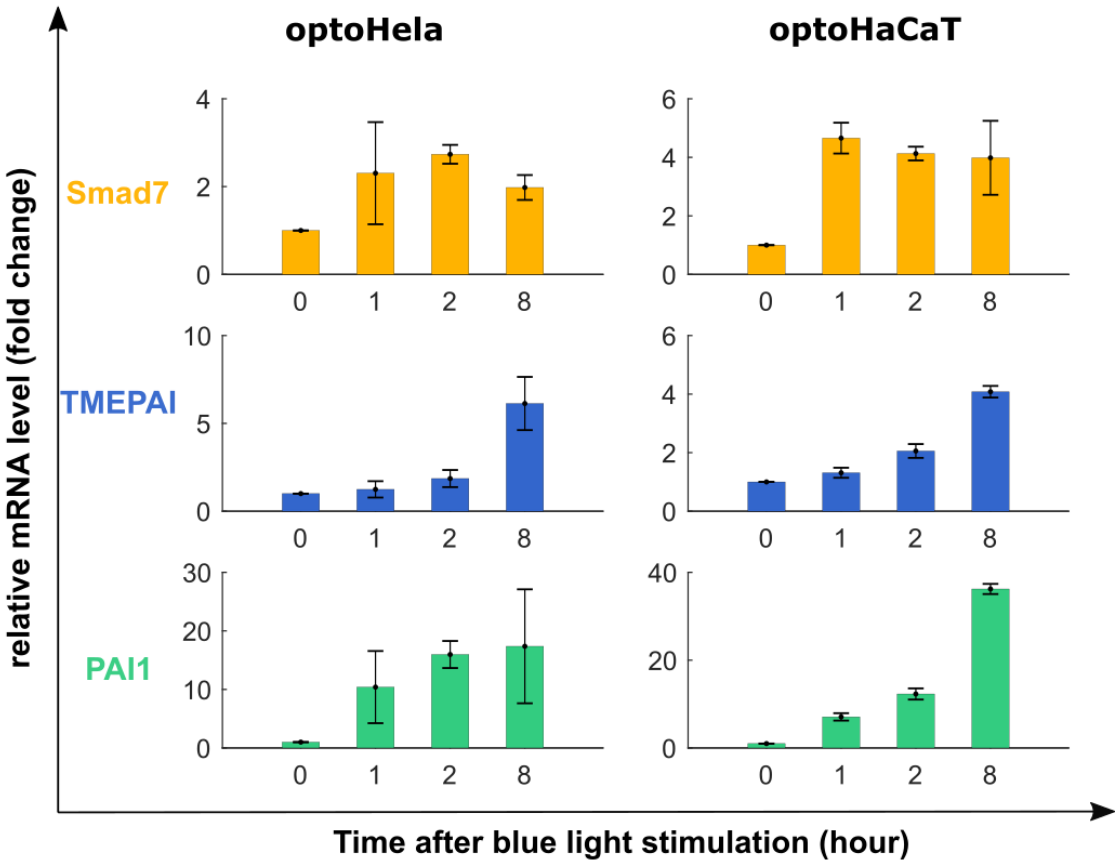

Figure 3.6.1 The optoTGFβ system can induce the expression of TGFβ responsive genes. Quantitative PCR assay for the expression of Smad7, TEMPAI and PAI1 genes in optoHela cells (left panels) and optoHaCaT cells (right panels) in response to blue light stimulation (488 nm, 4 mW/cm2). Samples were collected at 0, 1, 2 and 8 hours after blue light irradiation in the LEDs box. The averages and standard deviations calculated from three replicates were plotted.

4

Control of TGFβ Signaling by the optoTGFβ System

After characterizing the optoTGFβ system, in this chapter, we tried to quantitatively control the TGFβ signaling through manipulating blue light input for activating the optoTGFβ system. First, we would like to test the spatiotemporal controllability in the optoTGFβ system. We demonstrated that the optoTGFβ system enabled control of TGFβ signaling in single cells at high spatial and temporal resolution. Second, we would like to know if we can harness TGFβ signaling, and generate complex TGFβ signaling dynamics through manipulating the light input. As expected, by applying light stimulations of single pulse, frequent pulses and sparsely separated pulses, we generated transient, sustained and oscillated Smad2 signaling, respectively. Third, we made comparisons between light stimulation and ligand stimulation, in terms of the Smad2 signaling activation dynamics. We found that with the optoTGFβ system, we could generate similar Smad2 dynamics by manipulating the light input, mimicking the patterns of ligand stimulation. Further than that, the optoTGFβ system expands the range of Smad2 activation by its ability to induce stronger Smad2 activation.

4.1 Control of TGFβ Signaling in Time and Space

In comparison with ligand stimulation, one of the largest advantages of light stimulation is the spatiotemporal control of stimulation at relatively high resolution. Since the laser beam on the confocal laser scanning microscopy could achieve high precision (i.e., at the subcellular level), the stimulation of the optoTGFβ system could be limited to specific single cells. In theory, only the light-sensitive proteins that are illuminated should be activated, hence only the portion of optoTβRII that is hit by the laser beam would undergo plasma membrane recruitment. Therefore, if we stimulate only one designate cell at a time, then only the optoTβRII proteins in this specific cell would translocate onto the plasma membrane and trigger the initiation of TGFβ signaling. In contrast, TGFβ signaling in other surrounding cells should stay inactive: no plasma membrane translocation of optoTβRII, and no nuclear translocation of iRFP-Smad2, or the endogenous Smad2.

To demonstrate the spatiotemporal control property of the optoTGFβ system, we implemented sequential light stimulation, and restricted the irradiation region to be in one specific cell by using a confocal laser scanning microscopy. At different time points (every 15 minutes), we irradiated one specific optoHela cell with a short pulse of blue light, while the surrounding cells were kept in dark (**Figure 4.1.1**). At time point 0 min, when we stimulated only the cell labeled as 'cell1', only the iRFP-Smad2 in this specific cell was activated and started to translocate from the cytosol into the nucleus in the following several minutes (**Figure 4.1.1** A, upper row). At time point 15 min, we similarly stimulated the cell labeled as 'cell2' and kept all the other cells in dark, only cell2 showed nuclear translocation of iRFP-Smad2 following this stimulation (**Figure 4.1.1** A, middle row). We did the same stimulation to cell3 at time point 30min, and then observed its specific activation (**Figure 4.1.1** A, lower row). During the whole experiment, cell4 and cell5 stayed in the dark and thus never had been activated, hence the distribution of iRFP-Smad2 in these two cells stayed the same. Quantification of the iRFP-Smad2 nuclear translocation (**Figure 4.1.1** C) in each of the five cells confirms that Smad2 signaling was activated in each cell sequentially, in accordance with the same sequence of the pulsed blue light stimulation (**Figure 4.1.1** B). This result suggests that it is possible to control the TGFβ signaling activation in single cells at high spatial and temporal resolution using the optoTGFβ system.

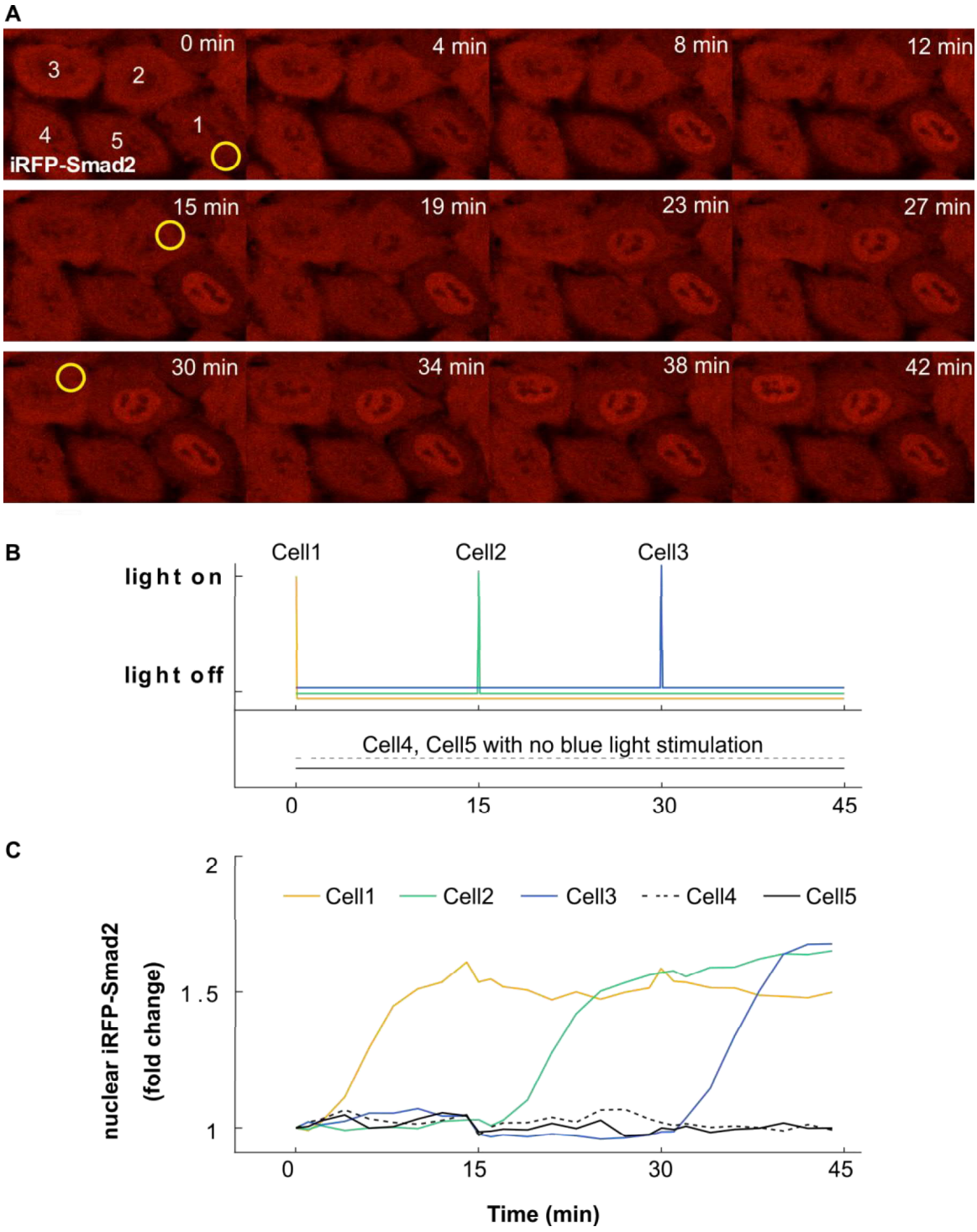

Figure 4.1.1 Spatiotemporal control of Smad2 signaling in optoHela cells. (A) One short pulse of blue light (488 nm, 12.4 μW, pixel dwell time: 100 μs) was used to sequentially stimulate the yellow circular region of cell 1, cell 2 and cell 3 at 0 min, 15 min and 30 min, respectively. Representative fluorescent images of iRFP-Smad2 in optoHela cells showed specific and sequential nuclear Smad2 accumulation. (B) Schematic representation of the light stimulations for the cells marked in panel A. (C) Quantification of the nuclear Smad2 signaling dynamics of the cells labeled in panel A. Scale bar: 10 μm.

4.2 Generating complex Smad2 signaling dynamics

Compared with ligand stimulation, another advantageous property of light stimulation is enabling us to manipulate the pattern of input conveniently, and avoid medium change. Furthermore, with the optoTGFβ system, we could simultaneously monitor signaling dynamics of both optoTβRs and Smad2 in response to various light irradiation patterns.

First, we implemented a single pulse stimulation (**Figure 4.2.1** B). We stimulated the optoHela cells with a very short pulse of blue light (pixel dwell time: 3.15 μs/pixel, which is the time the focused laser dwells on each pixel). As shown both by video observation (**Figure 4.2.1** A, yellow channel) and by image quantification (**Figure 4.2.1** D), upon light irradiation, optoTβRII was immediately depleted from the cytosol, recruited to the plasma membrane, reaching the maximal extend of recruitment within seconds. After that, optoTβRII dissociated from the plasma membrane-localized optoTβRI and gradually returned to the cytoplasm, recovering to its pre-stimulation level within 15 min. In contrast, the Smad2 activation and deactivation processes were much slower. It took minutes for the Smad2 nuclear translocation to arrive its maximal level, and took hours for its recovery (**Figure 4.2.1** A, red channel; **Figure 4.2.1** C). Notably, although the amplitude of Smad2 signaling varies among individual cells, the peaking time of Smad2 nuclear accumulation is very robust, at about 20 min after the exposure to the short pulse of blue light. The deactivation of Smad2 was also much slower than the recovery of cytoplasmic optoTβRII signal. However, it is consistent with the relatively slow dynamical property of the Smad2 nuclear-cytoplasmic shuttling process[133]. These results also suggest that the dynamics of Smad2 signaling and TGFβ receptors activations occur on different time scales.

As there is a delay of around 90 minutes between the Smad2 deactivation and the TGFβ receptors complex dissociation, we speculate that this delay feature would enable the TGFβ signaling pathway to remember the previous input signal and sustain the signaling for a short time. In this way, the TGFβ signaling could filter out input signal changes at high frequencies. To test this hypothesis, we monitored the TGFβ signaling dynamics in optoHela cells upon repeated pulses of blue light stimulation at high or low frequencies.

When the cells were stimulated every 10 minutes (**Figure 4.2.2** B), which is a period that is much shorter than the delay time between the receptors deactivation and the Smad2 deactivation, the Smad2 signaling showed a sustained response (**Figure 4.2.2** A, red channel; **Figure 4.2.2** C). Notably, the maximal level of Smad2 nuclear translocation in this experiment is generally much higher than that in single pulse stimulation experiments, and the time for peaking is also longer (around two hours after the first pulse of stimulation). This

is justified, as a single pulse doesn't provide sufficient energy for a saturate Smad2 signaling, the effect of multiple pulses would accumulate until the saturation of signaling. Furthermore, as the phosphorylation level of Smad2 is correlated with the intensity of light input (**Figure 3.5.2**), the peaking time could vary depending on the total amount of light per unit of time a cell receives, i.e., the more intensive the illumination, the faster the Smad2 signaling would peak.

As expected, when the cells were stimulated with pulsed light at a low frequency (**Figure 4.2.3** B), an oscillated transient Smad2 signaling response was observed (**Figure 4.2.3** A， red channel; **Figure 4.2.3** C). As the activation of the light-sensitive module is reversible, the optoTβRII recruitment dynamics also showed an oscillated pattern (**Figure 4.2.3** A, yellow channel; **Figure 4.2.3** D). The period of Smad2 activation oscillation is in accordance with the period of input light pulses. Therefore, it is beyond dispute that we could generate other Smad2 oscillations by manipulating the stimulation patterns, i.e., varying the frequency of input light pulses.

In addition, it should be noted that, we did not implement continuous stimulation by live cell imaging. This is due to the nature of the laser scanning process of confocal microscopy, which operates on one single pixel at a time. Therefore it is in theory impossible to stimulate the entire image region simultaneously and continuously. However, as the continuous stimulation falls in the regime of highly frequent pulsed stimulation, the Smad2 signaling dynamics in response to continuous light stimulation should show a sustained response pattern, similar to the above response upon pulsed stimulation in high frequencies (**Figure 4.2.2**).

Furthermore, depending on the dynamical properties of the downstream TGFβ responsive gene expressions, various patterns of TGFβ responsive transcription dynamics could also be generated by manipulate the light irradiation input. Cellular response in single cells could thus be adjusted accordingly.

In summary, with the optoTGFβ system, we can easily generate three categories of Smad2 signaling dynamics: transient, sustained or oscillated, by modulating the patterns of blue light inputs. Moreover, by integrating these plentiful input patterns, we could further design more sophisticate light input patterns, and thus generate a variety of more complex Smad2 signaling dynamics, as well as a variety of TGFβ responsive gene expression dynamics. TGFβ signaling could therefore be better investigated, and the TGFβ signaling could also be better controlled in therapeutic applications.

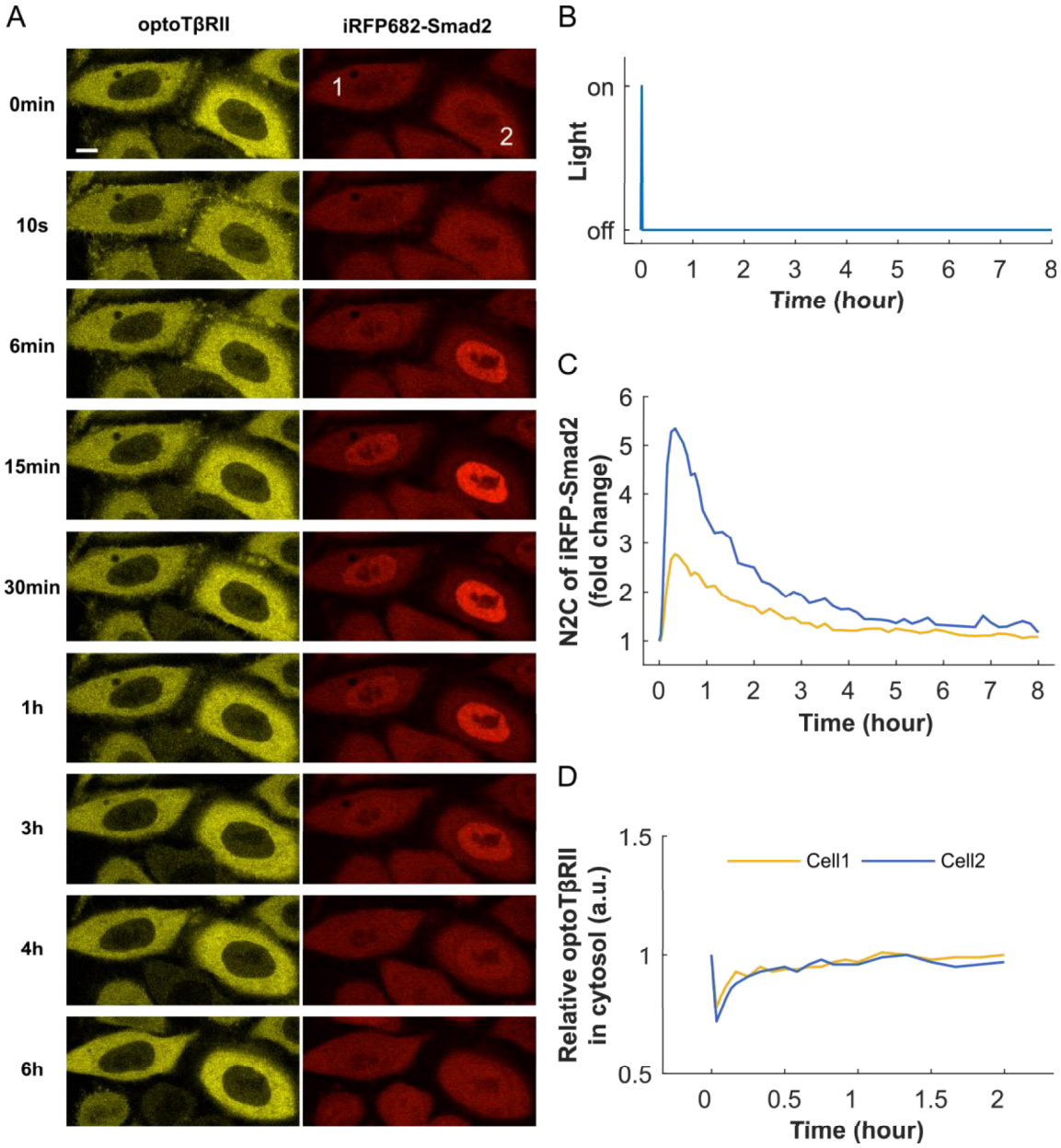

Figure 4.2.1 Dynamics of Smad2 signaling upon one short pulse of blue light irradiation in the optoTGFβ system. (A) Representative fluorescent images of optoTβRII (yellow) and iRFP-Smad2 (red) in optoHela cells in response to a pulse of 488nm light irradiation. Light power for the pulse: 12.4 μW. Pixel dwell time: 3.15 μs. Scale bar: 10 μm. (B) Input pattern of the blue light stimulation. (C) Quantification of the nuclear Smad2 signaling dynamics in the cells labeled in panel A. (D) Quantification of the optoTβRII signaling dynamics shown in the cells labeled in panel A.

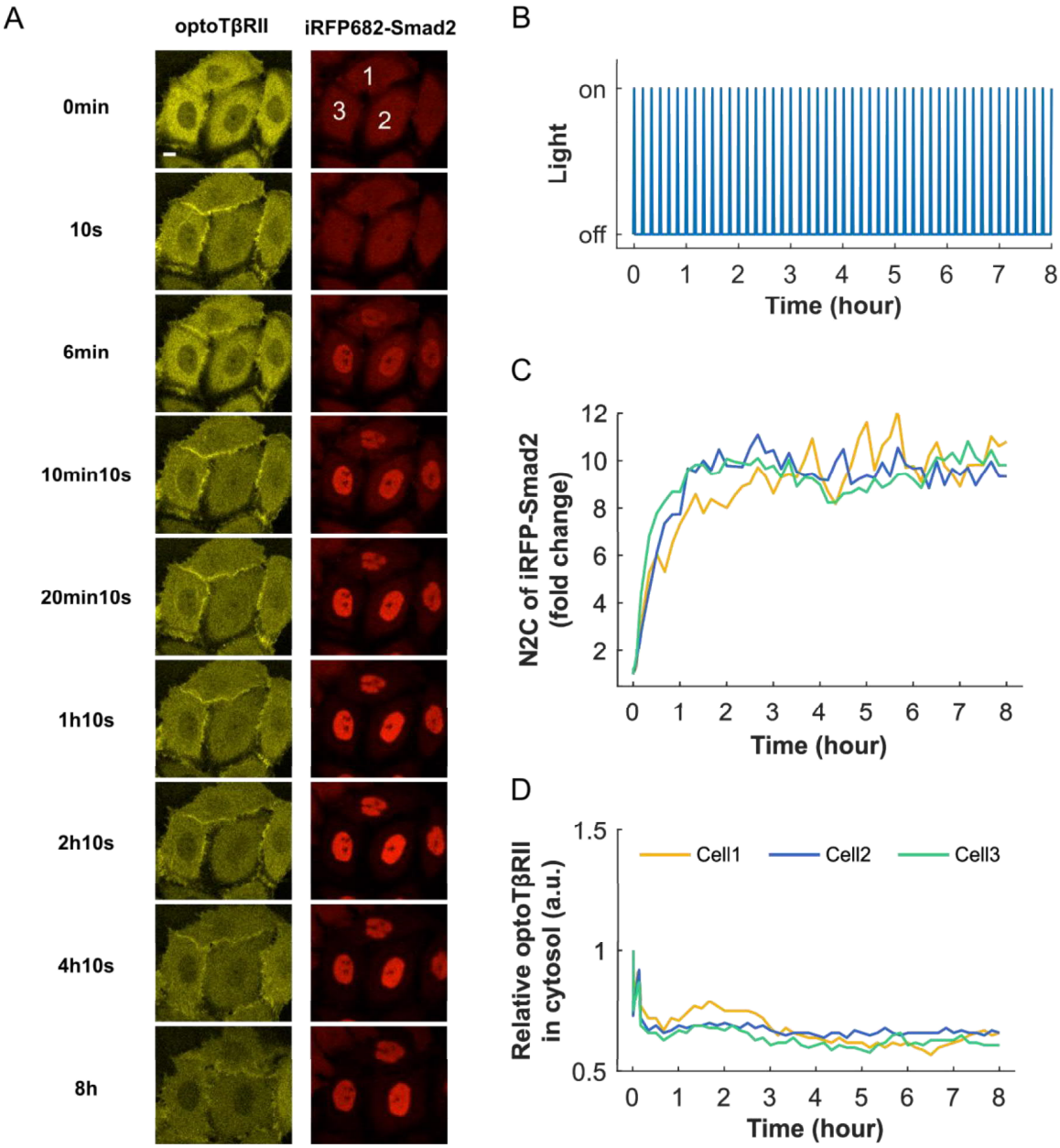

Figure 4.2.2 Dynamics of Smad2 signaling upon a highly frequent pulsed irradiation in the optoTGFβ system. (A) Representative fluorescent images of optoTβRII (yellow) and iRFP-Smad2 (red) in optoHela cells in response to repeated pulses of 488nm light stimulation. Scale bar: 10 μm. Period of the pulses: 10 minutes. Light power for each pulse: 12.4 μW. Pixel dwell time: 3.15 μs. (B) Input pattern of the blue light stimulation. (C) Quantification of the nuclear Smad2 signaling dynamics in the cells labeled in panel A. (D) Quantification of the optoTβRII signaling dynamics shown in the cells labeled in panel A.

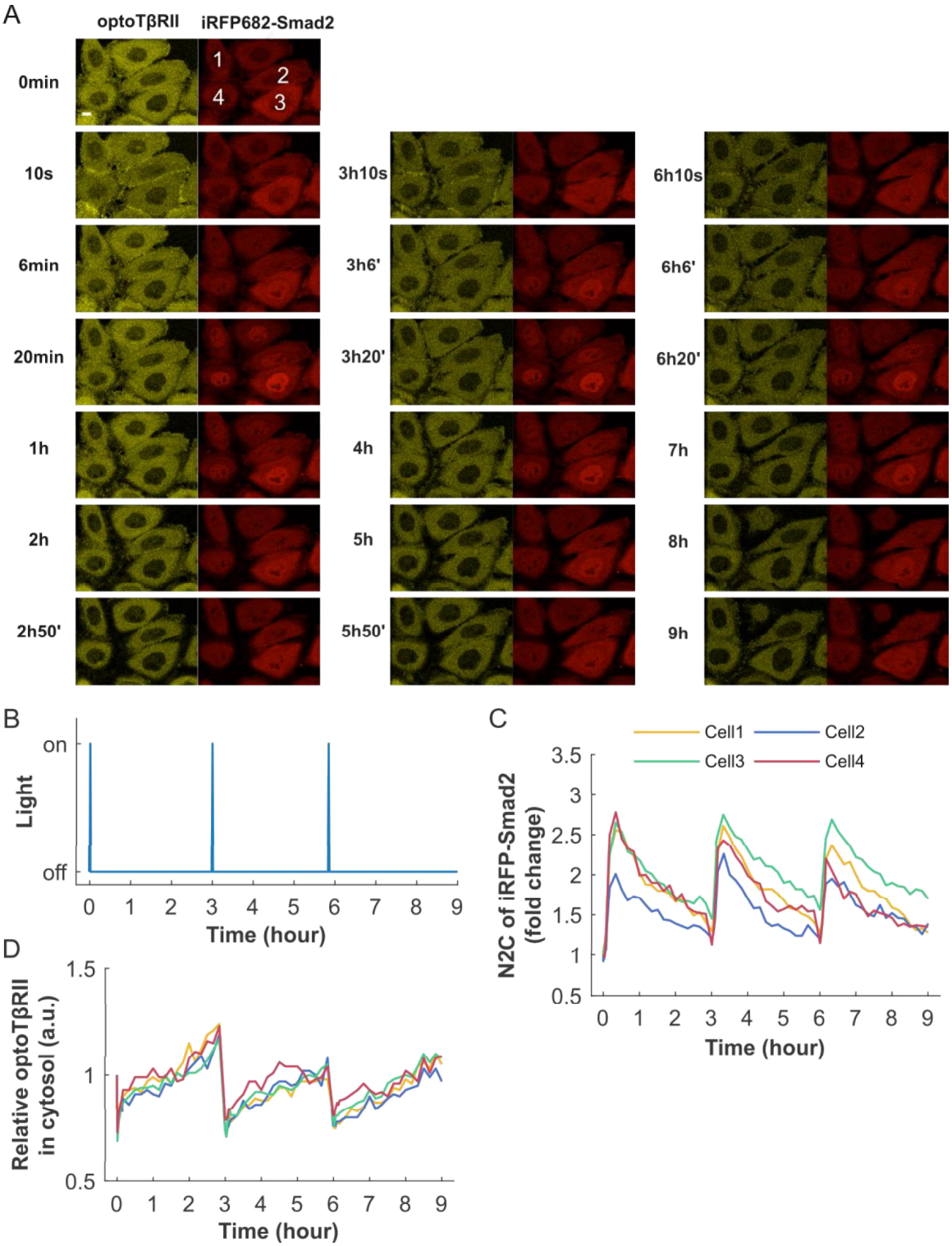

Figure 4.2.3 Dynamics of Smad2 signaling upon a low frequent pulsed irradiation in the optoTGFβ system. (A) Representative fluorescent images of optoTβRII (yellow) and iRFP-Smad2 (red) in optoHela cells in response to 3 pulses of 488nm light stimulation. Scale bar: 10 μm. Period of the pulses: 3 hours. Light power for each pulse: 12.4 μW. Pixel dwell time: 3.15 μs. (B) Input pattern of the stimulation. (C-D) Quantification of the nuclear Smad2 signaling dynamics (C) or the optoTβRII signaling dynamics (D) in the cells labeled in panel A.

4.3 Smad2 signaling upon light vs. ligand stimulation

4.3.1 Similar signaling dynamics upon similar patterns of stimulation

Although both blue light and TGFβ ligand could induce Smad2 signaling, we still need to check whether blue light stimulation mimics similar TGFβ ligand stimulation for Smad2 signaling activation, i.e., we would like to know whether the Smad2 signaling dynamics upon the two different kinds of stimulations are similar when the input patterns are similar. Here we planned to check the Smad2 signaling in response to both kinds of stimulations in three types of input patterns: single pulse, frequent pulses and infrequent pulses.

For results of TGFβ ligand stimulation, due to the necessity of double medium changes for every pulsed stimulation, it is very inconvenient to implement pulsed ligand stimulation, especially for pulses at high frequencies. Therefore, here we tried to use a published mathematical model to predict the Smad2 signaling in response to the three patterns of TGFβ stimulations: single pulse, pulses with a period of 10 minutes, and pulses with a period of 3 hours (**Figure 4.3.1** A-C, upper panels). The Smad2 dynamics are predicted to be transient, sustained and oscillated with a period of 3 hours, respectively (**Figure 4.3.1** A-C, lower panels).

For results of blue light stimulation, through time-lapse live cell imaging, we stimulated optoHela cells with the three patterns of light input: one single pulse, one pulse in every 10 minutes, and one pulse in every 3 hours (**Figure 4.3.1** D-F, upper panels). The iRFP-Smad2 signaling dynamic responses in dozens of individual cells were recorded and quantified subsequently.

Despite the variations of Smad2 signaling among individual cells in response to the same blue light stimulation, the Smad2 signaling dynamics in optoHela cells showed transient, sustained or oscillated responses upon light stimulation patterns of single pulse, frequent pulses or infrequent pulses, respectively (**Figure 4.3.1** D-F, lower panels). These results are consistent with the Smad2 dynamic responses upon the corresponding input patterns of TGFβ ligand stimulation, which were experimentally measured or theoretically predicted at the population level (**Figure 4.3.1** A-C, lower panels) [136,232,233]. Therefore, with similar stimulation input pattern, light and ligand induce similar dynamics of Smad2 signaling responses.

We therefore conclude that similar patterns of light stimulation or TGFβ ligand stimulation would induce similar dynamics of Smad2 signaling activations.

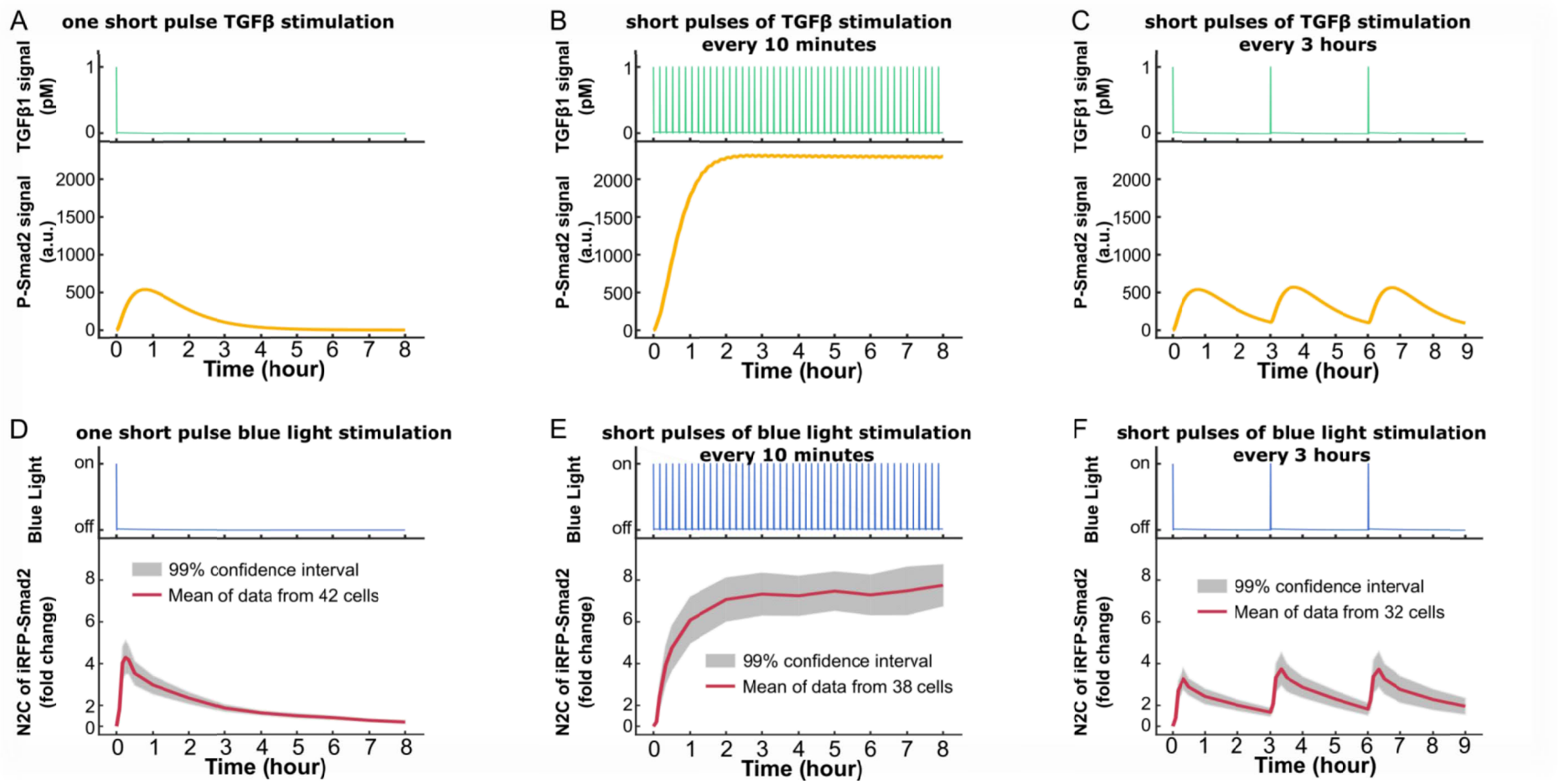

Figure 4.3.1 Dynamics of Smad2 signaling in response to pulses of TGFβ or blue light stimulations.

(A-C) Predicted dynamics of P-Smad2 response upon different TGFβ stimulations using a published mathematical model[136]. (D-F) Quantification of Smad2 signaling is response to similar patterns of blue light stimulations in optoHela cells. The 99% confidence interval is based on Student's t-distribution.

4.3.2 The optoTβRs could induce stronger Smad2 signaling

Despite the fact that the static cellular structures encode substantial information about biological functions, more and more studies suggest that biological information is also encoded in another dimension: dynamics of signaling over time[216]. The dynamics of signaling is the pattern of signal changes over time, and the 'signal' could be any aspect, such as molecular concentration, chemical modification, and translocation, etc[217]. Examples for the measurable features of signaling dynamics are: delay (the duration from the stimulation until the onset of activation), duration of activation, duration of peak retention, duration of deactivation, cumulative level, amplitude and frequency, etc. (**Figure 4.3.2**). Needless to say, these temporal codes enormously extend the complexity of the cellular information. Therefore, decoding and controlling the dynamics of signaling are important for investigating and modulating the related cellular functions.

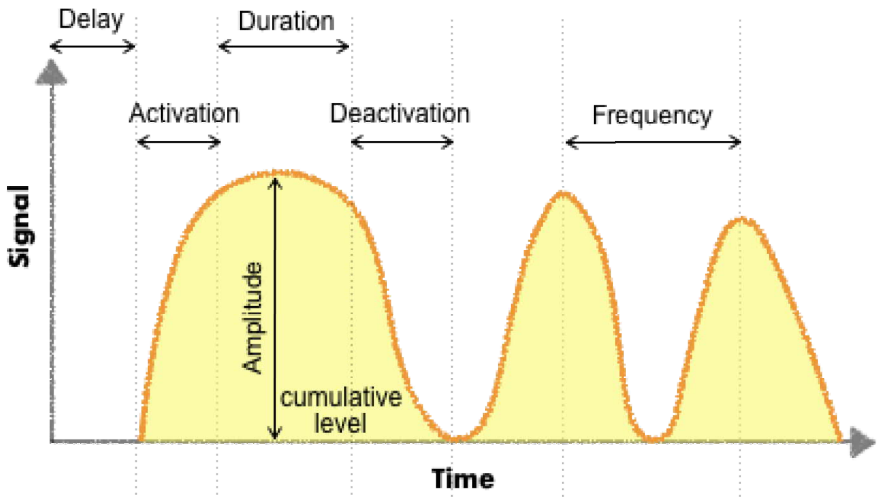

Figure 4.3.2 Illustration for some measureable features of signaling dynamics. Delay is the duration from the stimulation until the onset of activation; Activation is the duration between the onset of activation and the time when reaching the maximal level; Duration is the time range of peak retention; Deactivation is the duration of signal decreasing; Amplitude is the maximal level of activation a signal could reach; Frequency is the duration between consecutive peaking time; cumulative level is the total accumulated signal, i.e., the area under the curve of signal dynamics.

In this study, cells expressing the optoTGFβ system contain two versions of TGFβ receptor pairs: one is the endogenous pair, which responds to TGFβ ligands in the surrounding medium; the other is the chimeric optoTβRs pair, which responds exclusively to blue light irradiation. Though both of these two receptor pairs induce similar downstream signaling transmission pathways, when discerning carefully, we could find that there exist differences between the dynamics induced by TGFβ ligand and that by blue light, even for similar

patterns of stimulation input. Upon blue light stimulation, most of the Smad2 could translocate into the nucleus (**Figure 4.3.3** B). In contrast, there were still observable traces of Smad2 remaining in the cytosol at the maximal level of response (~ 60 minutes after stimulation), even though the cells are treated with a saturating dose (100 pM) of TGFβ ligand (**Figure 4.3.3** A) [136,234]. Quantification confirms this observation. While the nuclear-to-cytoplasmic (N2C) ratio of iRFP-Smad2 upon blue light stimulation could reach higher than 10, it was less than 4 in the case of ligand stimulation (**Figure 4.3.3** D). In addition, when checking the raw data, intensities of the cells in this experiment were at the same scale (**Figure 4.3.3** C), which means the abundances of iRFP-Smad2 in the representative cells were similar and thus comparable. These results suggest that blue light could induce stronger Smad2 nuclear translocation.

Besides the difference of amplitude, the speed of activation, i.e. the time needed to peak the activation is also different between TGFβ ligand and blue light stimulation. While in response to blue light stimulation, iRFP-Smad2 could translocate to the maximal extend in less than 20 minutes, the peaking time of iFRP-Smad2 translocation upon TGFβ ligand stimulation was around one hour. And there was still a large amount of iRFP-Smad2 in the cytoplasmic region 15 minutes after adding a saturating dose of TGFβ ligand (**Figure 4.3.3** A, left panels). Therefore, blue light could induce faster Smad2 activation.

These differences might be resulted from the different molecular regulations on the specific responsive receptor pair, which is in turn determined by its specific molecular mechanism. For example, negative feedback regulations might have different impacts on the endogenous and light-controllable TGFβ signaling. In the endogenous system, TGFβ ligand binds to TβRII which then recruits and phosphorylates TβRI, the activated TβRI then activates Smads. During this time, the negative feedbacks gradually build up and act on receptors or Smads to maintain the signaling at a certain level. However, in the optoTGFβ system, light induces a much faster reaction of receptor binding and activation, which immediately activates Smad2 to a higher extent before the negative regulations are building up. In addition, due to the chimeric structures of optoTβRs, negative feedbacks regulating the endogenous TβRs might fail to regulate optoTβRs. Therefore the TGFβ signaling could reach a higher level in the optoTGFβ system.

On the one hand, the stronger Smad2 signaling induced in the optoTGFβ system in turn reveals the effects of negative regulations in the endogenous TGFβ signaling. On the other hand, due to the convenient control of the optoTGFβ system, it is easy to generate any TGFβ signaling dynamics that the TGFβ ligand could trigger, through adjusting the input light intensity or stimulation pattern. Therefore, the optoTGFβ system provides a wider range of signaling activation, which we could apply to modulate TGFβ signaling in specific cells.

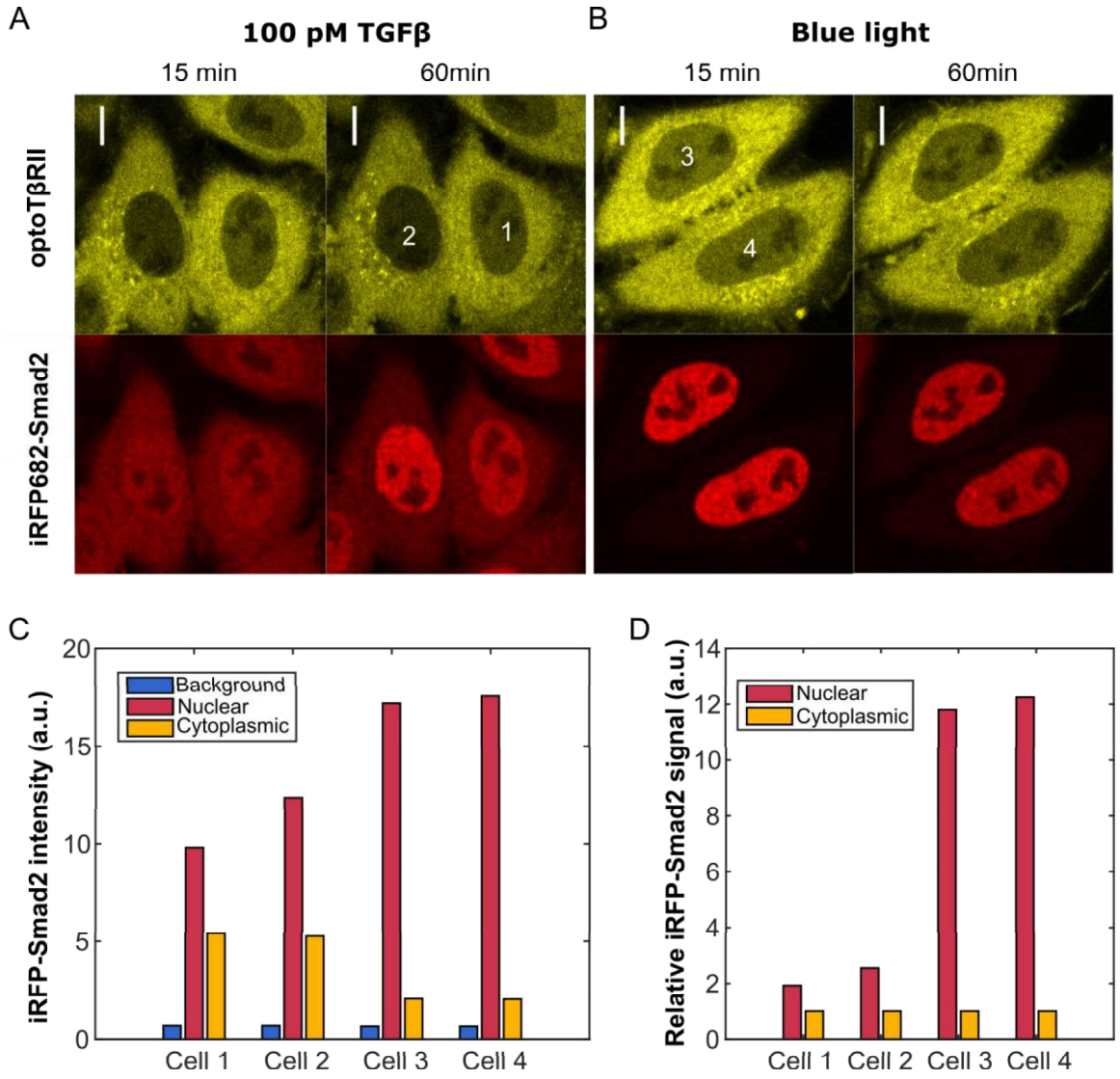

Figure 4.3.3 optoTβRs could induce stronger Smad2 signaling. optoHela cells were stimulated by 100pM TGFβ (Cell1 and Cell2), or illuminated by a single pulse of blue light (Cell3 and Cell4; light: 488 nm, 12.4 μW, with pixel dwell time of 3.15 μs). Representative image of iRFP-Smad2 localization after 15 minutes, 1 hour of TGFβ stimulation (A) or a pulse of blue light stimulation (B). Yellow signal: optoTβRII; red signal: iRFP-Smad2. Scale bar: 10 μm. (C) Quantification of the mean iRFP-Smad2 signal in both nuclear and cytoplasmic compartments, in the cells labeled on panel A. Cell1 and Cell2 were quantified for the 60 minute timepoint after TGFβ ligand stimulation; Cell3 and Cell4 at the 15 minute timepoint after blue light stimulation were quantified. Regions without cells were measured as background signal. (D) Normalized iRFP-Smad2 signal in the cells as on panel C. Intensities of both nuclear and cytoplasmic iRFP-Smad2 were subtracted by the corresponding background intensity, and then normalized by the cytoplasmic signal of the corresponding cell.

5

Development of a Mathematical Model for the optoTGFβ System

To better describe the dynamic properties of the optoTGFβ system, and to facilitate further applications of the optoTGFβ system, in this chapter, we formulated a mathematical model by integrating a light controllable module to a previously developed model of the endogenous canonical TGFβ/Smad signaling. As the previous models were built on experimental datasets of HaCaT cells, whose physiological background is not exactly the same as Hela cells which were used in our project, we calibrated our new model with fresh quantitative experimental datasets based on Hela or optoHela cells.

One thing we'd like to point out here is that, compared with the previous model calibration processes, we obtained quantitative data more efficiently and precisely by the optoTGFβ system. Therefore, the optoTGFβ system facilitates mathematical model development, and further promotes better characterization of TGFβ signaling.

After model construction and parameter estimation, we validated the model performance by assessing in-sample fit and out-sample fit. Taking the advantages of model simulation, we scanned several parameters to explore several characteristics of the optoTGFβ system. These were then followed by a summary of the model.

5.1 Model conception

The chimeric optoTGFβ system (**Figure 5.1.1**) was generated from two different systems: the light responsive protein pair that controls the activity of the receptors (optoTβRs), and the downstream TGFβ signaling. Therefore, the model contains 2 major parts:

I. The optoTβRs activation and deactivation, including:
   a. The optoTβRII activation (transformation of the light-sensitive domain PHRi → PHRa by light irradiation);
   b. Activated optoTβRII forms receptors complex (optoRC) with optoTβRI;
   c. The optoRC dissociation;

II. The Smads activation and deactivation, including:
   a. The nucleocytoplasmic shuttling of Smad2/Smad4;
   b. The association and dissociation of Smad2/Smad4;
   c. The phosphorylation and dephosphorylation of Smad2.

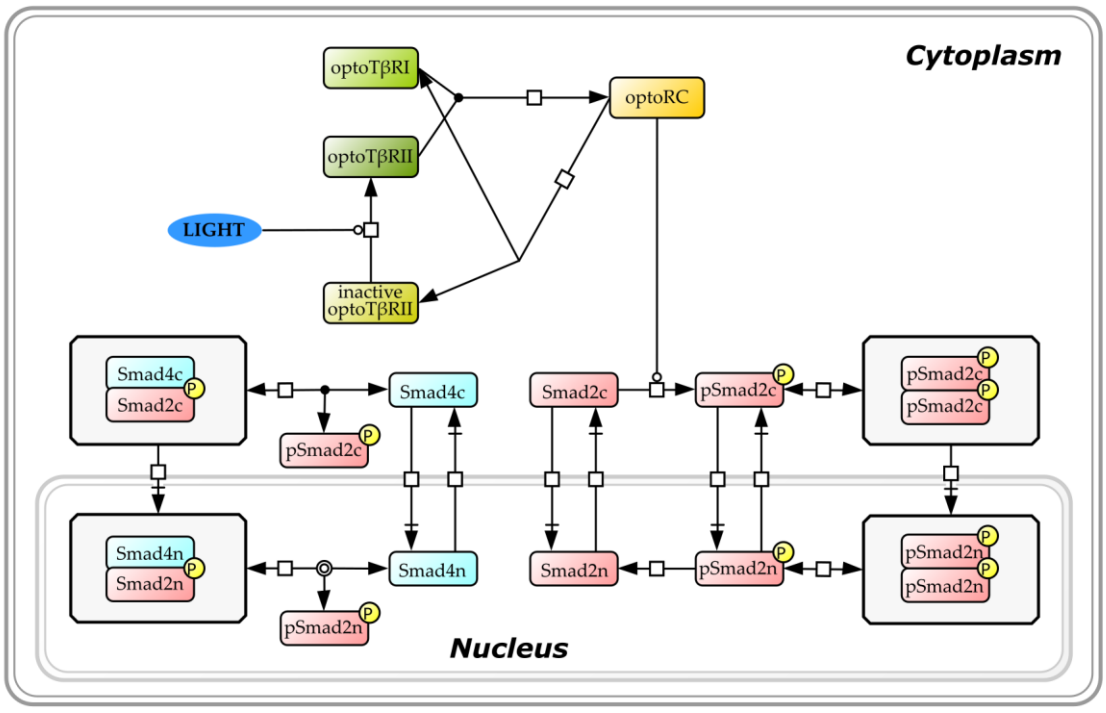

Figure 5.1.1 Schematic model of the optoTGFβ system. optoRC, activated optoTβRs complex; pSmad2n, phosphorylated Smad2 in the nucleus; etc. It should be noted that the cytoplasmic region of TβRII in optoTβRII is constitutively active for activating TβRI. It is the light-sensitive PHR domain in optoTβRII that is activated by light irradiation, followed by association with the binding partner, i.e., CIBN in optoTβRI.

5.2 Model assumptions

I. The optoTβRs complex formation upon light activation is very fast and reaches its maximum within one minute. It should be noted here that the cytoplasmic region of TβRII in optoTβRII is constitutively active for activating TβRI. It is the light-sensitive PHR domain in optoTβRII that is activated by light stimulation, which then binds with its partner, i.e., CIBN in optoTβRI. When we stimulated optoHela cells with a short pulse (< 1 s) of blue light, we could observe a depletion process of optoTβRII from the cytoplasmic region during the first minute after the stimulation (**Figure 5.3.1**). This indicates that, to model the light activation, there are clearly two steps that we should describe separately:
    1) a very fast reaction of optoTβRII activation by light stimulation;
    2) a relatively slow reaction of optoTβRs association to form the optoTβRs complex (optoRC).

   As the TGFβ signaling in the optoTGFβ system saturates for light intensities above a certain threshold (**Figure 3.5.2**), we assume a Michaelis-Menten kinetic for the optoTβRII activation step, which transforms the inactivate optoTβRII pool (ioptoT2R) to a pool of activated optoTβRII (optoT2R). Its two parameters (V_{max} and K_M) could be assigned arbitrarily as long as all of optoTβRII could be activated within 1 second upon a saturating light intensity. Here, we assigned the two parameters (**Table 5.3-2**) by assuming that a light intensity of 1 (with an arbitrary unit) could activate over 90 percent of the inactivate optoTβRII pool (ioptoT2R) in one second. The optoTβRs association step was modeled by mass action kinetic, just as the rest reactions in the model.

II. Being in accordance with Zi's model, we assumed that the phosphorylation rate of Smad2 is proportional to the concentration of the cytoplasmic Smad2 and the activated optoTβRs complex (optoRC). Besides, we also assumed that dephosphorylation only happens in the nucleus as there is little cytoplasmic phosphatase activity targeting Smads complex[133].

III. Similar to the previous models[133,136], we assumed Smad3 undergoes the same reactions as Smad2, and therefore omitted Smad3 in the model.

IV. As the total amount of optoTβRs and Smad2 proteins varied little in the time scale of our experiment, independent of the presence or absence of perturbation. We assumed the amounts of all the proteins involved in the model are constant. Although degradation and production exist in the cell, they are in balance. Therefore, for simplification, production and degradation of all the proteins were not explicitly modeled in this model.

Table 5.2-1 Equations of the mathematical model

Ordinary differential equations*

Receptor Module

$$\frac{\mathrm{d}[\mathrm{optoT2R}]}{\mathrm{d}t} = \frac{V_{max}\,[\mathrm{Light}]}{K_M + [\mathrm{Light}]}\,[\mathrm{ioptoT2R}] - k_{on}^{optoTRs}\,[\mathrm{optoT1R}]\,[\mathrm{optoT2R}]$$

$$\frac{\mathrm{d}[\mathrm{ioptoT2R}]}{\mathrm{d}t} = k_{diss}^{optoTRs}\,[\mathrm{optoRC}] - \frac{V_{max}\,[\mathrm{Light}]}{K_M + [\mathrm{Light}]}\,[\mathrm{ioptoT2R}]$$

$$\frac{\mathrm{d}[\mathrm{optoRC}]}{\mathrm{d}t} = k_{on}^{optoTRs}\,[\mathrm{optoT1R}]\,[\mathrm{optoT2R}] - k_{diss}^{optoTRs}\,[\mathrm{optoRC}]$$

$$\frac{\mathrm{d}[\mathrm{optoT1R}]}{\mathrm{d}t} = k_{diss}^{optoTRs}\,[\mathrm{optoRC}] - k_{on}^{optoTRs}\,[\mathrm{optoT1R}]\,[\mathrm{optoT2R}]$$

Smad Module

$$\frac{\mathrm{d}[\mathrm{S2}_c]}{\mathrm{d}t} = \frac{\mathrm{V_{nuc}}}{\mathrm{V_{cyt}}}\,k_{exp}^{S2}\,[\mathrm{S2}_n] - k_{imp}^{S2}\,[\mathrm{S2}_c] - k_{phos}^{S2}\,[\mathrm{S2}_c]\,[\mathrm{optoRC}]$$

$$\frac{\mathrm{d}[\mathrm{S2}_n]}{\mathrm{d}t} = \frac{V_{cyt}}{V_{nuc}}\,k_{imp}^{S2}\,[\mathrm{S2}_c] - k_{exp}^{S2}\,[\mathrm{S2}_n] + k_{dephos}^{S2}\,[\mathrm{pS2}_n]$$

$$\frac{\mathrm{d}[\mathrm{S4}_c]}{\mathrm{d}t} = \frac{V_{nuc}}{V_{cyt}}\,k_{exp}^{S4}\,[\mathrm{S4}_n] - k_{imp}^{S4}\,[\mathrm{S4}_c] + k_{off}^{Smads}\,[\mathrm{pS2S4}_c] - k_{on}^{Smads}\,[\mathrm{S2}_c]\,[\mathrm{S4}_c]$$

$$\frac{\mathrm{d}[\mathrm{S4}_n]}{\mathrm{d}t} = \frac{V_{cyt}}{V_{nuc}}\,k_{imp}^{S4}\,[\mathrm{S4}_c] - k_{exp}^{S4}\,[\mathrm{S4}_n] + k_{off}^{Smads}\,[\mathrm{pS2S4}_n] - k_{on}^{Smads}\,[\mathrm{pS2}_n]\,[\mathrm{S4}_n]$$

$$\begin{aligned}\frac{\mathrm{d}[\mathrm{pS2}_c]}{\mathrm{d}t} = {} & \frac{V_{nuc}}{V_{cyt}}\,k_{exp}^{S2}\,[\mathrm{pS2}_n] - k_{imp}^{S2}\,[\mathrm{pS2}_c] + k_{phos}^{S2}\,[\mathrm{S2}_c]\,[\mathrm{optoRC}] \\ & - k_{on}^{Smads}\,[\mathrm{pS2}_c]\,[\mathrm{S4}_c] + k_{off}^{Smads}\,[\mathrm{pS2S4_c}] \\ & - 2\,k_{on}^{Smads}\,[\mathrm{pS2}_c]\,[\mathrm{pS2}_c] + 2\,k_{off}^{Smads}\,[\mathrm{pS2S2_c}]\end{aligned}$$

$$\frac{d[pS2_n]}{dt} = \frac{V_{cyt}}{V_{nuc}} k_{imp}^{S2} [pS2_c] - k_{exp}^{S2} [pS2_n] - k_{dephos}^{S2} [pS2_n] + k_{off}^{Smads} [pS2S4_n] - k_{on}^{Smads} [pS2_n] [S4_n] + 2 k_{off}^{Smads} [pS2S2_n] - 2k_{on}^{Smads} [pS2_n] [pS2_n]$$

$$\frac{d[pS2S2_c]}{dt} = k_{on}^{Smads} [pS2_c] [pS2_c] - k_{off}^{Smads} [pS2S2_c] - k_{imp}^{Smads} [pS2S2_c]$$

$$\frac{d[pS2S2_n]}{dt} = \frac{V_{cyt}}{V_{nuc}} k_{imp}^{Smads} [pS2S2_c] - k_{off}^{Smads} [pS2S2_n] + k_{on}^{Smads} [pS2_n] [pS2_n]$$

$$\frac{d[pS2S4_c]}{dt} = k_{on}^{Smads} [pS2_c] [S4_c] - k_{off}^{Smads} [pS2S4_c] - k_{imp}^{Smads} [PS2S4_c]$$

$$\frac{d[pS2S4_n]}{dt} = \frac{V_{cyt}}{V_{nuc}} k_{imp}^{Smads} [pS2S4_c] - k_{off}^{Smads} [pS2S4_n] + k_{on}^{Smads} [pS2_n] [S4_n]$$

Assignment rules and compartment parameters

$$Smad2_{N2C} = \frac{[S2_n] + [pS2_n] + 2 [pS2S2_n] + [pS2S4_n]}{[S2_c] + [pS2_c] + 2 [pS2S2_c] + [pS2S4_c]}$$

$$pSmad2_{totalAmount} = ([pS2_n] + 2 [pS2S2_n] + pS2S4_n))*602 + ([pS2_c] + 2 [pS2S2_c] +[pS2S4_c]) *2.66*602$$

* See tables **Table 5.3-2** and **Table 5.3-3** for annotation of each parameters and species, respectively.

5.3 Parameter estimation

Model parameters were estimated either by experimental measurement, or by data fitting. Some parameters could be easily measured through experimental approaches available in our lab; several others could be inferred by referring to the literature or public databases. The remaining four parameters, which were hard to access directly through experimental measurement, were estimated through data fitting. We generated three independent experimental datasets by live cell imaging, and quantified the iRFP-Smad2 signal in both nuclear and cytoplasmic region in multiple cells at various time points. These data were used to estimate the four parameters. After that, another two new datasets were used for model validation.

The model frame of the second part was based on the model developed by Zi et al[136], however, the physiological background of Hela cell is different from that of HaCaT cell, upon which Zi's model was built. Therefore, we used different parameters, which were determined in this work through experimental measurement or parameter estimation.

5.3.1 Deriving parameter values by experimental measurement

5.3.1.1 Determination of the volumes of cellular compartment

A typical Hela cell has a diameter of 20 microns[235] (consistent with the image observations in this study). Considering the ratio of cytoplasmic-to-nuclear volume estimated in the following section *5.3.1.5* (~ 2.66), the volumes of nucleus and cytoplasm could be estimated as 1 pl (picoliter, = 1×10^{-12} L) and 2.66 pl, respectively.

5.3.1.2 The initial steady state before perturbation

Concentrations of all the relevant endogenous proteins were estimated by referring to GeneCards[236] and MaxQB[237] databases, which include numerous protein expression data measured in Hela cells. Concentrations of the chimeric proteins in the optoTGFβ system were estimated by comparing to their respective endogenous counterparts on western blots.

Here we used the relative expression value measured as ppm (parts per million). By considering the protein density for a typical mammalian cell of $2.6*10^6$ proteins/um^3 [238], concentrations of the corresponding proteins could be estimated accordingly.

Table 5.3-1 Definition of the protein concentrations at steady state

Name	Rel. Expression (ppm)	Concentration (nM)	Surface (nM)	Cytoplasm (nM)	Nucleus (nM)
TβRI	16	71.74	7.17*	64.56	0
TβRII	0.55	2.47	0.25*	2.22	0
Smad2	58	260.05	0	291.32	176.87
Smad4	22	98.64	0	61.4	197.7
optoTβRI	TβRI * 0.55	39.46	39.46	0	0
optoTβRII	TβRII * 3.6	8.88	0	8.88	0
iRFP-Smad2	Smad2 * 1.7	442.08	0	495.24	300.68

* Calculated by referring to the estimation that around 10 percentages of TGFβ receptors locate on the plasma membrane[108,136].

5.3.1.3 Determination of the optoTβRs association kinetics

The kinetic parameter for the optoTβRs association ($k_{on}^{optoTRs}$) was measured by frequent imaging of the optoTβRII signal following a pulsed stimulation. Briefly, optoHela cells were stimulated by a short pulse of blue light, images of the optoTβRII channel were taken before and after the light stimulation at a frequency of 2s-per-image (**Figure 5.3.1** A). Dynamics of the cytoplasmic optoTβRII signal depletion in multiple cells were quantified and fitted to a mass action kinetic ODE (**Figure 5.3.1** B), using the Curve Fitting Toolbox in MATLAB. The association parameter could therefore be obtained (**Figure 5.3.1** C).

Specifically, the optoTβRs association process is at the scale of seconds, while the activation of optoTβRII is super fast (at the scale of ~us), and the dissociation process of optoRC (the optoTβRs complex) is slow (at the scale of minutes). We assumed that optoTβRII is immediately activated and the dissociation of optoRC could be ignored during the first minute after light activation. Therefore, we could use a mass action kinetic ODE to describe the optoTβRs association process:

$$\frac{\mathrm{d}x}{\mathrm{d}t} = -k_{on} \cdot x \cdot (x + d) \qquad (1)$$

Where x denotes the concentration of cytoplasmic optoTβRII, $(x + d)$ denotes the concentration of optoTβRI, and d denotes the difference between the concentration of optoTβRII and optoTβRI. d could be calculated by:

$$d = x_0 \cdot (R - 1) \tag{2}$$

Where x_0 denotes the initial level of x, R denotes the ratio of (the concentration of) optoTβRI to optoTβRII, which could be calculated by referring to **Table 5.3-1**.

Solving the ODE (1), we can get:

$$x_t = \frac{d}{e^{\ln\left(\frac{d+x_0}{x_0}\right) + d \cdot k_{on} \cdot t} - 1} \tag{3}$$

By live cell imaging and image quantification, we could get a series of $x_t$with the corresponding t. By fitting these data to function (3), the parameter k_{on} could be obtained, which is the kinetic parameter for optoTβRs association ($k_{on}^{optoTRs}$).

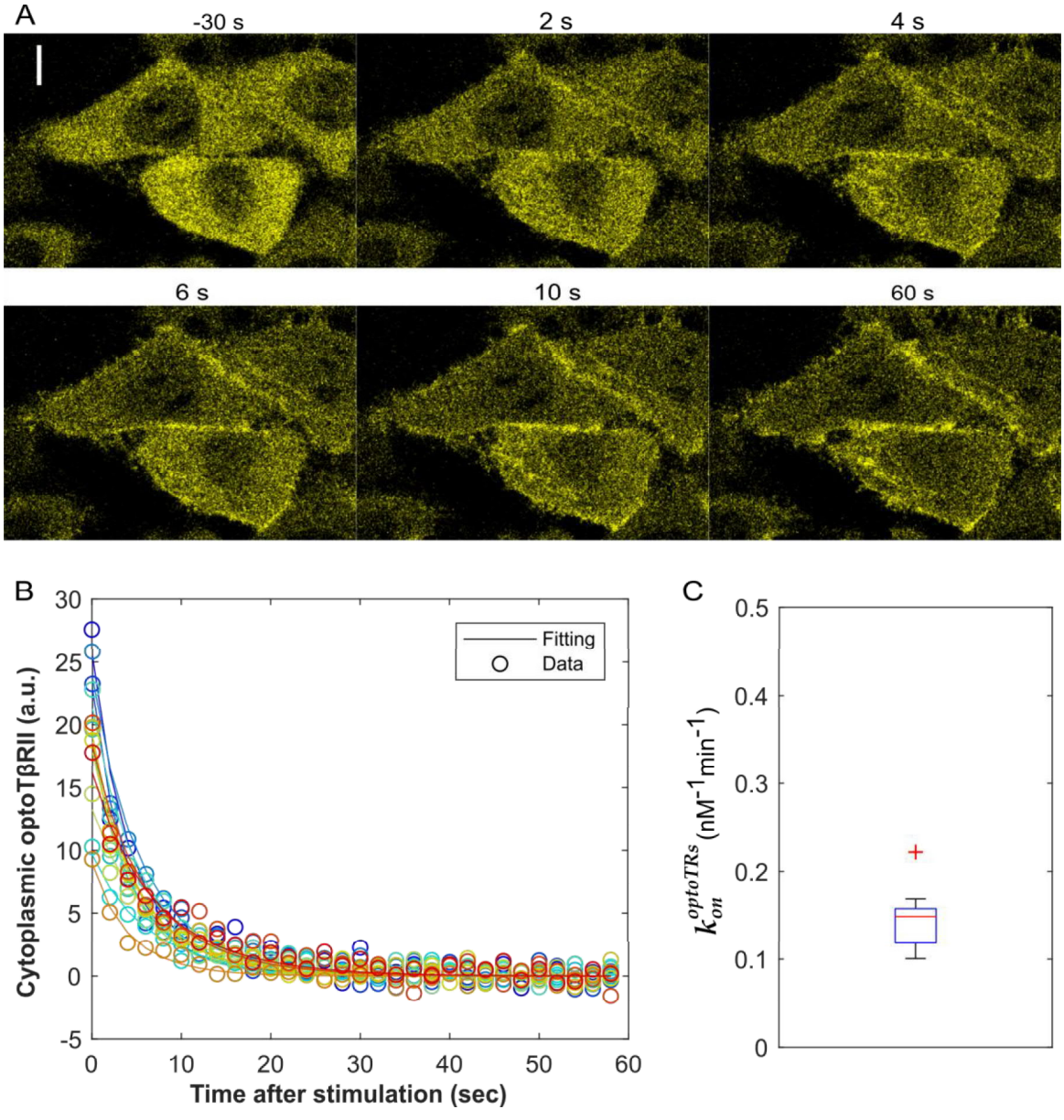

Figure 5.3.1 Determination of the optoTβRs association kinetics. optoHela cells were stimulated by a short pulse of blue light, images for the optoTβRII channel were taken at a frequency of 2s-per-image, the quantified optoTβRII dynamics were fitted to obtain the association parameter. (A) Representative images of optoTβRII translocation onto the plasma membrane upon light stimulation. Upper panels, from left to right, t=30 sec before, t= 2 sec, t=4 sec after photoactivation; lower panels, from left to right, t=6 sec, 10 sec, 60 sec after photoactivation. Scale bar: 10μm. (B) Quantification of cytoplasmic optoTβRII intensity in multiple cells over time (open circles). Data were normalized by subtracting the corresponding intensities when reaching the highest recruitment. Activation was done at the time point 0. In the corresponding color, are the fitted curves. (C) Boxplot of the optoTβRs association kenitics from the fits in (B).

5.3.1.4 Determination of the optoTβRs dissociation kinetics

The kinetics of optoTβRs dissociation ($k_{diss}^{optoTRs}$) was determined by quantifying images of optoTβRII signal following a pulsed stimulation, with a longer time scale. Briefly, optoHela cells were stimulated by a short pulse of blue light, images of the optoTβRII channel were taken before and after the light stimulation at a frequency of 30s-per-image (**Figure 5.3.2** A). After that, the dynamics of the cytoplasmic optoTβRII signal recovery in multiple cells were quantified and fitted to an exponential decay function (**Figure 5.3.2** B), using the Curve Fitting Toolbox in MATLAB. Therefore the dissociation parameter could be obtained (**Figure 5.3.2** C).

Specifically, the association of optoTβRs reaches the maximal extent in 1 minute after a pulse of light stimulation, after that, the dissociation of optoRC dominates. Therefore, we could use a first-order mass action kinetic ODE to describe this optoTβRs dissociation process:

$$\frac{\mathrm{d}x}{\mathrm{d}t} = k_{diss} \cdot (x_{tot} - x) \tag{4}$$

Where x denotes the concentration of cytoplasmic optoTβRII, $(x_{tot} - x)$ denotes the concentration of optoRC, i.e., the portion of optoTβRII in optoRC at the plasma membrane, and x_{tot} denotes the total amount of optoTβRII, which is the concentration of cytoplasmic optoTβRII at the steady state in the dark.

Solving the ODE (4), we can get:

$$x_t = x_{tot} + e^{-k_{diss} \cdot t} \cdot (x_0 - x_{tot}) \tag{5}$$

By live cell imaging, we could get a series of $x_t$with the corresponding t (we used the data between 1min and 10min after photoactivation). By fitting these data to function (5), the parameter k_{diss} could be obtained, which is the kinetic parameter for optoTβRs dissociation ($k_{diss}^{optoTRs}$).

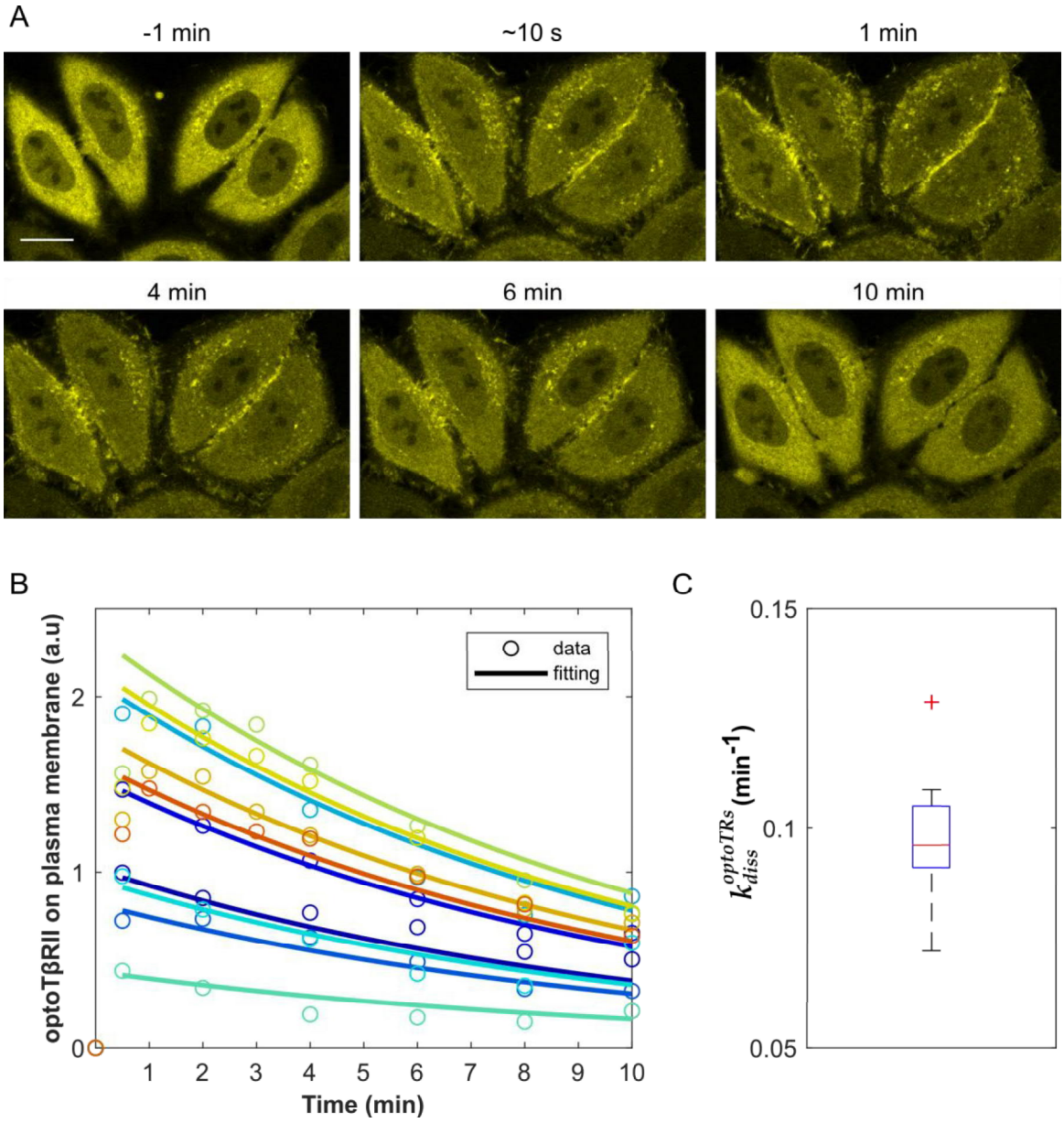

Figure 5.3.2 Determination of the optoTβRs dissociation kinetics. optoHela cells were stimulated by a short pulse of blue light, dynamics of the optoTβRII signal were quantified and fitted to obtain the dissociation parameter. (A) Representative images of optoTβRII translocation onto the plasma membrane upon light stimulation, and its recovery afterwards. Upper panels, from left to right, t=1 min before, t= 10s, t=1 min after photoactivation; lower panels, from left to right, t=4 min, t= 6 min, t=10 min after photoactivation. Scale bar= 20µm. (B) Quantification of the optoTβRII signal in multiple cells over time (open circles). Data were normalized by the respective initial intensities (at 1min after photoactivation). Activation was done at the 0 minute time point. In the corresponding color, are the fitting curves according to the optoTβRs dissociation model. (C) Boxplot of the characteristic parameter of optoTβRs dissociation from the fits in (B).

5.3.1.5 Determination of the accessible cytoplasmic-to-nuclear volume ratio

While western blotting data indicate the total amounts of specific proteins, fluorescent protein intensities quantified on microscopic images indicate the concentrations of the corresponding proteins. To parallelize and compare these two types of data, cell volume is needed additionally. While it is difficult to infer the volume of either nuclear or cytoplasmic compartment by western blotting experiments, it is possible to measure the volumes of these two compartments by microscopy. Then the total amount of a specific protein could be calculated by converting the concentration data of both compartments, which could match the western blotting data. To simplify the experiments, rather than measuring the exact physical data of the volumes, we could get the ratio of the accessible cytoplasmic-to-nuclear volume by using the already available data collected in most of the live-cell imaging experiments in this study.

During the process of fluorescence-tagged Smad2 translocation from the cytosol into the nucleus, an increase of the fluorescence signal in the nuclear compartment (ΔF_{nuc}) is companioned by a decrease of the fluorescent signal in the corresponding cytoplasmic compartment (ΔF_{cyto}). The total flux of the iRFP-Smad2 could be written as:

$$\Delta J_{Smad2} = \Delta F_{nuc} \cdot V_{nuc} = -\Delta F_{cyt} \cdot V_{cyt} \quad (6)$$

where V_{nuc} and V_{cyto} are the volumes of the accessible nuclear and cytoplasmic compartments, respectively. Therefore, the ratio of the accessible cytoplasmic-to-nuclear volume could be calculated by:

$$R = V_{cyt}/V_{nuc} = -\Delta F_{nuc}/\Delta F_{cyt} \quad (7)$$

To determine the accessible cytoplasmic-to-nuclear volume ratio for Hela cells, here we chose the one-hour-long live cell imaging data for optoHela cells upon a short pulse of blue light stimulation. Images of the iRFP-Smad2 channel were taken before and after the light stimulation, recording the process of Smad2 nuclear translocation. The Smad2 signal in both the nuclear and the cytoplasmic regions were quantified at various time points. For each specific cell, the nuclear iRFP-Smad2 signal difference between two random time points was calculated as ΔF_{nuc}, the corresponding change of the cytoplasmic Smad2 signal was calculated as ΔF_{cyt}, then the ratio of them was calculated by $R = -\Delta F_{nuc}/\Delta F_{cyt}$ to represent the ratio of the accessible cytoplasmic-to-nuclear volume for this specific cell (**Figure 5.3.3** A). After calculating for various time point pairs and for various cells, we obtained a value of 2.66 +/- 0.02 (**Figure 5.3.3** B), which is a reasonable result, and in good agreement with other studies[133].

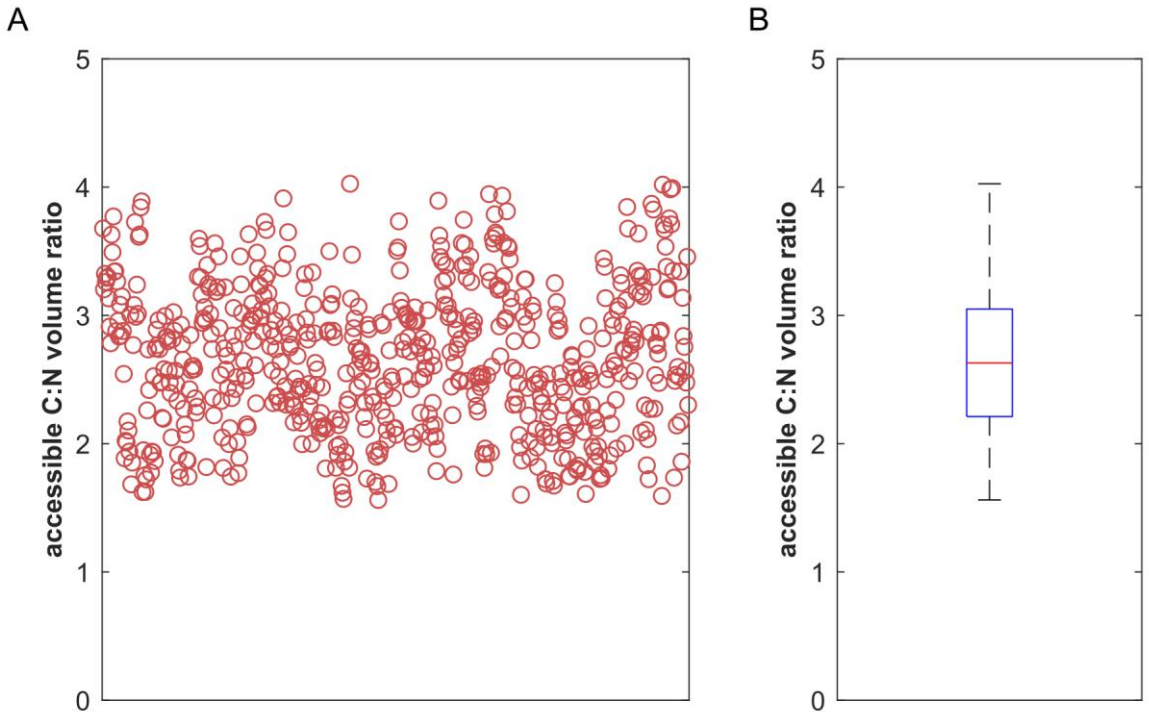

Figure 5.3.3 Determination of the accessible cytoplasmic-to-nuclear volume ratio. optoHela cells were stimulated by a short pulse of blue light, dynamics of the Smad2 signal in both the nuclear and the cytoplasmic regions were quantified. The ratio of their changes was calculated as $R = -\Delta F_{nuc}/\Delta F_{cyt}$ to represent the ratio of the accessible cytoplasmic-to-nuclear volume for the corresponding cell, which was represented as a red circle on the panel (A). (B) Boxplot of the R (ratios of accessible cytoplasmic-to-nuclear volume) for multiple time point pairs (~ 10 timepoints) for multiple cells (141 cells) as represented on the panel (A). The typical R is 2.66 +/- 0.02.

5.3.1.6 Determination of the Smad2 translocation kinetics

To estimate the import and export rate constants for the constitutive shuttling processes of iRFP-Smad2, we implemented whole compartment FRAP of nuclear iRFP-Smad2. In the absence of stimulation, optoHela cells stay in a steady state where only the basal nucleocytoplasmic shuttling of Smads is taking place. Photobleaching of the nuclear localized iRFP-Smad2 disturbs this steady state, and the ratio of nuclear-to-cytoplasmic (N2C) fluorescence will recover to the steady state due to the basal nucleocytoplasmic shuttling of Smads. Nuclear importing and exporting rates (k_{imp} and k_{exp}, respectively) could thus be inferred by curve fitting to the measured fluorescence recovery curves.

Assuming first order kinetics for both import and export:

$$\frac{dC_{nuc}}{dt} = k_{imp} \cdot C_{cyt} - k_{exp} \cdot C_{nuc} \quad (8)$$

where C_{cyt} and C_{nuc} denote the concentrations of nuclear and cytoplasmic Smad2, respectively; k_{imp} and k_{exp} are Smad2 nuclear import and export rates, respectively.

During the fluorescence recovery process, the total amount of fluorescence does not change, which is equal to the total amount of cytoplasmic fluorescence immediately after photobleaching (assuming a complete photobeaching, i.e., $C_{nuc}\,(t = 0) = 0$). Thus there is the mass conservation:

$$C_{cyt0} = C_{cyt} + C_{nuc}/R \tag{9}$$

where C_{cyt0} denotes $C_{cyt}\,(t = 0)$, i.e., the initial concentration of cytoplasmic fluorescent signal immediately after photobleaching; R denotes the accessible cytoplasmic-to-nuclear volume ratio calculated in section *5.3.1.5*.

The change of nuclear fluorescence, i.e., the ODE (8) could then be solved analytically as follows[239]:

$$C_{nuc}(\mathrm{t}) = C_{cyt0} \cdot \frac{R \cdot k_{imp}(1 - \mathrm{e}^{-(R \cdot k_{exp} + k_{imp}) \cdot \mathrm{t}})}{R \cdot k_{exp} + k_{imp}} \tag{10}$$

At steady state, i.e., $t \to \infty$,

$$C_{nucsteady} = C_{cyt0} \cdot \frac{R \cdot k_{imp}}{R \cdot k_{exp} + k_{imp}} \tag{11}$$

Therefore, the function (10) could be rewritten as:

$$C_{nuc}(\mathrm{t}) = C_{nucsteady} \cdot (1 - \mathrm{e}^{-(R \cdot k_{exp} + k_{imp}) \cdot \mathrm{t}}) \tag{12}$$

By fitting the data of nuclear FRAP curve to (12), $(R \cdot k_{exp} + k_{imp})$ could be obtained. Then combining with equation (11), both k_{imp} and k_{exp} could be derived.

To implement, briefly, unstimulated live optoHela cells were photobleached in the whole nuclear region, the reappearance of iRFP signal was monitored at a frequency of 2s-per-image (**Figure 5.3.4** A), until a steady state was reached. Dynamics of the nuclear iRFP signal in multiple cells were quantified and fitted to the exponential function (12) using the Curve Fitting Toolbox in MATLAB (**Figure 5.3.4** B), the import and export rate parameters for iRFP-Smad2 could therefore be obtained (**Figure 5.3.4** C).

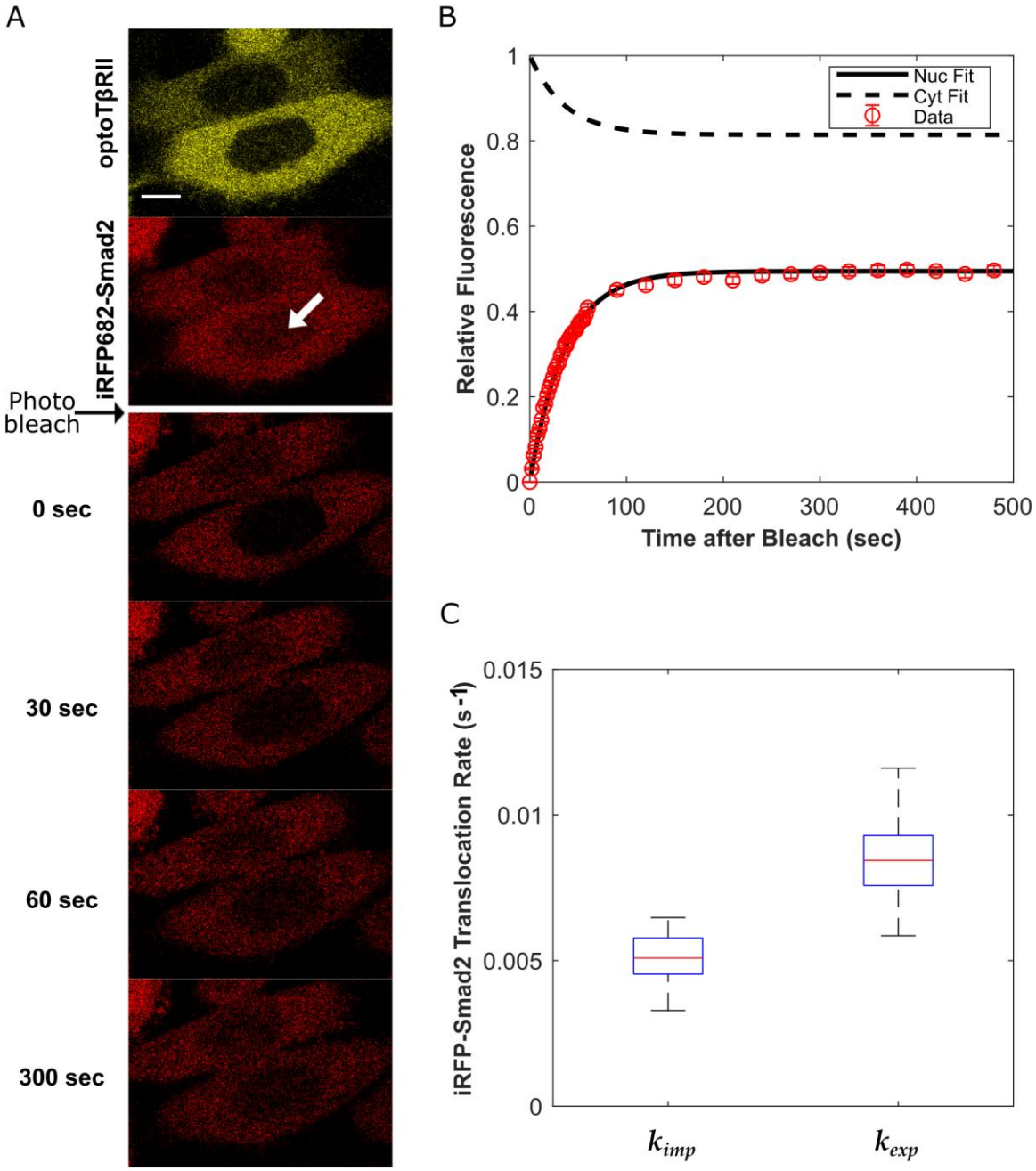

Figure 5.3.4 Determination of the Smad2 translocation kinetics. (A) Representative images of a photobleaching experiment. The channel for optoTβRII (yellow) was used for nucleus segmentation for photobleaching. Images of the iRFP-Smad2 channel (red) were taken before and after photobleaching: t = 1 min before, t = 0 sec, t = 30 sec, t = 60 sec and t = 300 sec after photobleaching. Scale bar= 10µm. (B) Quantification of nuclear iRFP intensity in multiple cells over time, normalized by the cytoplasmic fluorescence immediately after the bleach (open circles, n= 10, +/-SD). The solid black line represents the model fitting with the obtained values of k_{imp} (0.0051 s^{-1}) and k_{exp} (0.0084 s^{-1}), the black dashed line represents the corresponding cytoplasmic iRFP signal dynamics. (C) Boxplots of the characteristic parameters.

In addition, the steady state of the cytoplasmic concentration could also be derived:

$$C_{cytsteady} = C_{cyt0} \cdot \frac{R \cdot k_{exp}}{R \cdot k_{exp} + k_{imp}} \tag{13}$$

The Smad2 N2C ratio at steady state could be derived by combing (11) and (13):

$$\frac{C_{nucsteady}}{C_{cytsteady}} = \frac{k_{imp}}{k_{exp}} \tag{14}$$

The total amount of iRFP-Smad2 is already known to be 260.05 nM (**Table 5.3-1**), which could be calculated by:

$$\frac{C_{nucsteady} \cdot 1 + C_{cytsteady} \cdot R}{1 + R} = C_{total} \tag{15}$$

Combing equations (14) and (15), the initial steady state concentrations of both nuclear and cytoplasmic Smad2 could be calculated. The detailed values are shown in **Table 5.3-3**.

Concerning the endogenous Smad4 in Hela cells, immunofluorescence experiments showed that the steady-state N2C ratio of Smad4 before perturbation in Hela cells is around 3.22, which equals the ratio of its nuclear import to export rate, as indicated by equation (14). As the Smad4 nuclear import occurs with comparable rate to that of Smad2[133], we used the same import rate of Smad2 for Smad4. The nuclear export rate of Smad4 could therefore be deduced. By knowing the total amount of Smad4 to be 98.64 nM (**Table 5.3-1**), the initial steady state concentrations of both nuclear and cytoplasmic Smad4 could then be calculated by combing equations (14) and (15). The detailed values are shown in **Table 5.3-3**.

Table 5.3-2 Summary of the derived parameter values based on experimental data or published models

Parameter	Value *	Annotation	Reference
Receptor Module			
V_{max}	5 sec^{-1}	maximum rate of optoTβRI activation	this work
K_M	0.1	light intensity at which the reaction rate is half of the V_{max}	this work
$k_{on}^{optoTRs}$	0.144 $nM^{-1}min^{-1}$	optoTβRs association rate constant	this work
$k_{diss}^{optoTRs}$	0.1 min^{-1}	optoTβRs dissociation rate constant	this work
Smad Module			
k_{imp}^{S2}	0.306 min^{-1}	Smad2 nuclear import rate constant	this work
k_{exp}^{S2}	1.34 min^{-1}	Smad2 nuclear export rate constant	this work
k_{imp}^{S4}	0.306 min^{-1}	Smad4 nuclear import rate constant	this work , [240,241]
k_{exp}^{S4}	0.253 min^{-1}	Smad4 nuclear export rate constant	this work
k_{off}^{Smads}	1 min^{-1}	Smad complexes dissociation rate constant	[240]
Compartment parameters			
V_{cyt}	2.66 pl	Volume of the cytoplasmic compartment	this work, [235]
V_{nuc}	1 pl	Volume of the nuclear compartment	this work, [235]

* The parameters were rounded to 3 significant digits.

Table 5.3-3 Summary of model initial conditions

Species	Value [a]	Annotation	Compartment
Receptor Module			
Light	1	light intensity	Cytoplasm
optoT1R	39.46 nM	optoTβRI	Cytoplasm [b]
ioptoT1R	8.88 nM	optoTβRII before light stimulation	Cytoplasm
optoT2R	0 nM	activated optoTβRII upon light stimulation	Cytoplasm
optoRC	0 nM	optoTβRs complex	Cytoplasm [b]
Smad Module			
$S2_c$	495.2 nM	Smad2	Cytoplasm
$S2_n$	300.7 nM	Smad2	Nucleus
$S4_c$	61.4 nM	Smad4	Cytoplasm
$S4_n$	197.7 nM	Smad4	Nucleus
$pS2_c$	0 nM	phosphorylated Smad2 monomer	Cytoplasm
$pS2_n$	0 nM	phosphorylated Smad2 monomer	Nucleus
$pS2S2_c$	0 nM	phosphorylated Smad2 dimer	Cytoplasm
$pS2S2_n$	0 nM	phosphorylated Smad2 dimer	Nucleus
$pS2S4_c$	0 nM	phosphorylated Smad2-Smad4 complex	Cytoplasm
$pS2S4_n$	0 nM	phosphorylated Smad2-Smad4 complex	Nucleus

a) The initial concentration values were rounded to 3 effective digits.

b) Its actual localization is the plasma membrane, but still could be considered to be the cytoplasm for simplification.

5.3.2 Estimation of unknown parameters

While the above-mentioned parameter values could be measured by experiments, other parameters are more difficult to access directly, including the following parameters:

- k_{phos}^{S2} ($nM^{-1}min^{-1}$):
  Rate constant for iRFP-Smad2 phosphorylation by the activated receptor complex (optoRC);
- k_{dephos}^{S2} (min^{-1}):
  Rate constant for iRFP-Smad2 dephosphorylation by phosphatase in the nucleus. Here we assumed a constant level of phosphatase and mass action kinetics, hence we omitted the concentration of phosphatase, and used a single parameter k_{dephos}^{S2} to represent the rate for iRFP-Smad2 dephosphorylation;
- k_{on}^{Smads} ($nM^{-1}min^{-1}$):
  The rate constant for Smads complex dissociation (k_{diss}^{Smads}) characterizes the Smad complex stability, and is the ratio of two kinetic rates: k_{off}^{Smads} over k_{on}^{Smads}. Here we used the same estimated off-rate of 1 min^{-1} as in Schmierer's paper[133], which corresponds to an averaged complex life time of approximate 1 min. Sensitivity analysis showed that k_{off}^{Smads} does not significantly influence system behavior. The corresponding k_{on}^{Smads} was optimized and the dissociation rate constant could be calculated.
- k_{imp}^{Smads} (min^{-1}):
  Rate constant for Smads complex nuclear import.

These parameters were optimized by simultaneously fitting several experimental data sets. The optimal set of parameters was then used for the subsequent simulations. To do this, we used a parallel parameter estimation tool[242], which applied the algorithm of stochastic ranking evolution strategy (SRES)[243]. Three datasets generated under different stimulation conditions were used for the estimation:

- Time course of Smad2 N2C ratio in response to frequent light stimulation (1 pulse every 10 minutes);
- Time course of Smad2 N2C ratio to in response to a single pulse of light stimulation;
- Time course of Smad2 N2C ratio in response to pulsed light stimulations at a low frequency (1 pulse every 180 minutes).

5.3.3 Statistical analysis of the estimated parameters

Due to the noise inherent in biological systems as well as in experimental measurements, the best-fit values might not be the only set of parameters that could fit within the error-bars of the experimental data. Certain deviation of the parameters from their best-fit values will still produce reasonable fits. However, due to the different properties of different parameters, the confidence intervals of these parameters could vary a lot. Here we implemented statistical analysis for the best-fit parameters. For calculating their 95% confidence intervals, we utilized a profile likelihood exploit algorithm[244]. In the meantime, we also tried to generate a series (5000 sets) of new synthetic data sets from the experimental data sets by the bootstrap method[245], and independently performed parameter estimations to obtain 5000 best fit parameter sets, which was followed by calculating their distributions as well as standard deviations. Both of these two statistical analyses were implemented in a parallel parameter estimation tool SBML-PET-MPI[242]. Results were shown in **Table 5.3-4**.

Table 5.3-4 Statistical analysis of the estimated parameters

Parameter (Unit)	Best fit [a]	95% confidence interval [b]	Mean ± SD [c]	Bounds in parameter estimation
k_{phos}^{S2} ($nM^{-1}min^{-1}$)	0.005936	(0.005639; 0.006530)	0.00616 ± 0.000679	0.001 ~ 1000
k_{dephos}^{S2} (min^{-1})	1.668	(1.335;2.002)	2.37 ± 2.43	0.001 ~ 1000
k_{on}^{Smads} ($nM^{-1}min^{-1}$)	2.300	(2.285; 2.303)	5.36 ± 13.5	0.001 ~ 1000
k_{imp}^{Smads} (min^{-1})	0.4549	(0.3639; 0.4563)	0.607 ± 0.621	0.001 ~ 1000

a) The estimated parameters were rounded to 4 significant digits.

b) The 95% confidence intervals derived from profile likelihood analysis.

c) The mean and 1 standard deviation calculated from 5000 optimizations from synthetic data sets by the bootstrap method.

5.3.4 Parameter correlation analysis

We calculated the correlation coefficients (Spearsman's rho) among the four estimated parameter by using the above obtained 5000 best fit parameter sets. We also plotted the four estimated parameters against each other for visualization (**Figure 5.3.5**). Correlation between k_{dephos}^{S2} and k_{on}^{Smads} was observed, this could explain the less constrained results of the above statistical analysis on them (**Table 5.3-4**).

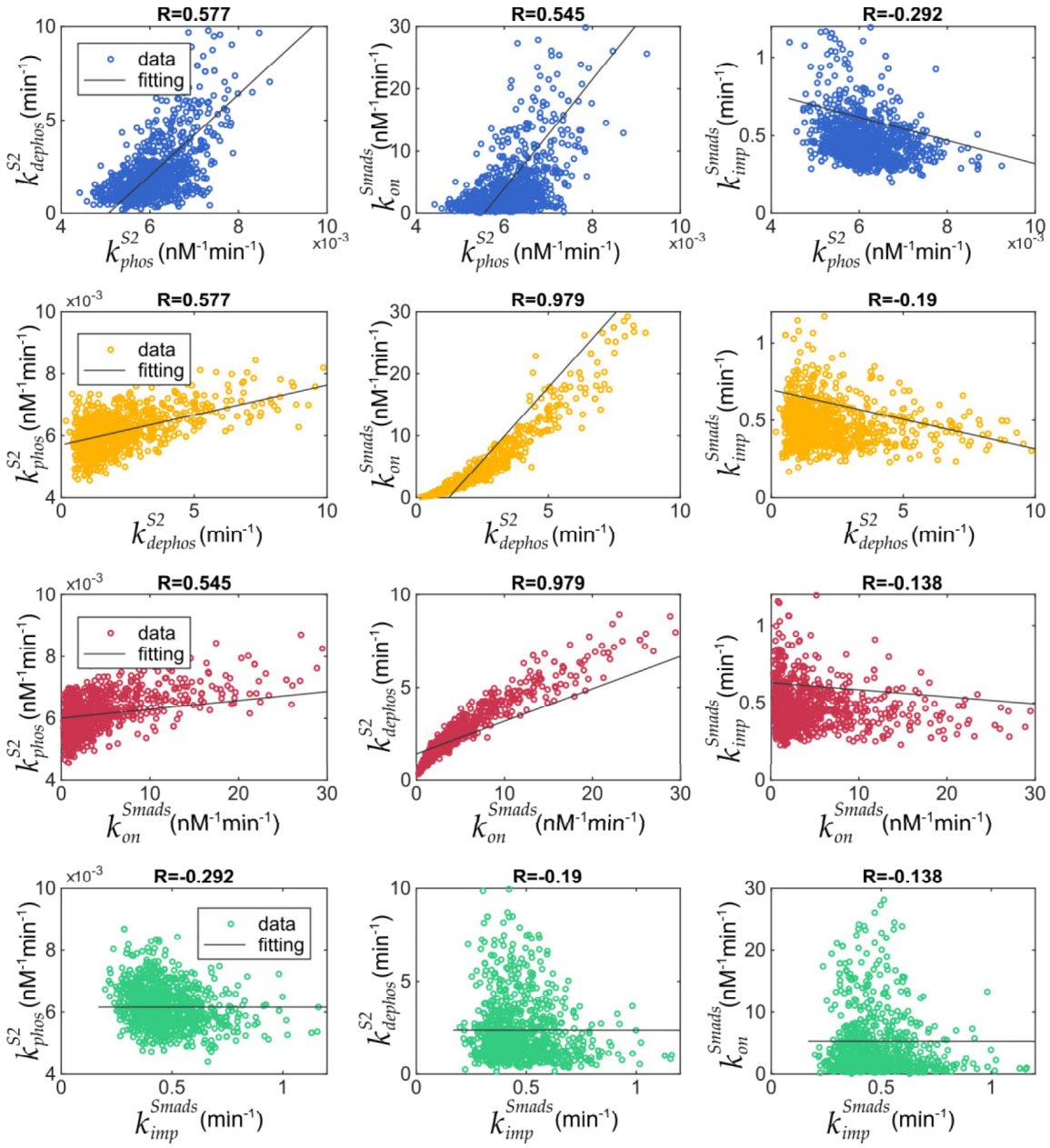

Figure 5.3.5 Parameter Correlation Analysis. The estimated parameters were plotted against each other by using the 5000 sets of best fit parameters obtained during the statistical analysis (section 5.3.3). Correlation between k_{on}^{Smads} and k_{dephos}^{S2} was observed.

5.3.5 Sensitivity analysis

Parameter sensitivity analysis is a measure for the magnitude of the effect on the system output by changing a specific parameter. For parameter sensitivity analysis, each parameter was varied and the corresponding change of the output was evaluated. Here we defined the maximal nuclear-to-cytoplasmic iRFP-Smad2 signal as the output. Therefore the scaled sensitivity coefficients are calculated as the following:

$$S_{p_i} = \frac{\frac{\partial(Smad2\_N2C)}{Smad2\_N2C}}{\frac{\partial p_i}{p_i}} \tag{16}$$

where $Smad2\_N2C$ is the maximal nuclear-to-cytoplasmic iRFP-Smad2 in response to a pulsed light stimulation; p_i denotes each individual parameters.

As shown in **Figure 5.3.6**, Smad2 signaling (N2C ratio of Smad2) is sensitive to the changes of k_{imp}^{S2}, k_{exp}^{S2}, k_{phos}^{S2} and $k_{diss}^{optoTRs}$, while it is relatively robust against changes of other parameters, especially, k_{imp}^{S4}, k_{exp}^{S4}, $k_{on}^{optoTRs}$ and K_M.

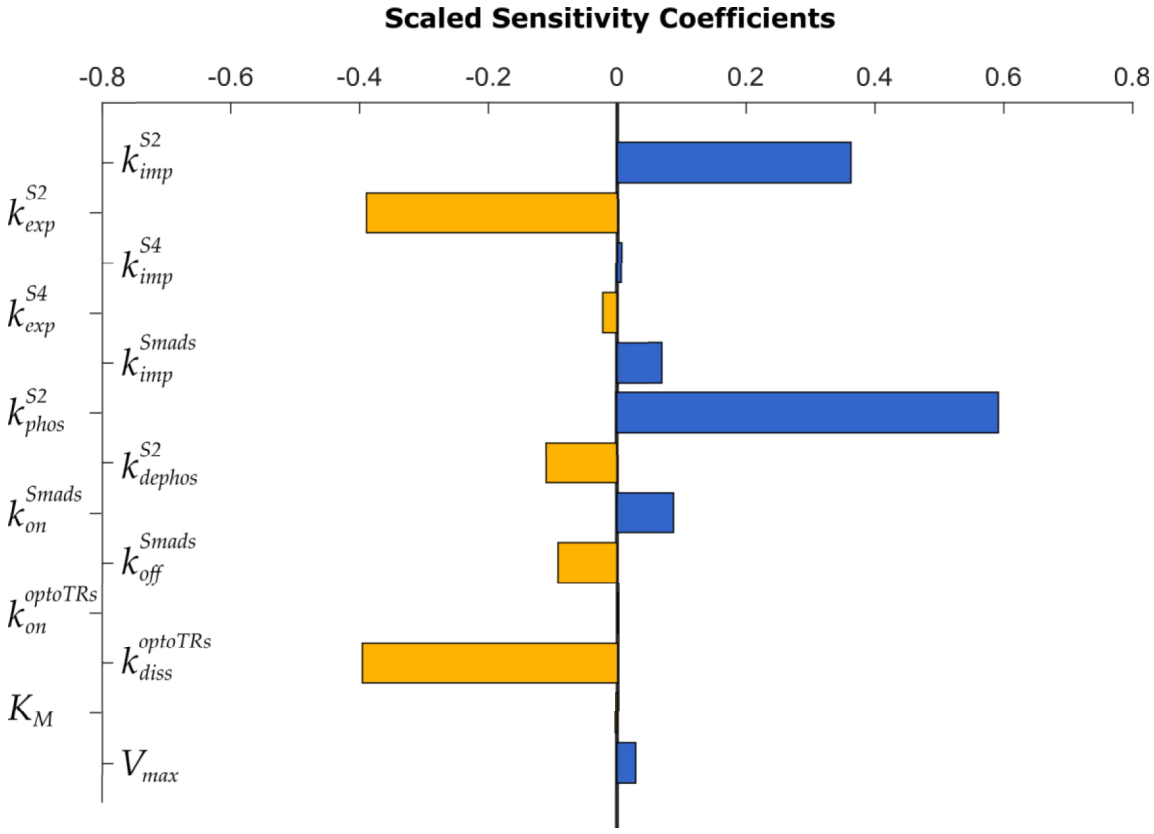

Figure 5.3.6 Sensitivity analysis of the parameters on Smad2 signaling response. Scaled sensitivity coefficients for the maximal N2C iRFP-Smad2 signal to variations of individual parameters.

5.4 Model performance

5.4.1 In-sample fit

To assess how good could the model fit the experimental data sets used in the procedure of parameter estimation, we checked whether model simulations could reproduce those data sets. Simulation results showed that the simulations were within the error bars for all the three different experimental conditions, indicating a good agreement between the model simulations and the experimental data that were used in parameter estimation (**Figure 5.4.1**).

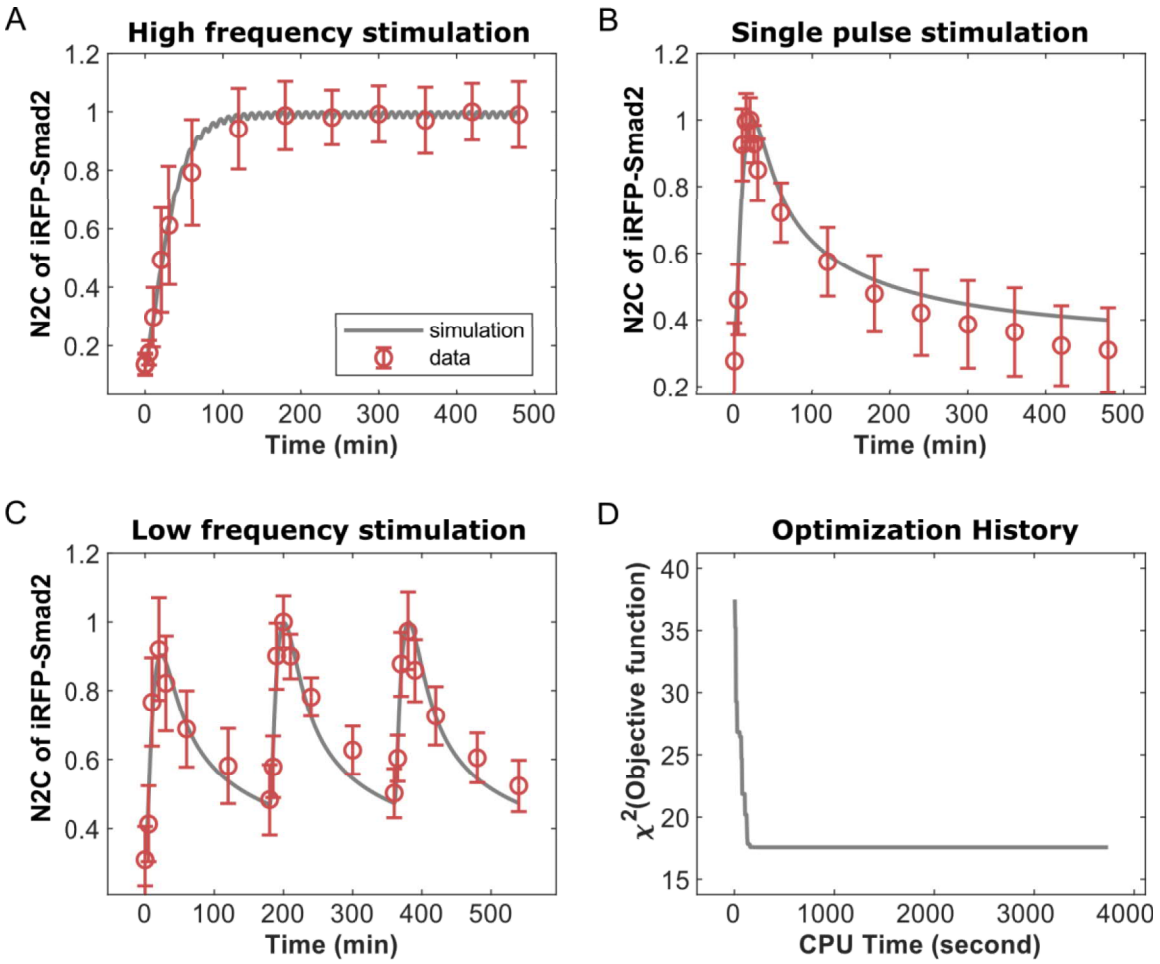

Figure 5.4.1 Comparisons of simulation results and the experimental data that were used for parameter estimation. Red circles with error bars denote the quantitative experimental data; the companioning grey curves denote the corresponding model predictions with the optimized parameters. Both the experimental data and model predictions were scaled by the maximum value in the respective data set. (A) Results of a frequent pulsed stimulation (1 pulse every 10 minutes). (B) Results of a single pulsed stimulation. (C) Results of a less frequent pulsed stimulation (1 pulse every 180 minutes). (D) Parameter optimization history.

5.4.2 Out-sample fit

To do model validation, we tested whether the model could also accurately predict Smad2 responses upon alternative stimulation patterns. We did new live-cell imaging experiments in which cells were stimulated by a short pulse of blue light in every one hour, or every two hours. Both the two experimental results agreed well with the corresponding model simulation results (**Figure 5.4.2**). Therefore, the model could successfully predict iRFP-Smad2 signaling behaviors of the optoTGFβ system upon various patterns of light stimulation.

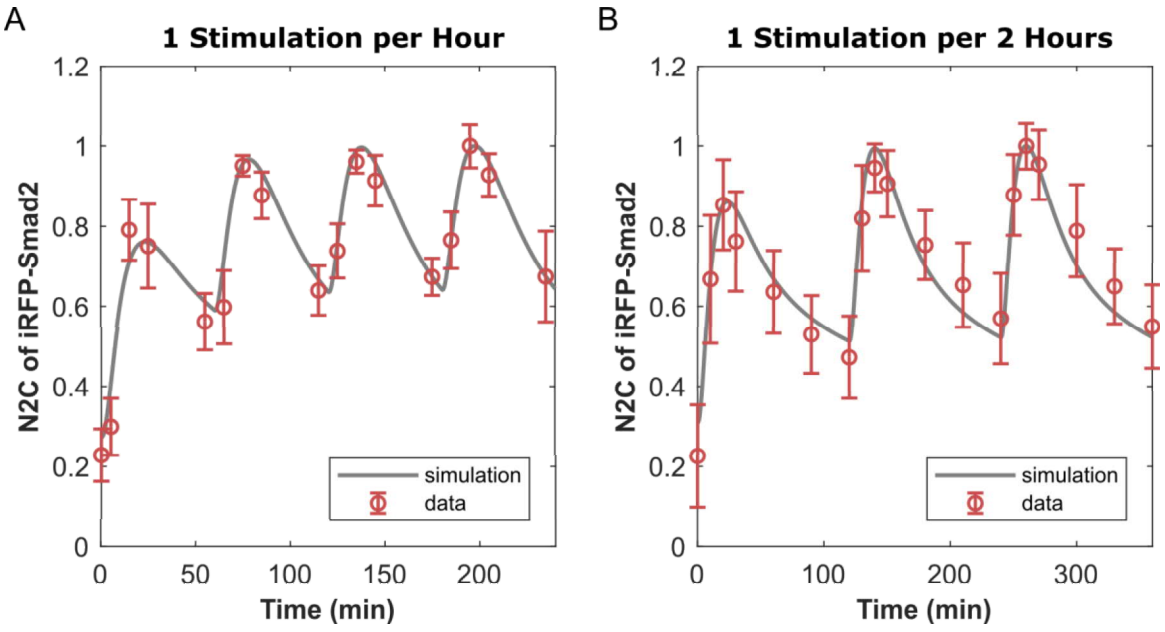

Figure 5.4.2 Comparisons of simulation results and the experimental data that were not used for parameter estimation. Red circles with error bars denote the experimental data; the companioning grey curves denote the corresponding model predictions. Both the experimental data and model predictions were normalized by the maximal value in the respective data set. (A) Results of experiments in which cells were stimulated by one pulse per hour. (B) Results of experiments in which cells were stimulated by one pulse per two hours.

5.4.3 Frequency responses of the optoTGFβ system

Continuous or frequent blue light irradiation would induce Smad2 activation that could be sustained for eight hours (**Figure 3.5.1** B & D). This indicates the absence of efficient negative feedback controls during this time range. In addition, below a certain intensity threshold, blue light with a higher intensity could induce a higher level of Smad2 phosphorylation (**Figure 3.5.2**). This suggests that an input with higher energy could trigger a stronger Smad2 response, as long as the input is within the unsaturation range. Since a higher frequency of pulsed

light stimulation means higher light energy being inputted during a defined time range (each single pulse has the same defined amount of energy), therefore, the higher frequency of pulsed light we implement, the higher level of Smad2 signaling we should observe.

To test if light stimulation with a higher frequency induces a stronger Smad2 response, we simulated Smad2 activities in response to various frequencies of pulsed light stimulation. To quantify the Smad2 response, we calculated both the amount of phosphorylated Smad2 (**Figure 5.4.3** A & B), and the N2C ratio of Smad2 (**Figure 5.4.3** C & D). As expected, below a threshold of ~10^{-2} Hz, higher frequency indeed triggered stronger Smad2 response, no matter in terms of the maximum level, or in terms of the cumulative level (the total accumulated signal, i.e., the area under the curve of signal dynamics).

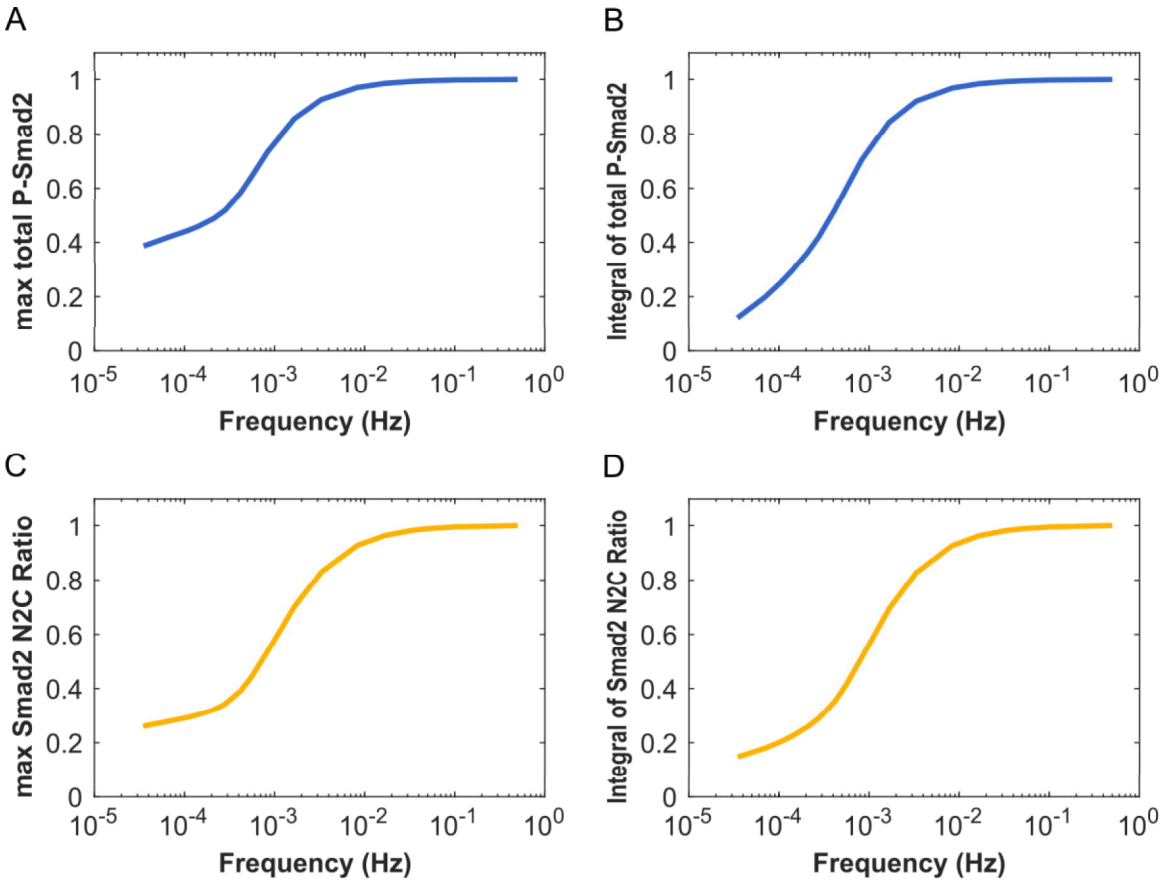

Figure 5.4.3 Frequency responses of the optoTGFβ system. The Smad2 activation responses were plotted versus pulsed light input frequencies. The responses were measured in terms of the maximum level of phosphorylated Smad2 (A), or the cumulative level of phosphorylated Smad2 during the first eight hours of stimulation (B), or the maximum level of Smad2 N2C ratio (C), or the cumulative level of Smad2 N2C ratio during the first eight hours of stimulation (D).

5.4.4 Parameter scanning for protein abundance

To explore the correlation between the signaling activity and the abundance of the involved proteins, we did parameter scan for the abundance of the four proteins: optoTβRII, optoTβRI, Smad2 and Smad4. For each protein, we set the scanning range to be between half of its measured concentration (minimum) and two-fold of its measured concentration (maximum).

First we ran simulations for single pulsed stimulation experiments, and used the time course of Smad2 N2C ratio as the readout of TGFβ signaling activity. Simulation results showed that the signaling activity varied a lot when scanning the abundance of optoTβRII (**Figure 5.4.4** A), but nearly stayed at the same level when varying the abundance of optoTβRI (**Figure 5.4.4** B). Similar results were observed for continuous stimulation experiments (**Figure 5.4.4** E-F).

The fact that the results of varying each of the two receptors are poles apart might arise from the inconsistent expression levels of the two chimeric receptors. Due to the longer sequence and thus larger conformation of the PHR domain in the optoTβRII construct, the expression level of optoTβRII is much lower than that of optoTβRI. Therefore, the pool of optoTβRI is always saturate with respect to the optoTβRII proteins. Varying the amount of optoTβRI in a certain range does not affect the signaling a lot, as long as it is in the range of saturation. In fact, concerning the protein expression levels in the optoHela cells in this study, optoTβRII is only ¼ of optoTβRI (**Table 5.3-1**). Therefore, the smallest value in the scanning range for optoTβRI abundance is larger than all the scanned values for the abundance of optoTβRII. Varying the optoTβRI abundance within this saturation range would certainly have little impact on the signaling. In contrast, the amount of optoTβRII is essential for determining the strength of signaling.

Interestingly, while increasing the abundance of either Smad2 or Smad4 could lift the signaling activation level under continuous stimulation conditions (**Figure 5.4.4** G-H), in the experiments of single pulsed stimulation, it lowered the signaling activity when raising the Smad2 abundance within a certain range (**Figure 5.4.4** C). This might be the consequence of adopting the N2C ratio of Smad2 as the readout. Upon the same intensity of light stimulation, (and within a certain range of Smad2 abundance,) less amount of Smad2 leads to less Smad2 remaining in the cytoplasmic compartment following signaling activation (i.e. higher depletion percentage of the cytoplasmic Smad2), which results in larger N2C ratio. In the continuous stimulation experiments, more and more cytoplasmic Smad2 could enter the nucleus before reaching a steady state, at which the N2C ratio is higher in the cells containing more Smad2. However, the total amount of phosphorylated Smad2 should not decrease when raising the Smad2 abundance under both stimulation conditions, which was confirmed by the same parameter scanning simulations.

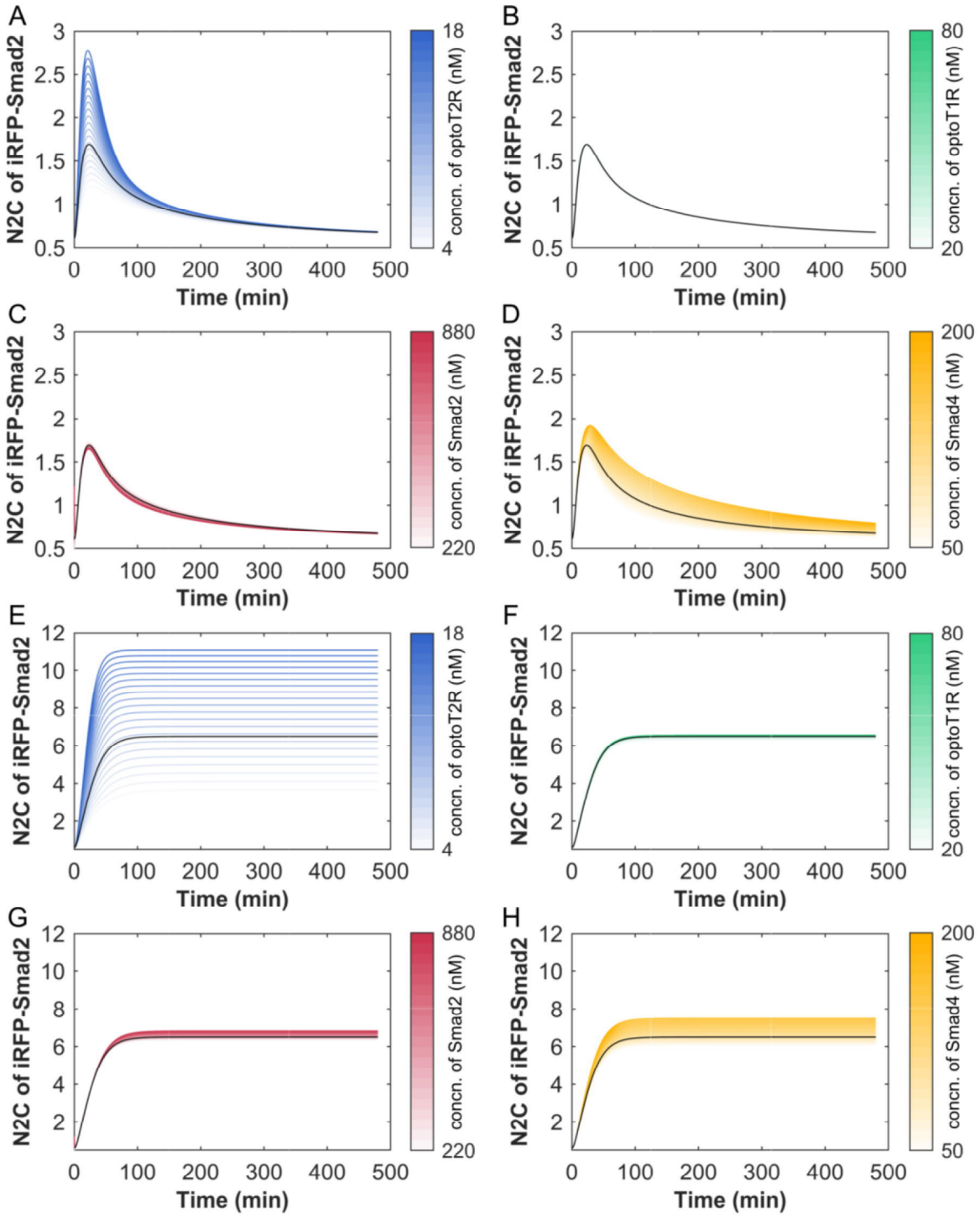

Figure 5.4.4 Results of parameter scanning for protein abundances. (A-D) Results for single pulsed stimulation; (E-H) Results for continuous stimulation. Curves represent the dynamics of Smad2 N2C ratio. The color of the curves codes the varied protein (blue, green, red or yellow denote varying the abundance of optoTβRII, optoTβRI, Smad2 or Smad4, respectively). The darker the color is, the more abundant the respective protein is. The black curves represent the simulation result without varying parameters.

5.5 Summary

In this chapter, we built a mathematical model on the chimeric optoTGFβ system by combining the two modules: the light-sensitive protein pair for controlling the activities of the receptors (optoTβRs), and the downstream Smad2 signaling network. This model is composed of 15 species, 17 reactions and 13 kinetic parameters (**Table 5.3-3**, **Table 5.2-1** and **Table 5.3-2** & **Table 5.3-4**, respectively). The initial concentrations of the involved proteins were inferred by comparing to that of their endogenous counterparts, which were in turn determined by referring to the public databases. Among the 13 kinetic parameters, 9 of them were determined by experiments or based on justifiable assumptions; the remaining 4 parameters were optimized by data fitting. The calibrated model could not only reproduce the data sets used for parameter estimation, but also predict dynamic behaviors of Smad2 under new stimulation conditions. By using the characterized properties (i.e. the kinetic parameter values) of the Smad2 signaling module, with additional data of signaling activation upon TGFβ ligand stimulation, it is possible to further infer the dynamic properties of the endogenous receptor module (e.g., ligand binding, receptor internalization and recycling, etc.) in the Hela cells.

6

General Discussion and Future Perspectives

In addition to the discussions following the above detailed results, here, I would like to make some general discussions regarding the entire project from the following perspectives: (1) We compared the optogenetic approach used in this project with other experimental approaches that are used for manipulating TGFβ signaling. We concluded that it is complementary to other approaches, and provides additional control of TGFβ signaling. (2) Combining with mathematical modeling, we found that optoTβRs are not internalized when activating TGFβ signaling in response to blue light irradiation, which suggests that endocytosis of TGFβ receptors is not necessary for Smad signaling. (3) We further discussed other explanations for the observations that light could induce faster and stronger TGFβ signaling. (4) We also discussed the higher precision of light stimulation, i.e., stimulation at the subcellular level. (5) We then talked about one of the primary advantages of the optoTGFβ system, isolating the signaling circuits specifically conducted by the two receptors (i.e., TβRI and TβRII), which facilitates better interrogation and control of TGFβ signaling. (6) We also discussed possible improvements and potential applications of the optoTGFβ system.

6.1 Comparison of the optoTGFβ system and other TGFβ signaling systems

Although traditional chemical and genetic approaches (e.g., small molecule inhibition, RNA silencing, genetic knockdown/knockout perturbations) have helped us manipulate TGFβ signaling, or identify the functions of key molecular mechanisms in regulating TGFβ signaling, these tools have common limitations. For instance, there might be potential off-target effects on cellular responses; it might be difficult to remove the chemicals, or reverse their effects when necessary; it is hard to control TGFβ signaling with high spatial precision by these approaches. Moreover, it has been shown that TGFβ ligands are internalized and degraded by the responsive cells[246,247]. The ligand depletion makes it difficult to control the dose of TGFβ ligand in the medium over time. The optoTGFβ system shows great advantages to overcome these problems, due to the technical specificities of the optical control. Compared with the traditional chemical treatment, the optoTGFβ system enables precise stimulation in thousands of patterns. More importantly, the optoTGFβ system can be used to control TGFβ signaling dynamics with high spatiotemporal precision at the single cell level, while it is hard to apply the classical biological tools to manipulate cell behaviors at the single cell resolution.

Another powerful and competing tool for precise signaling perturbation is the microfluidics technology. However, although temporal perturbation could be achieved conveniently in most contexts, precise spatial stimulation is still difficult to be implemented in the microfluidic systems. Presently, it only allows generating limited types of chemical gradient in the microfluidic channels, rather than implementing various patterns of spatially restricted stimulation. Besides, even for the temporal control, it is hard to implement sharp transitions of stimulation. When flushing the channels at high speed to implement a sudden change of input, unwanted responses might be induced, this could interfere with the experimental results. Furthermore, it is usually very expensive to build up a microfluidic system, or purchase commercially available equipment or devices, as it heavily relies on the advanced technologies of manufacturing microminiaturized devices. In contrast, with the advantageous properties of the light controllable optoTGFβ system, it is possible to apply any types of temporally and spatially restricted perturbations.

Therefore, although the optoTGFβ system could not completely replace the role of the endogenous TGFβ signaling machinery, it is complementary to other tools, and provides additional control of TGFβ signaling activity by facilitating various perturbations in time and space.

6.2 Endocytosis of optoTβRs is not necessary for Smad2 signaling

Instead of using the entire proteins of the endogenous TGFβ receptors, we only employed the cytoplasmic region of them to construct optoTβRs. This is consistent with the previous studies (**Figure 2.1.1**), and again confirms that neither the extracellular domain nor the transmembrane region of TβRs is indispensable for TGFβ signaling activation. As long as their cytoplasmic domains could be brought close enough to facilitate phosphorylation of TβRI by the constitutively activated TβRII, TGFβ signaling could be initiated. However, from the evolutional perspective, the extracellular domain is a rational design of the nature. For better adaptation and evolvement, cells need to communicate with each other or with their environment now and then, by responding to the numerous and specific types of cues. On the other hand, as an evolution product, plasma membrane functions as a protective wall surrounding all the machinery of a cell against the complex extracellular environment, and is only selectively permeable to the necessary materials for its survival. Not everything could enter the living cells easily. Even for the molecules that could really enter the cells, not all of them are transported through the same biophysical mechanism. TGFβ is a small protein, but much larger than small chemicals such as carbon dioxide (CO_2), ion, and even sugars or amino acids. Therefore, it can neither pass the plasma membrane freely by passive osmosis or diffusion, nor enter the cells by transmembrane proteins channels or transporters easily. Producing membrane receptors with extracellular domains specific to the TGFβ ligand structure is the most convenient and rational way to sense the TGFβ signal.

Upon ligand activation, the ligand-receptors complex (LRC) is internalized, which on the one hand facilitates signaling via the clathrin-dependent manner, on the other hand removes the signal via the lipid-raft-dependent manner (**Figure 1.2.7**). Penheiter et al. have shown that the internalization of LRC is necessary for Smad2/Smad3 activation and downstream signaling. However, this conclusion was based on the study of blocking internalization by low temperature treatment. The absence of Smads activation might result from a low temperature-dependent response, rather than a direct effect of non-endocytosis[248]. On the contrary, another study by depleting intracellular potassium or expressing a mutant dynamin suggested that receptor internalization is dispensable for TGFβ induced Smad2 activation[249]. The contrast between these two conclusions might arise from the differences between the specific cell lines they investigated on. Nonetheless, it didn't rule out the necessity of signaling taking place on the plasma membrane.

In the endogenous TGFβ signaling pathway, the plasma membrane participates in the signaling by engulfing LRC. How about in the optoTGFβ

system? As the Myr sequence was inserted randomly to the plasma membrane, it is not likely that light could trigger specific endocytosis of the activated receptors.

Although it is difficult to interrogate if the activated optoTβRs undergo endocytosis upon light activation, we could examine it easily by mathematical modeling (**Figure 6.2.1** A). In theory, under sparse pulsed stimulation conditions, it is difficult to distinguish whether internalization happens or not, as optoTβRII always returns from the plasma membrane following a pulsed stimulation, no matter it is internalized or not. However, under frequent stimulation conditions, if endocytosis exists, a certain portion of optoTβRI will be internalized and thus stay in the cytoplasm. Therefore the depletion of cytoplasmic optoTβRII upon the next light stimulation should decrease, which means there always exists a certain portion of optoTβRII in the cytoplasm throughout the experiment. On the contrary, if the activated optoRCs do not undergo endocytosis, all optoTβRI should stay on the plasma membrane, and the depletion of optoTβRII following each light pulse will always be complete. Therefore, we could easily distinguish whether internalization exists or not by frequent stimulation experiments.

To test this "thought experiment" by model simulation, we included the endocytosis processes in the model (**Figure 6.2.1** A), and performed parameter estimation as before (**Figure 6.2.1** B). The new model fit the data well. We next ran a simulation for a frequent stimulation experiment (one pulse in every 10 minutes), and found that indeed the bulk of optoTβRII kept staying in the cytoplasm after several minutes. Although the amount of cytoplasmic optoTβRII (including the inactivated optoTβRII, activated optoTβRII, and endocytosed optoTβRs complex) fluctuated in accordance with light stimulation, as time goes on, less and less optoTβRII would translocate onto the plasma membrane following each stimulation. Finally, from the 4th hour on, a plateau was reached where almost all optoTβRII kept staying in the cytoplasm (**Figure 6.2.1** C). According to this model prediction, we should observe a sharp decline of cytoplasmic optoTβRII to the lowest level after the first stimulation, and at least half of the total optoTβRII remaining in the cytoplasm from the second stimulation onwards.

However, it was not the case in reality. When we quantified cytoplasmic optoTβRII signal in the experiments with the same stimulation condition, it declined upon the first stimulation, but continued to decrease upon the following stimulations (**Figure 6.2.1** D). We also ran a simulation by assuming that internalization isn't involved in the optoTGFβ signaling, the localization of optoTβRII was consistent with the experimental observations (**Figure 6.2.1** D, grey curve). These results imply that the activated optoRCs do not undergo endocytosis upon activation. This suggests that endocytosis of TGFβ receptors is dispensable for Smad2 activation, which is consistent with the previous finding that Smad2 could still be activated in the absence of receptor internalization[249].

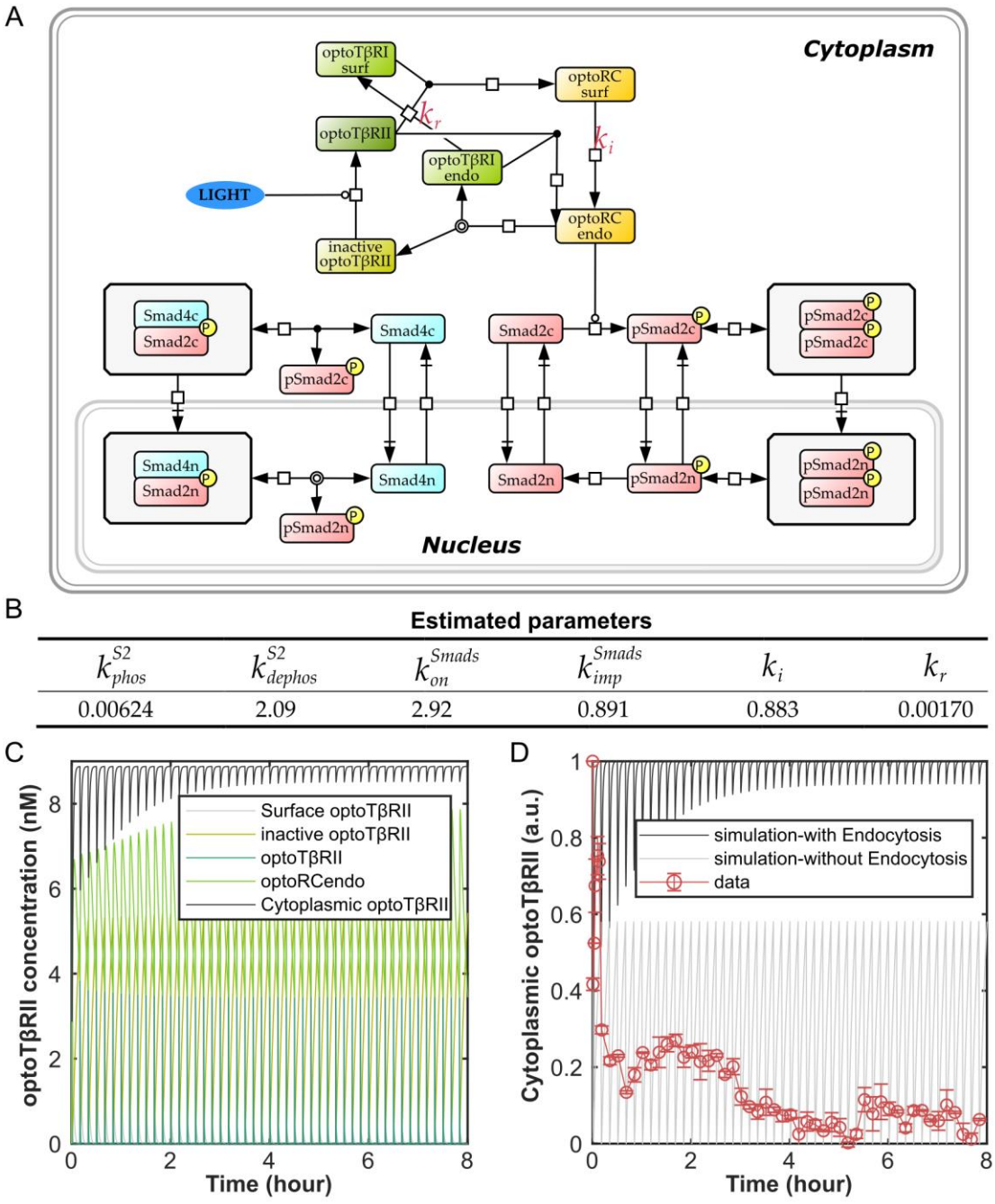

Figure 6.2.1 optoTβRs do not undergo endocytosis when activated. (A) Scheme of an optoTGFβ model involving receptor endocytosis processes. (B) Values of the estimated parameters. (C) Dynamics of different species containing optoTβRII upon frequent stimulation in model simulation. (D) Inconsistency between simulation (black curve) and image quantification (red circles). For comparison, simulation result based on the model (Figure 5.1.1) without endocytosis was also shown (grey curve). Note that compared with model simulations, experiments couldn't capture data continuously, therefore, only a few discrete data points were shown in the figure. optoHela cells were stimulated by one pulse of blue light in every 10 minutes, cytoplasmic optoTβRII signal (immediately after each pulsed stimulation) was quantified and compared with model predictions. Data were scaled between 0 and 1. k_i, receptor internalization rate; k_r, receptor recycling rate.

Experimental verification could be done by directly monitoring the localization dynamics of fluorescence-labeled optoTβRII or optoTβRI following light stimulations in a TIRFM (total internal reflection fluorescent microscopy), or by checking if optoTβRII has the same localization with endosome marker proteins such as the small GTPase Rab11[99,104] , clathrin adaptor protein DAB2[105] or subunits of the clathrin-associated adaptor complex AP2[91]. Furthermore, as optoTβRI is hung on the inner side of the plasma membrane, and the activation of the optoTGFβ system is through the translocation of cytoplasmic optoTβRII to the plasma membrane, we still cannot exclude the necessity of the plasma membrane for activating the TGFβ type I receptor.

6.3 Light induces faster and higher level of TGFβ signaling

Compared with TGFβ ligand stimulation, blue light stimulation could induce faster and stronger iRFP-Smad2 signaling (Section *4.3.2*). One of the possible explanations might be the faster kinetics of receptor interaction and activation in the optoTGFβ system. It might also result from the amount of the receptors that actually mediate the signaling. According to the previous studies on the endogenous TGFβ signaling pathway[108,136], only around 10 percent of TβRI is on the cell surface. This plasma membrane localized portion of TβRI is the functional pool, which directly perceives TGFβ ligands and participates in the TGFβ signaling activation. In this surface pool of TβRI, only around 40 percent is activated in the first hour, even in response to a saturating dose of TGFβ stimulation[136]. However, in the optoTGFβ system, almost the entire ensemble of the chimeric receptor pool could be activated upon light activation, resulting in a higher saturation level of receptor activation. This indicates that, we could possibly expand the response regime and functionality of TGFβ signaling with the optoTGFβ system.

There are also possibilities that optoTβRII also phosphorylates and activates the endogenous TβRI following light activation, which further increases the level of activated type I receptors. However, the possibility is very low. On the one hand, a typical Hela cell has a diameter of 20 microns[235], corresponding to a surface area of over 1000 um^2; a ~70 kDa size optoTβRI is a protein whose diameter is less than 6 nanometer[250], and an endogenous TβRI is ~50kDa thus even smaller. Therefore the size of TβRI or optoTβRI is very small relative to the entire plasma membrane. On the other hand, the estimated protein expression level of the endogenous TβRI in a Hela cell is around 16 ppm (parts per million) [237,251], which is higher than the optoTβRI expression level according to the western blotting experiment in our study (**Figure 2.4.3**). By assuming these proteins are evenly distributed on the plasma membrane, and knowing the total number of proteins in a Hela cell is ~ 10^10[238], we could estimate the numbers of optoTβRI

and the endogenous TβRI on the plasma membrane are around 86000 and 16000 molecules, respectively. Considering the large area of the plasma membrane, and the small volume of these proteins, this calculation suggests that both optoTβRI and the endogenous TβRI locate sparsely on the plasma membrane. Therefore, an endogenous TβRI could be activated upon light stimulation only if it happens to reside close to one of the sparsely distributed optoTβRI, whose probability is very low. In addition, a previous study showed that integrin-rich focal adhesions organize TβRII around a segregated pool of TβRI, and immobilize TβRI at these sites[252]. This further implies that TβRI is very unlikely to stay close to optoTβRI. Therefore, although it might occasionally happen that a light-activated optoTβRII phosphorylates an endogenous TβRI, the possibility would be very little.

Light could induce stronger Smad2 activation, which is the upstream step of the TGFβ signaling pathway. It is highly possible that the downstream TGFβ responses are also affected, including the various targeted transcriptional activities, and the non-canonical TGFβ signaling circuits. By lifting the maximal level of upstream receptor activation as well as facilitating the stimulation input control, various cellular responses could be modulated easily with the optoTGFβ system, and even novel responses could possibly be developed.

6.4 Stimulation precision at the subcellular level

When demonstrating the spatiotemporal control of the optoTGFβ system (**Figure 4.1.1**), although we irradiated cells only at a specific small region within the cell (yellow circles), Smad2 translocated into the nucleus evenly from every direction. This might be due to the imprecision of stimulation, or the rapid diffusion of activated Smad2 throughout the cytoplasm. The imprecision of stimulation might be in turn due to the technical limitation of the laser source, or the inherent scattering of light by the materials it passes through (such as air, plastic, cell culture medium or cell biomass). Thus the entire collection of optoTβRII in the cell was activated simultaneously. Although this imprecision is trivial in most studies, it is still important to improve it for generalizing the application of the optoTGFβ system to a wider range of studies.

The stimulation precision at the subcellular resolution is essential in some contexts, such as studies on cell polarity. Studies on polarized epithelial cells have revealed that the TGFβ receptors are exclusively basolateral at high cell density, which prevents Smad signaling by apical TGFβ [253,254]. Loss of polarity was observed during early carcinogenesis, which may lead to TGFβ mediated EMT[255,256] and cancer cell dissemination[257,258]. However, the detailed molecular mechanism is still not clear. It was quite difficult to precisely control polarized signaling activation and to untangle the role of polarity in carcinogenesis. Now the optoTGFβ system sheds light on solving this problem. By improving the

stimulation precision, subcellular TGFβ signaling control could be realized, which could benefit the field of studies on cell polarity.

In addition, single cell mathematical models have been developed to explore the spatial intercellular signaling. A lot of interesting characteristics were predicted on unbalanced signaling transduction in individual cells[259-263]. However, some direct evidences from biological experiments are still difficult to achieve. Now the optogenetics shows great potential as a new yet powerful approach to validate those single cell model predictions.

The desire for subcellular controllable tools raises the question of how to improve the precision of optical control. There are several ways, from the technical aspect to the manipulation perspective. On the one hand, technical imprecision is mainly caused by the transmission medium or light source. Therefore technical precision could be increased by methods such as replacing the plastic slices with glass ones[264]. Multi-photon excitation is an alternative option due to its more confined region of excitation at the focal plane, compared with single-photon excitation[265]. Finer spatial stimulation could also be realized by DMD (digital micro-mirror device), which is composed of an array of microscopic mirrors that can be toggled individually to project any pattern of light. On the other hand, the input pattern of irradiation should be precisely controlled. For example, when precise and predictable control of optoTβRII is necessary, pulsed light stimulation is better than continuous illumination with comparable light energy[215]. There are several reasons. First of all, it limits unnecessary light irradiation on cells. If a short pulse is enough to activate all the light-sensitive proteins that present in the illumination volume, further illumination is redundant. Even if new inactivated light-sensitive proteins might diffuse into this illumination volume, most of the proteins in this illumination volume are already activated. Second, pulsed illumination avoids considering diffusion, which is hard to be predicted, and thus increases the predictability and reproducibility of the experiments. Third, pulsed illumination allows protein interactions to reset and be re-activated, which might improve the activation efficiency. For instance, in the optoTGFβ system, the reset of optoTβRII enables it to activate more optoTβRI upon the following pulsed stimulations. Usually, the ideal length and intensity of light stimulation are necessary to be optimized before experiments. It should be short but strong enough to activate all the light-sensitive proteins in the illumination volume, but should avoid diffusion and replenishment with inactive proteins.

By improving the stimulation precision, it is possible to apply the optoTGFβ system to manipulate TGFβ signaling at a specific subcellular region, which would benefit future studies at the subcellular level.

6.5 Dissection of the two receptors by the optoTGFβ system

In this study, we focused on the TGFβ signaling specifically triggered by ligands of the TGFβ subfamily, which is only a branch of a large TGFβ superfamily. Although members of the TGFβ superfamily employ similar molecular mechanisms for signaling activation, each member has its unique binding affinities and activities, and thus implements distinct tasks in various cell types or different developmental stages. Examples of the TGFβ superfamily ligand are BMPs, Activin, Nodal, TGFβ, GDFs and AMH. To specifically perceive these ligands, there is a family of receptors, including various type I receptors and a series of type II receptors. Among them, the human genome encodes seven and five different type I and type II receptors, respectively. Despite the binding specificities of the ligands, some of the ligands could bind and activate multiple receptors (**Figure 1.2.3**). For example, besides binding to TβRI/TβRII to trigger the Smad2/Smad3 pathway, TGFβ ligands could also bind to ALK1/TβRII to activate the Smad1/Smad5/Smad8 pathway[26,65,126]. The employment of receptors in the TGFβ superfamily signaling can also overlap. TβRI could be interacted and activated by other type II receptors than TβRII, such as ActRIIB[266,267]. In the optoTGFβ system, the specific interaction between PHR and CIBN induces the specific binding between optoTβRI and optoTβRII, which originate from TβRI and TβRII, respectively. This avoids interference from signaling through other receptor pairs (e.g. ALK1/TβRII), which could also be induced by TGFβ ligands. Hence we could focus only on the TGFβ signaling transmitted through the TβRI/TβRII receptor pair.

Besides, the endocytosis process involved in the endogenous TGFβ signaling further complicates the signaling pathway, which subjects the signaling to more delicate and elaborate regulations. However, this also makes it difficult to interrogate the properties of the pathway, especially when applying mathematical modeling methods on it. The optoTGFβ system simplifies the signaling process by excluding the endocytosis steps. Without endocytosis, which is subject to numerous regulations, TGFβ signaling in the optoTGFβ system could therefore be manipulated in a more predictable way. Mathematical models built on it are also easier to be calibrated. Moreover, it is also possible to compensate for the absent signaling regulations through precisely controlling the light stimulation pattern.

Furthermore, when diving into the TGFβ ligand subfamily, there are mainly 3 different isoforms of TGFβ: TGFβ1, TGFβ2 and TGFβ3. They differ in their coding gene's sequences[268,269], chromosomal localizations[270-272], and their protein conformations, which lead to their differential biological activities[32,273,274]. Due to their unique physiological activities[275], as well as their tissue-specific expression levels[276], all the isoforms are indispensable in vivo, which was confirmed by the knock-out/null-mutation studies: TGFβ1 null mutation in mice could lead to

inflammatory diseases or early death[277,278]; TGFβ2 knock-out mice have distinctive developmental defects[279]; mice lacking TGFβ3 exhibit cleft palate which results from failures in secondary palate fusion[280]. In addition, gene replacement studies on the three isoforms showed partial rescue of the null-mutant defective phenotypes[281,282], which implies both their redundant and non-overlapping functions. Nonetheless, they all signal through the same pair of receptors (TβRI/TβRII), which means that this pair of receptors could discern and transmit different information to downstream effectors via different activities of themselves. The conveniences of the optoTGFβ system could help to elucidate how exactly the receptors differentially mediate these signals, for example, through manipulating the dynamics of receptor activation to mimic the activities induced by the specific isoform, or to rescue the null-mutant phenotypes. Eventually, the same optoTGFβ system could be placed into specific tissues to implement unique functions by modulating light stimulation in vivo.

Taken together, the optoTGFβ system dissects and isolates the two specific receptors from their isogenous counterparts, which could not only overcome the complexity of regulations on the ligand perceiving process (i.e., from ligands binding, until receptor activation), but also help to identify the differences among the signaling induced by different TGFβ isoforms. Endocytosis of activated receptors is also absent in the optoTGFβ system, which not only confirms the dispensability of it, but also facilitates investigation and mathematical modeling. In summary, these simplifications in the optoTGFβ system could help us better investigate the signaling pathway, and implement more predictable controls on it.

6.6 Possible improvements of the current optoTGFβ system

The current generation of the optoTGFβ system still has some limitations and could be further optimized for studying and manipulating the TGFβ signaling. For example, optoTβRI, optoTβRII and iRFP-Smad2 proteins are constitutively overexpressed with exogenous promoters. In the future, it would be useful to replace their endogenous counterparts with these chimeric proteins, thus express these proteins from their endogenous promoters by approaches such as the CRISPR/Cas9-mediated knock-in technology[283,284]. Such a version of the optoTGFβ system would be valuable for studying the TGFβ signaling under conditions more close to the physiological state. An alternative design is to control the expression of these chimeric proteins at different levels through using inducible gene expression systems. Furthermore, because of the multi-functional property of the TGFβ signaling, it would also be interesting to investigate the spatiotemporal control of downstream responses, by expressing reporters for specific TGFβ responsive genes, or markers of specific TGFβ dependent cellular responses.

6.7 Potential application of the optoTGFβ system

Although the function of TGFβ signaling is versatile and context dependent, the signaling engine is essentially the same one. Therefore, the optoTGFβ system is potential for studying the TGFβ signaling at various levels.

In the optoTGFβ system, iRFP-Smad2 is co-expressed to indicate the downstream Smad signaling in single cells. This property allows us to simultaneously monitor the dynamics of both receptor and Smad activation at the single cell level. This could help us establish quantitative relationships between the upstream TGFβ receptor activity and the downstream Smad signaling, which would facilitate quantitative modeling of the canonical TGFβ signaling pathway.

In addition, benefited from its convenient way of stimulation implementation and data acquisition, the optoTGFβ system has great potential to help us investigate how cells respond to complex signals, such as repeated pulses of signal inputs, increasing input ramp or noisy signal inputs[136,232,285]. Mathematical models of the signaling pathway could then be developed or calibrated more precisely and efficiently. In such ways, the TGFβ signaling could be better characterized, and even new functions of TGFβ signaling might be revealed.

Besides the canonical TGFβ signaling, quantitative studies on non-canonical signaling (Section *1.2.2*) could also be facilitated by modulating light input and observing specific outputs with the optoTGFβ system. For instance, for cells undergoing EMT, in addition to the transcriptional effects of the canonical TβRI-Smad pathway[256,286], the activated TβRII directly phosphorylates PAR6, which recruits SMURF1 to induce RhoA degradation, followed by dissolution of tight junctions as well as polarized migration[287,288]. By expressing optoTβRs and additional signaling reporters in these epithelial cells, each of these steps could be conveniently and quantitatively studied. In the end, the processes of EMT might even be harnessed by simply modulating the light input. Crosstalks of TGFβ signaling with other signaling pathways such as MAPK[289] and PI3K[290,291] pathways could also be interrogated, the biochemical links that might play crucial roles in some pathological processes[292,293] could then be identified.

Furthermore, the optoTGFβ system could be potentially generalized to other receptor-multimerization-dependent signaling pathways. Especially, the basic design of the optoTGFβ system can be adopted to build light controllable signaling systems for other branches of the TGFβ superfamily signaling. Some members of the TGFβ superfamily regulate important biological processes such as morphogen gradient formation and embryonic development. For these processes, it is essential to precisely control the temporal and spatial distribution of signaling activation. A recent study adapted the light-oxygen-voltage (LOV) optogenetic module to develop a photoactivatable Nodal receptor pair, Opto-

acvr1b and Opto-acvr2b, for activating Nodal signaling[220]. In this Opto-acvr1b/2b system, both types of the Nodal receptors were expressed at the plasma membrane by injecting zebrafish embryos with their mRNAs. This Opto-acvr1b/2b system was helpful and adequate to elucidate the pivotal role of Nodal signaling duration for cell fate specification at the population level. However, as the two types of receptors were not differentially labeled in this system, it is not convenient to monitor the expression level or the dynamics of the upstream Nodal receptor signaling in single cells.

Compared with the Opto-acvr1b/2b system, the optoTGFβ system differentiates the two types of receptors: optoTβRI is attached to the plasma membrane, while optoTβRII is expressed in the cytoplasmic region and tagged with a fluorescent protein. On the one hand, the spatial separation of optoTβRI and optoTβRII could avoid a high level of basal TGFβ signaling before perturbation. On the other hand, as the subcellular localization of optoTβRII can be changed upon light irradiation, the optoTGFβ system is able to report the activities of the TGFβ receptors by visualizing the formation and dissociation of the receptors complexes. Therefore, compared with the design of the Opto-acvr1b/2b system, our optoTGFβ system allows monitoring and charactering the dynamics of the TGFβ receptors, which would help to discover their quantitative relationships with the upstream signal input patterns, and with the various downstream responses in single cells. Since other branches of the TGFβ superfamily signaling (e.g. BMPs, Activin, GDFs, etc.) also employ the receptor-multimerization strategy to initiate signaling, the optoTGFβ system could be easily generalized to these signaling pathways.

Last but not least, due to the important roles of TGFβ signaling in various pathological processes, the optoTGFβ system is also a latent tool for medical application. Its spatiotemporal precision property makes optogenetics a promising and superior approach for targeted therapies. The earlier growth of photosensitive neuronal switches has promoted the evolvement of therapeutic strategies for in vivo manipulation with light[294-300]. In vivo perturbations of cellular behavior or metabolic activities have also been achieved in cells other than neurons[301-304]. Even clinical trials for a few optogenetic therapies have been launched in recent years[305,306]. All these strategies could be adopted for the in vivo application of the optoTGFβ system. For instance, gene delivery of optoTβRs to specific cells or tissues could be implemented by viral vectors or in vivo transfection such as PEI-mediated transfection. Multi-site, as well as customizable patterns of light stimulation could be delivered through implantable laser-coupled fiber optics or μLED probes. Cellular activities regulated by TGFβ signaling could thus be controlled, and the related signaling circuits could be logically rewired to achieve targeted therapy. Despite the present technical limitations, realistic perspectives are quickly emerging.

6.8 Summary

The multifunctional property of TGFβ signaling makes it an intriguing target for investigation. However, the lack of tools to control this pathway limits our understanding of it. In this thesis, we developed a light controllable TGFβ signaling system (the optoTGFβ system) by fusing light-sensitive proteins to the TGFβ receptors, and using fluorescence labeled Smad2 as the signaling indicator. After successfully establishing cell lines expressing the optoTGFβ system, we characterized it from various aspects, and compared it with the endogenous TGFβ signaling system. We found that the optoTGFβ system mimics the endogenous TGFβ signaling upon light stimulation, but has more flexibility through expanding the extent of signaling activation. In addition, we demonstrated the spatiotemporal controllability of the optoTGFβ system at the single cell level. By building a mathematical model on the optoTGFβ system, we not only better characterized it, but also equipped it with a computational tool for further investigation, and confirmed the dispensable role of endocytosis for Smad signaling. Altogether, the spatial and temporal precision of optical control allows the optoTGFβ system to work as not only a novel analytical tool for disentangling TGFβ signaling in various studies, but also a potential therapeutic tool for TGFβ signaling related diseases.

7

Materials and Methods

7.1 Plasmids preparation

To generate the light-inducible TβRs system, we used the sequence encoding the photolyase homology region of cryptochrome 2 (PHR, amino acids 1-489) that was codon optimized for mammalian expression[307], and the N-terminal part of CIB1 (CIBN, amino acid 1-147) from Arabidopsis thaliana[170]. The PCR-amplified sequence encoding CIBN was cloned into pmCerulean-C1 vector (Clontech), which resulted in a plasmid encoding CIBN-mCerulean. The myristoylation sequence of Lyn (amino acids 1-11) was added to the N-terminus of CIBN, and the cytoplasmic region of mouse TβRI (amino acids 148-502) was inserted between the myristoylation sequence and CIBN. To generate optoTβRI (Myr-cytoTβRI-CIBN), the mCerulean sequence was deleted and blunted with Klenow enzyme. The optoTβRII (cytoTβRII-CRY2PHR-tdTomato) construct was generated by inserting sequence encoding PHR into the pmCitrine-C1 vector (Clontech). mCitrine was replaced with tdTomato and the cytoplasmic region of mouse TβRII (amino acids 190-567) was cloned into the N terminus of PHR. Finally, we generated a pLNCX2-optoTβRs plasmid by combining optoTβRI (Myr-cytoTβRI-CIBN) and optoTβRII (cytoTβRII-CRY2PHR-tdTomato) with 1:1 ratio using a P2A bicistronic linker sequence (**Figure 7.1.1** B). The piRFP682-N1 plasmid was a gift from Vladislav Verkhusha (Addgene, #45459)[223]. To generate the iRFP682-C1 plasmid, the mCitrine sequence in the pmCitrine-C1 vector was replaced with the FP-encoding sequence from the piRFP682-N1 plasmid. For the construction of iRFP682-Smad2, cDNA encoding Smad2 was amplified and inserted to the piRFP682-C1 plasmid. The iRFP682-Smad2 was then amplified and replaced the EYFP-Smad2 of pREX-EYFP-Smad2-IRES-BSD (a gift from Xuedong Liu) to generate the pREX-iRFP682-Smad2-IRES-BSD for retroviral transfection (**Figure 7.1.1** A).

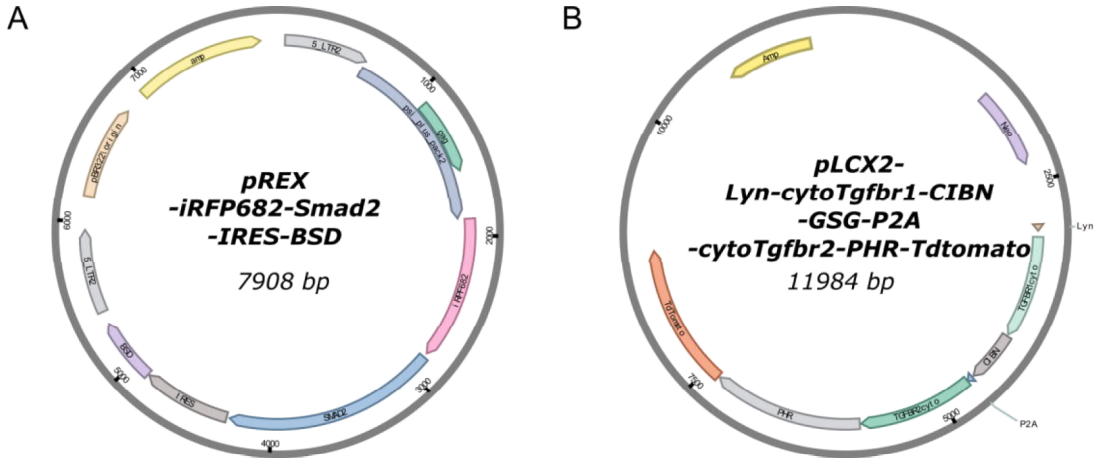

Figure 7.1.1 Brief maps for retroviral plasmids in this project. (A) The plasmid encoding the iRFP682-Smad2 protein. (B) The plasmid of the optoTβRs proteins: Myr-cytoTβRI-CIBN (optoTβRI), cytoTβRII-CRY2PHR-tdTomato (optoTβRII).

7.2 Cell culture, TGFβ stimulation, and transient transfection

Hela cells (American Type Culture Collection) or Human keratinocytes (HaCaT) were cultured in Dulbecco's Modified Eagle Medium (Lonza, Catalog #BE12-707F) or (GIBCO, Catalog #12800-082), respectively, with 10% fetal bovine serum (Merck Biochrom, Catalog #S0615), 2 mM L-Glutamine (Gibco, Catalog #25030-024), 100 units/mL penicillin and 100 µg/mL streptomycin (Gibco, Catalog #15140-122) at 37°C and in 5% CO2.

For handling cells expressing optoTβRs, ambient light should be avoided. All the operation steps were performed under red LED light (OSRAM).

For TGFβ stimulation experiments, cells were seeded 24 h before treatment with TGF-β1 (R&D Systems, 240-B-002). TβRs inhibitor LY364947 (Merck, Catalog #L6293) was added 2 hours before TGFβ treatment at a final concentration of 2.5 µM.

For transfection experiments, cells were seeded one day before transfection. After incubation overnight, cells were transiently transfected using Lipofectamine 3000 (Invitrogen) following the manufacturer's protocol. Transfected cells were incubated for at least 24 hours before experiments.

7.3 Stable cell line generation

We first generated cell lines stably expressing optoTβRI (Myr-cytoTβRI-CIBN) and optoTβRII (cytoTβRII-CRY2PHR-tdTomato) proteins. The packaging HEK293T cells were plated onto 60 mm dishes to be ~ 30% confluent at transfection. After 24 hours, the optoTβRs encoding plasmid pLNCX2- optoTβRs, as well as the pCL-Ampho Retrovirus packaging vector plasmid (a gift from Xuedong Liu) were co-transfected into the HEK293T cells using Lipofectamine 3000 (Invitrogen, Catalog # L3000001) following the manufacturer's protocol. Medium containing retroviral particles was filtered through a 0.45µm syringe filter (Carl Roth, Catalog #XH43.1) 48 hours after transfection. Viral supernatant was used immediately for retroviral transduction, or kept at −80 degrees for storage.

For retroviral transduction, the filtered supernatant was mixed with a final concentration of 8µg/ml of Polybrene (Merck Chemicals, Catalog #TR-1003-G) before added to the target Hela or HaCaT cells (~ 30% confluency at transduction) in 100mm dishes. Infected cells were transferred to T75 flasks (Greiner bio-one, Catalog # 658175) upon confluent, and then either treated with corresponding antibiotics for 2 weeks until clonal isolation, or enriched for successfully transduced cells by FACS. The selected clonal cell line was confirmed by live cell imaging. We then generated the cell lines stably expressing both optoTβRs and iRFP682-Smad2 by stably transfecting the plasmid pREX-iRFP682-Smad2-IRES-

BSD into the aforementioned cells (stably expressing optoTβRs) using a similar approach.

7.4 Fluorescence-activated cell sorting (FACS)

Cultured cells were trypsinized and suspended in phenol-red free DMEM (Gibco, Catalog #31053-028 and #11880-028 for HaCaT and Hela, respectively) at a concentration of ~ 1 million cells per 1 ml. All the samples were measured by BD FACS Aria II flow cytometer (BD Biocsiences, San Jose, USA). 561nm laser and 583/22-25 filter were used for tdTomato, 633nm laser and 670/14 filter were used for iRFP682. The data was analyzed by the FACSDivaTM software Version 6.1.3.

When sorting cells, Plasmocin ™ Prophylactic (InvivoGen, Catalog #ant-mpp) was supplied at a final concentration of 5 μg/ml for the prevention of mycoplasma contamination.

7.5 Cell lysate preparation and western blot

~1.5×10^6 cells were seeded in 60mm dishes (Greiner bio-one, Catalog # 628160) 24 h before TGFβ stimulation or photoactivation in the LEDs illumination box. Samples were taken out of the incubator after indicated stimulation conditions and washed by ice-cold DPBS (Gibco, Catalog #14190-094) twice before cell lysate preparation.

Cells were lysed in RIPA buffer (Cell Signaling, Catalog #9806), supplemented with 1 mM PMSF, 1 mM NaF, protease inhibitor cocktail (Roche, Catalog #04 693 132 001) and phosphatase inhibitor cocktail (Roche, Catalog #04 906 845 001). Protein concentrations were determined by using the Pierce BCA protein assay kit (Thermo Scientific, Catalog #23225) and a Infinite® F50 Absorbance Microplate Reader (Tecan Trading AG) according to the manufacturer's instructions.

SDS–PAGE gels were transferred onto nitrocellulose membranes. The following primary antibodies were used in this work: Phospho-Smad2 (Ser465/467) primary antibody (Cell Signaling, Catalog #3108) with a dilution of 1:500, Smad2 primary antibody (Cell Signaling, Catalog #3103) with a dilution of 1:1000, β-Actin primary antibody (Cell Signaling, Catalog #3700) with a dilution of 1:10000, optoTβRI primary antibody (Cell Signaling, Catalog #3712) with a dilution of 1:500, optoTβRII primary antibody (Santa Cruz, Catalog #sc-400) with a dilution of 1:200. All the primary antibodies were incubated overnight at 4°C. Secondary antibodies used for western blot were anti-rabbit IgG (H+L) DyLight

800 4X PEG Conjugate (Cell Signaling, Catalog #5151, dilution: 1:15000) and anti-mouse IgG (H+L) DyLight 680 Conjugate (Cell Signaling, Catalog #5470, dilution: 1:15000). Western blot images were acquired using the Odyssey CLx Imaging System (LI-COR Biosciences, Catalog # 9140) and the data was analyzed in the Image Studio Lite Ver 4.0.

7.6 Immunofluorescence

Cells were seeded in the μ-Slide 8 Well (ibidi, Catalog #80826) and incubated overnight. Samples were taken out of the incubator after indicated stimulation conditions and washed by DPBS (Gibco, Catalog #14190-094) for three times followed by fixation in 4% PFA for 10 minutes. Permeabilization was performed with pre-chilled 100% methanol for 10 minutes after another DPBS washing (three times). Samples were blocked in PBS Fish Gel (ROCKLAND, Catalog #MB-066-0100) overnight at 4°C. The primary antibody used in this work: Smad4 primary antibody (SANTA CRUZ, Catalog # sc-7966) with a dilution of 1:100. The secondary antibodies used for immunofluorescence were the Anti-mouse IgG (H+L), F(ab')2 Fragment (Alexa Fluor® 488 Conjugate) (Cell Signaling, Catalog # 4408, dilution: 1:500). Images were acquired using a Plan-Apochromat 40 x/0.95 Korr Ph 3 M27 objective (Zeiss, Catalog # 420661-9970) mounted on a Zeiss Axio-Observer Z1 fluorescence microscope. The data was analyzed automatically in the free open-source software CellProfiler (Version 3.0.0)[308].

7.7 Photoactivation in the LEDs illumination box

An illumination box with 475-nm LEDs (Roithner, Catalog #B56L5111P) was made according to a previous study[309]. The LEDs box was installed in a CO2 incubator for illuminating live cells. The LED illumination power was measured with an optical power sensor (THORLABS, Catalog #S170C).

To illuminate cells in the experiments for western blot assay, cell viability assays, RNA isolation and qPCR analysis, cells were seeded 24 h before being irradiated in the LEDs illumination box. The illumination power of LEDs in the box was adjusted to the specific value as indicated in the results. Samples were taken out at indicated time points after turning on the LEDs, and further processed for different experiments.

7.8 Live cell imaging and photoactivation

Cells were seeded in the μ-Slide 8 Well (ibidi, Catalog #80826) and incubated overnight. After replacing the medium with the phenol-red free DMEM, cells were ready for live cell imaging.

Live cell imaging were performed using a Zeiss LSM 710 NLO 2-photon/confocal laser scanning microscope, which was equipped with an incubator to maintain the samples at 37 °C and in 5% CO_2. Images were captured using a Plan-Apochromat 63x/1.40 Oil DIC M27 objective (Zeiss, Catalog #420782-9900).

A 633nm laser with an intensity of 5.0 % was used for imaging both tdTomato and iRFP682. The detection wavelength (band-pass filter set) for collecting emission light of tdTomato was 638-759 nm, and for iRFP682 is 548-647 nm. Except indicated otherwise, images were normally taken at a frequency of 1 image/min for the first 10 minutes following light stimulation (in order to capture the dynamics of optoTβRII), from then on, one image was captured every 10 minutes. Other detailed information for imaging was listed in **Figure 7.8.1**.

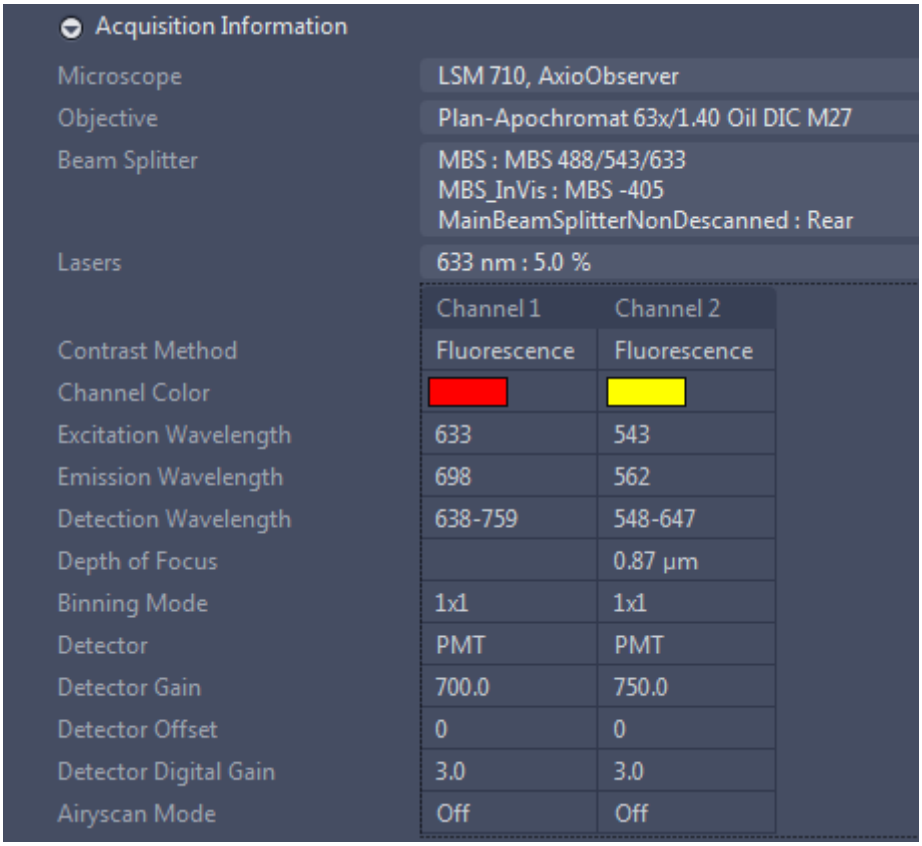

Acquisition Information

Microscope	LSM 710, AxioObserver	
Objective	Plan-Apochromat 63x/1.40 Oil DIC M27	
Beam Splitter	MBS : MBS 488/543/633 MBS_InVis : MBS -405 MainBeamSplitterNonDescanned : Rear	
Lasers	633 nm : 5.0 %	
	Channel 1	Channel 2
Contrast Method	Fluorescence	Fluorescence
Channel Color		
Excitation Wavelength	633	543
Emission Wavelength	698	562
Detection Wavelength	638-759	548-647
Depth of Focus		0.87 µm
Binning Mode	1x1	1x1
Detector	PMT	PMT
Detector Gain	700.0	750.0
Detector Offset	0	0
Detector Digital Gain	3.0	3.0
Airyscan Mode	Off	Off

Figure 7.8.1 Information for imaging. A screenshot of the acquisition information in the ZEN software (Zeiss). Channel 1 and Channel 2correspond to iRFP682 and tdTomato, respectively.

Cells expressing the optoTGFβ system were activated using an Argon laser at 488nm with power 5.0 %, which results in an illumination power of 12.4 μW (measured by the optical power sensor on the focus plane). The illumination power could be adjusted by changing the scan speed to fine-tune the pixel dwell time.

For 2-photom activation, a chameleon laser was used at power 5.0 %, and wavelength 860nm.

7.9 Image analysis

Due to the lack of nuclear marker, automatic image quantification was hard to be implemented. Therefore, the live cell imaging data was manually quantified with ImageJ. The Smad2 signal was quantified as the ratio of nuclear-to-cytoplasmic iRFP-Smad2 signal. Due to the difficulty of quantifying the fluorescence signal at the plasma membrane, the dynamics of optoTβRII were represented by the depletion of the cytoplasmic optoTβRII level. For comparison among different images, the mean tdTomato intensity (level of optoTβRII) in cytoplasmic area was normalized to that in the entire imaging field. Multiple corresponding areas were quantified and the average values were calculated.

7.10 Cell viability assays

Cell viability tests were performed with Trypan blue staining and MTT (3-(4,5-dimethylthiazol-2-yl)-2,5-diphenyltetrazolium bromide) assays. Cells were plated in 24-well plates (2.5×10^5 cells/well). After overnight incubation, cells were kept in dark or exposed to blue light (488 nm, 0.8 mW/cm2) in the LEDs illumination box for 24 hours. The percentages of viable cells were counted after Trypan blue staining in Bio-Rad TC20 cell counter according to the manufacturer's protocol. MTT assay was performed with the MTT reagent from SERVA (Catalog #20395) according to the manufacturer's instruction. The p-values were calculated using a two-sample t-test.

7.11 RNA isolation and qPCR analysis

~1.5×10^6 cells were seeded in 60mm dishes (greiner bio-one, Catalog # 628160) 24 h before photoactivation in the LEDs illumination box. Samples were taken out of the incubator after indicated illumination time before extraction of RNA using the QIAGEN RNeasy Plus Mini Kit (QIAGEN, Catalog #74134), according to the manufacturer's protocol. The mRNAs from the samples were converted to

cDNAs using the QIAGEN QuantiTect Reverse Transcription Kit (QIAGEN, Catalog #205311), and the cDNAs were amplified with the QuantiFast SYBR Green PCR Kit (QIAGEN, Catalog #204054) in the StepOnePlus Real-Time PCR System from the Applied Biosystems. Data was normalized by the signal of GAPDH. The primer sets are listed as below (**Table 7.11-1**):

Table 7.11-1 Sequences of the primers used in the study for qPCR

Primers	Sequence	
human GAPDH	Forward	CCACTCCTCCACCTTTGAC
human GAPDH	Reverse	ACCCTGTTGCTGTAGCCA
human SMAD7	Forward	ACCCGATGGATTTTCTCAAACC
human SMAD7	Reverse	GCCAGATAATTCGTTCCCCCT
human TMEPAI	Forward	GCACAGTGTCAGGCAACGG
human TMEPAI	Reverse	AGATGGTGGGTGGCAGGTC
human PAI1	Forward	GAGACAGGCAGCTCGGATTC
human PAI1	Reverse	GGCCTCCCAAAGTGCATTAC

7.12 Mathematical modeling

The system of ordinary differential equations was prepared in the free software CellDesigner (Version 4.4)[310]. Model simulations, data fitting were implemented with SBML-PET-MPI[242]. Details of the mathematical modeling, including initial conditions, parameter values and the system of ordinary differential equations, were described in the **chapter 5 (Developing a Mathematical Model for the optoTGFβ System)**.

Bibliography

1. Paluch EK, Nelson CM, Biais N, et al. Mechanotransduction: use the force(s). *Bmc Biol.* 2015;13.
2. Hohmann S. Osmotic stress signaling and osmoadaptation in Yeasts. *Microbiol Mol Biol R.* 2002;66(2):300-+.
3. Zhang XM. Molecular sensors and modulators of thermoreception. *Channels.* 2015;9(2):73-81.
4. Baylor D. How photons start vision. *P Natl Acad Sci USA.* 1996;93(2):560-565.
5. Lalli E, Sassonecorsi P. Signal-Transduction and Gene-Regulation - the Nuclear Response to Camp. *J Biol Chem.* 1994;269(26):17359-17362.
6. Szewczyk NJ, Jacobson LA. Signal-transduction networks and the regulation of muscle protein degradation. *Int J Biochem Cell B.* 2005;37(10):1997-2011.
7. Rosen OM. After insulin binds. *Science.* 1987;237(4821):1452-1458.
8. Sun Y, Liu WZ, Liu T, Feng X, Yang N, Zhou HF. Signaling pathway of MAPK/ERK in cell proliferation, differentiation, migration, senescence and apoptosis. *J Recept Sig Transd.* 2015;35(6):600-604.
9. Morgensztern D, McLeod HL. PI3K/Akt/mTOR pathway as a target for cancer therapy. *Anti-Cancer Drug.* 2005;16(8):797-803.
10. Rawlings JS, Rosler KM, Harrison DA. The JAK/STAT signaling pathway. *J Cell Sci.* 2004;117(8):1281-1283.
11. Hanahan D, Weinberg RA. The hallmarks of cancer. *Cell.* 2000;100(1):57-70.
12. Massague J. TGF beta signalling in context. *Nat Rev Mol Cell Bio.* 2012;13(10):616-630.
13. Blobe GC, Schiemann WP, Lodish HF. Mechanisms of disease: Role of transforming growth factor beta in human disease. *New Engl J Med.* 2000;342(18):1350-1358.
14. Gordon KJ, Blobe GC. Role of transforming growth factor-beta superfamily signaling pathways in human disease. *Bba-Mol Basis Dis.* 2008;1782(4):197-228.
15. Sporn MB, Roberts AB. The Transforming Growth Factor-Betas - Past, Present, and Future. *Ann Ny Acad Sci.* 1990;593:1-6.
16. Wrana JL, Attisano L, Carcamo J, et al. Tgf-Beta Signals through a Heteromeric Protein-Kinase Receptor Complex. *Cell.* 1992;71(6):1003-1014.
17. Feng XH, Derynck R. Specificity and versatility in TGF-beta signaling through Smads. *Annu Rev Cell Dev Bi.* 2005;21:659-693.
18. Hata A, Chen YG. TGF-beta Signaling from Receptors to Smads. *Csh Perspect Biol.* 2016;8(9).
19. Massague J, Seoane J, Wotton D. Smad transcription factors. *Gene Dev.* 2005;19(23):2783-2810.
20. Hill CS. Transcriptional Control by the SMADs. *Csh Perspect Biol.* 2016;8(10).
21. Weiss A, Attisano L. The TGFbeta Superfamily Signaling Pathway. *Wires Dev Biol.* 2013;2(1):47-63.

22. Huminiecki L, Goldovsky L, Freilich S, Moustakas A, Ouzounis C, Heldin CH. Emergence, development and diversification of the TGF-beta signalling pathway within the animal kingdom. *Bmc Evol Biol.* 2009;9.

23. De Robertis EM, Kuroda H. Dorsal-ventral patterning and neural induction in Xenopus embryos. *Annu Rev Cell Dev Biol.* 2004;20:285-308.

24. Ramis JM, Collart C, Smith JC. Xnrs and activin regulate distinct genes during Xenopus development: activin regulates cell division. *Plos One.* 2007;2(2):e213.

25. Eimon PM, Harland RM. Effects of heterodimerization and proteolytic processing on Derriere and Nodal activity: implications for mesoderm induction in Xenopus. *Development.* 2002;129(13):3089-3103.

26. Heldin CH, Moustakas A. Signaling Receptors for TGF-beta Family Members. *Csh Perspect Biol.* 2016;8(8).

27. Lawler S, Feng XH, Chen RH, et al. The type II transforming growth factor-beta receptor autophosphorylates not only on serine and threonine but also on tyrosine residues. *J Biol Chem.* 1997;272(23):14850-14859.

28. Groppe J, Hinck CS, Samavarchi-Tehrani P, et al. Cooperative assembly of TGF-beta superfamily signaling complexes is mediated by two disparate mechanisms and distinct modes of receptor binding. *Molecular Cell.* 2008;29(2):157-168.

29. Sebald W, Nickel J, Zhang JL, Mueller TD. Molecular recognition in bone morphogenetic protein (BMP)/receptor interaction. *Biol Chem.* 2004;385(8):697-710.

30. Sun PD, Davies DR. The Cystine-Knot Growth-Factor Superfamily. *Annu Rev Bioph Biom.* 1995;24:269-291.

31. Harrison CA, Al-Musawi SL, Walton KL. Prodomains regulate the synthesis, extracellular localisation and activity of TGF-beta superfamily ligands. *Growth Factors.* 2011;29(5):174-186.

32. Huang T, Schor SL, Hinck AP. Biological Activity Differences between TGF-beta 1 and TGF-beta 3 Correlate with Differences in the Rigidity and Arrangement of Their Component Monomers. *Biochemistry-Us.* 2014;53(36):5737-5749.

33. Huang SS, O'Grady P, Huang JS. Human transforming growth factor beta.alpha 2-macroglobulin complex is a latent form of transforming growth factor beta. *J Biol Chem.* 1988;263(3):1535-1541.

34. Munger JS, Harpel JG, Gleizes PE, Mazzieri R, Nunes I, Rifkin DB. Latent transforming growth factor-beta: structural features and mechanisms of activation. *Kidney Int.* 1997;51(5):1376-1382.

35. Annes JP, Chen Y, Munger JS, Rifkin DB. Integrin alphaVbeta6-mediated activation of latent TGF-beta requires the latent TGF-beta binding protein-1. *J Cell Biol.* 2004;165(5):723-734.

36. Buscemi L, Ramonet D, Klingberg F, et al. The single-molecule mechanics of the latent TGF-beta1 complex. *Curr Biol.* 2011;21(24):2046-2054.

37. Kim YW, Park J, Lee HJ, Lee SY, Kim SJ. TGF-beta sensitivity is determined by N-linked glycosylation of the type II TGF-beta receptor. *Biochem J.* 2012;445(3):403-411.

38. Partridge EA, Le Roy C, Di Guglielmo GM, et al. Regulation of cytokine receptors by Golgi N-glycan processing and endocytosis. *Science.* 2004;306(5693):120-124.

39. Ferreira IG, Pucci M, Venturi G, Malagolini N, Chiricolo M, Dall'Olio F. Glycosylation as a Main Regulator of Growth and Death Factor Receptors Signaling. *Int J Mol Sci.* 2018;19(2).

40. Luo K, Lodish HF. Positive and negative regulation of type II TGF-beta receptor signal transduction by autophosphorylation on multiple serine residues. *EMBO J.* 1997;16(8):1970-1981.

41. Lawler S, Feng XH, Chen RH, et al. The type II transforming growth factor-beta receptor autophosphorylates not only on serine and threonine but also on tyrosine residues. *J Biol Chem.* 1997;272(23):14850-14859.

42. Galliher AJ, Schiemann WP. Src phosphorylates Tyr284 in TGF-beta type II receptor and regulates TGF-beta stimulation of p38 MAPK during breast cancer cell proliferation and invasion. *Cancer Res.* 2007;67(8):3752-3758.

43. Heldin CH, Moustakas A. Signaling Receptors for TGF-beta Family Members. *Cold Spring Harb Perspect Biol.* 2016;8(8).

44. Chen X, Wang H, Liao HJ, et al. Integrin-mediated type II TGF-beta receptor tyrosine dephosphorylation controls SMAD-dependent profibrotic signaling. *J Clin Invest.* 2014;124(8):3295-3310.

45. Wang T, Li BY, Danielson PD, et al. The immunophilin FKBP12 functions as a common inhibitor of the TGF beta family type I receptors. *Cell.* 1996;86(3):435-444.

46. Chen YG, Liu F, Massague J. Mechanism of TGFbeta receptor inhibition by FKBP12. *EMBO J.* 1997;16(13):3866-3876.

47. Huse M, Muir TW, Xu L, Chen YG, Kuriyan J, Massague J. The TGF beta receptor activation process: an inhibitor- to substrate-binding switch. *Mol Cell.* 2001;8(3):671-682.

48. Wrana JL, Attisano L, Wieser R, Ventura F, Massague J. Mechanism of activation of the TGF-beta receptor. *Nature.* 1994;370(6488):341-347.

49. Souchelnytskyi S, ten Dijke P, Miyazono K, Heldin CH. Phosphorylation of Ser165 in TGF-beta type I receptor modulates TGF-beta1-induced cellular responses. *EMBO J.* 1996;15(22):6231-6240.

50. Shi W, Sun C, He B, et al. GADD34-PP1c recruited by Smad7 dephosphorylates TGFbeta type I receptor. *J Cell Biol.* 2004;164(2):291-300.

51. Griswold-Prenner I, Kamibayashi C, Maruoka EM, Mumby MC, Derynck R. Physical and functional interactions between type I transforming growth factor beta receptors and Balpha, a WD-40 repeat subunit of phosphatase 2A. *Mol Cell Biol.* 1998;18(11):6595-6604.

52. Batut J, Schmierer B, Cao J, Raftery LA, Hill CS, Howell M. Two highly related regulatory subunits of PP2A exert opposite effects on TGF-beta/Activin/Nodal signalling. *Development.* 2008;135(17):2927-2937.

53. Kavsak P, Rasmussen RK, Causing CG, et al. Smad7 binds to Smurf2 to form an E3 ubiquitin ligase that targets the TGF beta receptor for degradation. *Mol Cell.* 2000;6(6):1365-1375.

54. Ebisawa T, Fukuchi M, Murakami G, et al. Smurf1 interacts with transforming growth factor-beta type I receptor through Smad7 and induces receptor degradation. *J Biol Chem.* 2001;276(16):12477-12480.

55. Zhang L, Zhou F, Drabsch Y, et al. USP4 is regulated by AKT phosphorylation and directly deubiquitylates TGF-beta type I receptor. *Nat Cell Biol.* 2012;14(7):717-726.

56. Eichhorn PJ, Rodon L, Gonzalez-Junca A, et al. USP15 stabilizes TGF-beta receptor I and promotes oncogenesis through the activation of TGF-beta signaling in glioblastoma. *Nat Med.* 2012;18(3):429-435.

57. Al-Salihi MA, Herhaus L, Macartney T, Sapkota GP. USP11 augments TGFbeta signalling by deubiquitylating ALK5. *Open Biol.* 2012;2(6):120063.

58. Kang JS, Saunier EF, Akhurst RJ, Derynck R. The type I TGF-beta receptor is covalently modified and regulated by sumoylation. *Nat Cell Biol.* 2008;10(6):654-664.

59. Chen T, Yan W, Wells RG, et al. Novel inactivating mutations of transforming growth factor-beta type I receptor gene in head-and-neck cancer metastases. *Int J Cancer.* 2001;93(5):653-661.

60. Zuo W, Huang F, Chiang YJ, et al. c-Cbl-mediated neddylation antagonizes ubiquitination and degradation of the TGF-beta type II receptor. *Mol Cell.* 2013;49(3):499-510.

61. Murphy SJ, Shapira KE, Henis YI, Leof EB. A unique element in the cytoplasmic tail of the type II transforming growth factor-beta receptor controls basolateral delivery. *Mol Biol Cell.* 2007;18(10):3788-3799.

62. Kavsak P, Rasmussen RK, Causing CG, et al. Smad7 binds to Smurf2 to form an E3 ubiquitin ligase that targets the TGF beta receptor for degradation. *Molecular Cell.* 2000;6(6):1365-1375.

63. Itoh S, Itoh F. Inhibitory machinery for the TGF-beta family signaling pathway. *Growth Factors.* 2011;29(5):163-173.

64. Bai S, Cao X. A nuclear antagonistic mechanism of inhibitory Smads in transforming growth factor-beta signaling. *J Biol Chem.* 2002;277(6):4176-4182.

65. Moustakas A, Heldin CH. The regulation of TGF beta signal transduction. *Development.* 2009;136(22):3699-3714.

66. Shi Y, Wang YF, Jayaraman L, Yang H, Massague J, Pavletich NP. Crystal structure of a Smad MH1 domain bound to DNA: insights on DNA binding in TGF-beta signaling. *Cell.* 1998;94(5):585-594.

67. Yagi K, Goto D, Hamamoto T, Takenoshita S, Kato M, Miyazono K. Alternatively spliced variant of Smad2 lacking exon 3. Comparison with wild-type Smad2 and Smad3. *J Biol Chem.* 1999;274(2):703-709.

68. Lo RS, Chen YG, Shi Y, Pavletich NP, Massague J. The L3 loop: a structural motif determining specific interactions between SMAD proteins and TGF-beta receptors. *EMBO J.* 1998;17(4):996-1005.

69. Chen YG, Hata A, Lo RS, et al. Determinants of specificity in TGF-beta signal transduction. *Genes Dev.* 1998;12(14):2144-2152.

70. Chong PA, Lin H, Wrana JL, Forman-Kay JD. Coupling of tandem Smad ubiquitination regulatory factor (Smurf) WW domains modulates target specificity. *Proc Natl Acad Sci U S A.* 2010;107(43):18404-18409.

71. Sudol M. Newcomers to the WW Domain-Mediated Network of the Hippo Tumor Suppressor Pathway. *Genes Cancer.* 2010;1(11):1115-1118.

72. de Caestecker MP, Yahata T, Wang D, et al. The Smad4 activation domain (SAD) is a proline-rich, p300-dependent transcriptional activation domain. *J Biol Chem.* 2000;275(3):2115-2122.

73. Wrighton KH, Feng XH. To (TGF)beta or not to (TGF)beta: fine-tuning of Smad signaling via post-translational modifications. *Cell Signal.* 2008;20(9):1579-1591.

74. Tu AW, Luo K. Acetylation of Smad2 by the co-activator p300 regulates activin and transforming growth factor beta response. *J Biol Chem.* 2007;282(29):21187-21196.

75. Inoue Y, Itoh Y, Abe K, et al. Smad3 is acetylated by p300/CBP to regulate its transactivation activity. *Oncogene.* 2007;26(4):500-508.

76. Moren A, Hellman U, Inada Y, Imamura T, Heldin CH, Moustakas A. Differential ubiquitination defines the functional status of the tumor suppressor Smad4. *J Biol Chem.* 2003;278(35):33571-33582.

77. Lee PS, Chang C, Liu D, Derynck R. Sumoylation of Smad4, the common Smad mediator of transforming growth factor-beta family signaling. *J Biol Chem.* 2003;278(30):27853-27863.

78. Gronroos E, Hellman U, Heldin CH, Ericsson J. Control of Smad7 stability by competition between acetylation and ubiquitination. *Mol Cell.* 2002;10(3):483-493.

79. Inamitsu M, Itoh S, Hellman U, Ten Dijke P, Kato M. Methylation of Smad6 by protein arginine N-methyltransferase 1. *Febs Lett.* 2006;580(28-29):6603-6611.

80. Lee MK, Pardoux C, Hall MC, et al. TGF-beta activates Erk MAP kinase signalling through direct phosphorylation of ShcA. *EMBO J.* 2007;26(17):3957-3967.

81. Galliher-Beckley AJ, Schiemann WP. Grb2 binding to Tyr284 in TbetaR-II is essential for mammary tumor growth and metastasis stimulated by TGF-beta. *Carcinogenesis.* 2008;29(2):244-251.

82. Galliher AJ, Schiemann WP. Beta3 integrin and Src facilitate transforming growth factor-beta mediated induction of epithelial-mesenchymal transition in mammary epithelial cells. *Breast Cancer Res.* 2006;8(4):R42.

83. Sorrentino A, Thakur N, Grimsby S, et al. The type I TGF-beta receptor engages TRAF6 to activate TAK1 in a receptor kinase-independent manner. *Nat Cell Biol.* 2008;10(10):1199-1207.

84. Yamashita M, Fatyol K, Jin C, Wang X, Liu Z, Zhang YE. TRAF6 mediates Smad-independent activation of JNK and p38 by TGF-beta. *Mol Cell.* 2008;31(6):918-924.

85. Zihni C, Terry SJ. RhoGTPase signalling at epithelial tight junctions: Bridging the GAP between polarity and cancer. *Int J Biochem Cell Biol.* 2015;64:120-125.

86. Ozdamar B, Bose R, Barrios-Rodiles M, Wang HR, Zhang Y, Wrana JL. Regulation of the polarity protein Par6 by TGFbeta receptors controls epithelial cell plasticity. *Science.* 2005;307(5715):1603-1609.

87. Moustakas A, Heldin CH. Signaling networks guiding epithelial-mesenchymal transitions during embryogenesis and cancer progression. *Cancer Sci.* 2007;98(10):1512-1520.

88. Viloria-Petit AM, David L, Jia JY, et al. A role for the TGFbeta-Par6 polarity pathway in breast cancer progression. *Proc Natl Acad Sci U S A.* 2009;106(33):14028-14033.

89. Mu Y, Sundar R, Thakur N, et al. TRAF6 ubiquitinates TGFbeta type I receptor to promote its cleavage and nuclear translocation in cancer. *Nat Commun.* 2011;2:330.

90. Sorkin A, von Zastrow M. Endocytosis and signalling: intertwining molecular networks. *Nat Rev Mol Cell Biol.* 2009;10(9):609-622.

91. Yao D, Ehrlich M, Henis YI, Leof EB. Transforming growth factor-beta receptors interact with AP2 by direct binding to beta2 subunit. *Mol Biol Cell.* 2002;13(11):4001-4012.

92. Gillooly DJ, Simonsen A, Stenmark H. Cellular functions of phosphatidylinositol 3-phosphate and FYVE domain proteins. *Biochem J.* 2001;355(Pt 2):249-258.

93. Chen YG. Endocytic regulation of TGF-beta signaling. *Cell Res.* 2009;19(1):58-70.

94. Tsukazaki T, Chiang TA, Davison AF, Attisano L, Wrana JL. SARA, a FYVE domain protein that recruits Smad2 to the TGFbeta receptor. *Cell.* 1998;95(6):779-791.

95. Miura S, Takeshita T, Asao H, et al. Hgs (Hrs), a FYVE domain protein, is involved in Smad signaling through cooperation with SARA. *Mol Cell Biol.* 2000;20(24):9346-9355.

96. Chen YG, Wang Z, Ma J, Zhang L, Lu Z. Endofin, a FYVE domain protein, interacts with Smad4 and facilitates transforming growth factor-beta signaling. *J Biol Chem.* 2007;282(13):9688-9695.

97. Lin HK, Bergmann S, Pandolfi PP. Cytoplasmic PML function in TGF-beta signalling. *Nature.* 2004;431(7005):205-211.

98. Hocevar BA, Smine A, Xu XX, Howe PH. The adaptor molecule Disabled-2 links the transforming growth factor beta receptors to the Smad pathway. *EMBO J.* 2001;20(11):2789-2801.

99. Zerial M, McBride H. Rab proteins as membrane organizers. *Nat Rev Mol Cell Bio.* 2001;2(2):107-117.

100. Panopoulou E, Gillooly DJ, Wrana JL, et al. Early endosomal regulation of Smad-dependent signaling in endothelial cells. *J Biol Chem.* 2002;277(20):18046-18052.

101. Dore JJ, Jr., Yao D, Edens M, Garamszegi N, Sholl EL, Leof EB. Mechanisms of transforming growth factor-beta receptor endocytosis and intracellular sorting differ between fibroblasts and epithelial cells. *Mol Biol Cell.* 2001;12(3):675-684.

102. Mitchell H, Choudhury A, Pagano RE, Leof EB. Ligand-dependent and -independent transforming growth factor-beta receptor recycling regulated by clathrin-mediated endocytosis and Rab11. *Mol Biol Cell.* 2004;15(9):4166-4178.

103. Zerial M, McBride H. Rab proteins as membrane organizers. *Nat Rev Mol Cell Biol.* 2001;2(2):107-117.

104. Yakymovych I, Yakymovych M, Zang G, et al. CIN85 modulates TGFbeta signaling by promoting the presentation of TGFbeta receptors on the cell surface. *J Cell Biol.* 2015;210(2):319-332.

105. Penheiter SG, Singh RD, Repellin CE, et al. Type II transforming growth factor-beta receptor recycling is dependent upon the clathrin adaptor protein Dab2. *Mol Biol Cell.* 2010;21(22):4009-4019.

106. Yin X, Murphy SJ, Wilkes MC, Ji Y, Leof EB. Retromer maintains basolateral distribution of the type II TGF-beta receptor via the recycling endosome. *Mol Biol Cell.* 2013;24(14):2285-2298.

107. Razani B, Zhang XL, Bitzer M, von Gersdorff G, Bottinger EP, Lisanti MP. Caveolin-1 regulates transforming growth factor (TGF)-beta/SMAD signaling through an interaction with the TGF-beta type I receptor. *J Biol Chem.* 2001;276(9):6727-6738.

108. Di Guglielmo GM, Le Roy C, Goodfellow AF, Wrana JL. Distinct endocytic pathways regulate TGF-beta receptor signalling and turnover. *Nat Cell Biol.* 2003;5(5):410-421.

109. Kim S, Lee Y, Seo JE, Cho KH, Chung JH. Caveolin-1 increases basal and TGF-beta1-induced expression of type I procollagen through PI-3 kinase/Akt/mTOR pathway in human dermal fibroblasts. *Cell Signal.* 2008;20(7):1313-1319.

110. Zuo W, Chen YG. Specific activation of mitogen-activated protein kinase by transforming growth factor-beta receptors in lipid rafts is required for epithelial cell plasticity. *Mol Biol Cell.* 2009;20(3):1020-1029.

111. Schwartz EA, Reaven E, Topper JN, Tsao PS. Transforming growth factor-beta receptors localize to caveolae and regulate endothelial nitric oxide synthase in normal human endothelial cells. *Biochem J.* 2005;390(Pt 1):199-206.

112. Santibanez JF, Blanco FJ, Garrido-Martin EM, Sanz-Rodriguez F, del Pozo MA, Bernabeu C. Caveolin-1 interacts and cooperates with the transforming growth factor-beta type I receptor ALK1 in endothelial caveolae. *Cardiovasc Res.* 2008;77(4):791-799.

113. Zhang XL, Topley N, Ito T, Phillips A. Interleukin-6 regulation of transforming growth factor (TGF)-beta receptor compartmentalization and turnover enhances TGF-beta1 signaling. *J Biol Chem.* 2005;280(13):12239-12245.

114. Atfi A, Dumont E, Colland F, et al. The disintegrin and metalloproteinase ADAM12 contributes to TGF-beta signaling through interaction with the type II receptor. *J Cell Biol.* 2007;178(2):201-208.

115. Anders RA, Arline SL, Dore JJ, Leof EB. Distinct endocytic responses of heteromeric and homomeric transforming growth factor beta receptors. *Mol Biol Cell.* 1997;8(11):2133-2143.

116. Mullen AC, Orlando DA, Newman JJ, et al. Master transcription factors determine cell-type-specific responses to TGF-beta signaling. *Cell.* 2011;147(3):565-576.

117. Li MO, Flavell RA. TGF-beta: A master of all T cell trades. *Cell.* 2008;134(3):392-404.

118. Vincent T, Neve EP, Johnson JR, et al. A SNAIL1-SMAD3/4 transcriptional repressor complex promotes TGF-beta mediated epithelial-mesenchymal transition. *Nat Cell Biol.* 2009;11(8):943-950.

119. Macias MJ, Martin-Malpartida P, Massague J. Structural determinants of Smad function in TGF-beta signaling. *Trends Biochem Sci.* 2015;40(6):296-308.

120. Radaev S, Zou ZC, Huang T, Lafer EM, Hinck AP, Sun PD. Ternary Complex of Transforming Growth Factor-beta 1 Reveals Isoform-specific Ligand Recognition and Receptor Recruitment in the Superfamily. *J Biol Chem.* 2010;285(19):14806-14814.

121. Hinck AP, Archer SJ, Qian SW, et al. Transforming growth factor beta 1: Three-dimensional structure in solution and comparison with the X-ray structure of transforming growth factor beta 2. *Biochemistry-Us.* 1996;35(26):8517-8534.

122. Tebben AJ, Ruzanov M, Gao M, et al. Crystal structures of apo and inhibitor-bound TGF beta R2 kinase domain: insights into TGF beta R isoform selectivity. *Acta Crystallogr D.* 2016;72:658-674.

123. Boesen CC, Radaev S, Motyka SA, Patamawenu A, Sun PD. The 1.1 A crystal structure of human TGF-beta type II receptor ligand binding domain. *Structure.* 2002;10(7):913-919.

124. Han S, Loulakis P, Griffor M, Xie Z. Crystal structure of activin receptor type IIB kinase domain from human at 2.0 Angstrom resolution. *Protein Sci.* 2007;16(10):2272-2277.

125. Hinck AP. Structural studies of the TGF-betas and their receptors - insights into evolution of the TGF-beta superfamily. *Febs Lett.* 2012;586(14):1860-1870.

126. Shi Y, Massague J. Mechanisms of TGF-beta signaling from cell membrane to the nucleus. *Cell.* 2003;113(6):685-700.

127. Chai J, Wu JW, Yan N, Massague J, Pavletich NP, Shi Y. Features of a Smad3 MH1-DNA complex. Roles of water and zinc in DNA binding. *J Biol Chem.* 2003;278(22):20327-20331.

128. Wu JW, Hu M, Chai J, et al. Crystal structure of a phosphorylated Smad2. Recognition of phosphoserine by the MH2 domain and insights on Smad function in TGF-beta signaling. *Mol Cell.* 2001;8(6):1277-1289.

129. Massague J, Chen YG. Controlling TGF-beta signaling. *Gene Dev.* 2000;14(6):627-644.

130. Melke P, Jonsson H, Pardali E, ten Dijke P, Peterson C. A rate equation approach to elucidate the kinetics and robustness of the TGF-beta pathway. *Biophys J.* 2006;91(12):4368-4380.

131. Vilar JMG, Jansen R, Sander C. Signal processing in the TGF-beta superfamily ligand-receptor network. *Plos Comput Biol.* 2006;2(1):36-45.

132. Zi ZK, Klipp E. Constraint-Based Modeling and Kinetic Analysis of the Smad Dependent TGF-beta Signaling Pathway. *Plos One.* 2007;2(9).

133. Schmierer B, Tournier AL, Bates PA, Hill CS. Mathematical modeling identifies Smad nucleocytoplasmic shuttling as a dynamic signal-interpreting system. *P Natl Acad Sci USA.* 2008;105(18):6608-6613.

134. Clarke DC, Liu XD. Decoding the quantitative nature of TGF-beta/Smad signaling. *Trends Cell Biol.* 2008;18(9):430-442.

135. Chung SW, Miles FL, Sikes RA, Cooper CR, Farach-Carson MC, Ogunnaike BA. Quantitative Modeling and Analysis of the Transforming Growth Factor beta Signaling Pathway. *Biophys J.* 2009;96(5):1733-1750.

136. Zi ZK, Feng ZP, Chapnick DA, et al. Quantitative analysis of transient and sustained transforming growth factor-beta signaling dynamics. *Mol Syst Biol.* 2011;7.

137. Li LY, Klim JR, Derda R, Courtney AH, Kiessling LL. Spatial control of cell fate using synthetic surfaces to potentiate TGF-beta signaling. *P Natl Acad Sci USA.* 2011;108(29):11745-11750.

138. Luo KX, Lodish HF. Signaling by chimeric erythropoietin-TGF-beta receptors: Homodimerization of the cytoplasmic domain of the type I TGF-beta receptor and heterodimerization with the type II receptor are both required for intracellular signal transduction. *Embo Journal.* 1996;15(17):4485-4496.

139. Stockwell BR, Schreiber SL. Probing the role of homomeric and heteromeric receptor interactions in TGF-beta signaling using small molecule dimerizers. *Curr Biol.* 1998;8(13):761-770.

140. Anders RA, Leof EB. Chimeric granulocyte/macrophage colony-stimulating factor transforming growth factor-beta (TGF-beta) receptors define a model system for investigating the role of homomeric and heteromeric receptors in TGF-beta signaling. *J Biol Chem.* 1996;271(36):21758-21766.

141. Sawyer JS, Anderson BD, Beight DW, et al. Synthesis and activity of new aryl- and heteroaryl- substituted pyrazole inhibitors of the transforming growth factor-b type I receptor kinase domain. *J Med Chem.* 2003;46(19):3953-3956.

142. Laping NJ, Grygielko E, Mathur A, et al. Inhibition of transforming growth factor (TGF)-beta 1-induced extracellular matrix with a novel inhibitor of the TGF-beta type I receptor kinase activity: SB-431542. *Mol Pharmacol.* 2002;62(1):58-64.

143. Melisi D, Ishiyama S, Sclabas GM, et al. LY2109761, a novel transforming growth factor beta receptor type I and type II dual inhibitor, as a therapeutic approach to suppressing pancreatic cancer metastasis. *Mol Cancer Ther.* 2008;7(4):829-840.

144. Chang CB. Agonists and Antagonists of TGF-beta Family Ligands. *Csh Perspect Biol.* 2016;8(8).

145. Schlingensiepen KH, Fischer-Blass B, Schmaus S, Ludwig S. Antisense therapeutics for tumor treatment: the TGF-beta2 inhibitor AP 12009 in clinical development against malignant tumors. *Recent Results Cancer Res.* 2008;177:137-150.

146. Kwiatkowski W, Gray PC, Choe S. Engineering TGF-beta superfamily ligands for clinical applications. *Trends Pharmacol Sci.* 2014;35(12):648-657.

147. Lonning S, Mannick J, McPherson JM. Antibody Targeting of TGF-beta in Cancer Patients. *Curr Pharm Biotechno.* 2011;12(12):2176-2189.

148. Nagel G, Szellas T, Huhn W, et al. Channelrhodopsin-2, a directly light-gated cation-selective membrane channel. *P Natl Acad Sci USA.* 2003;100(24):13940-13945.

149. Zhang F, Prigge M, Beyriere F, et al. Red-shifted optogenetic excitation: a tool for fast neural control derived from Volvox carteri. *Nat Neurosci.* 2008;11(6):631-633.

150. Kalaidzidis IV, Kalaidzidis YL, Kaulen AD. Flash-induced voltage changes in halorhodopsin from Natronobacterium pharaonis. *Febs Lett.* 1998;427(1):59-63.

151. Han X, Chow BY, Zhou H, et al. A high-light sensitivity optical neural silencer: development and application to optogenetic control of non-human primate cortex. *Front Syst Neurosci.* 2011;5:18.

152. Chow BY, Han X, Dobry AS, et al. High-performance genetically targetable optical neural silencing by light-driven proton pumps. *Nature.* 2010;463(7277):98-102.

153. Gradinaru V, Zhang F, Ramakrishnan C, et al. Molecular and cellular approaches for diversifying and extending optogenetics. *Cell.* 2010;141(1):154-165.

154. Lozier RH, Bogomolni RA, Stoeckenius W. Bacteriorhodopsin: a light-driven proton pump in Halobacterium Halobium. *Biophys J.* 1975;15(9):955-962.

155. Gunaydin LA, Yizhar O, Berndt A, Sohal VS, Deisseroth K, Hegemann P. Ultrafast optogenetic control. *Nat Neurosci.* 2010;13(3):387-392.

156. Berndt A, Yizhar O, Gunaydin LA, Hegemann P, Deisseroth K. Bi-stable neural state switches. *Nat Neurosci.* 2009;12(2):229-234.

157. Gradinaru V, Thompson KR, Deisseroth K. eNpHR: a Natronomonas halorhodopsin enhanced for optogenetic applications. *Brain Cell Biol.* 2008;36(1-4):129-139.

158. Pastrana E. Optogenetics: controlling cell function with light. *Nat Methods.* 2011;8(1):24-25.

159. Guru A, Post RJ, Ho YY, Warden MR. Making Sense of Optogenetics. *Int J Neuropsychopharmacol.* 2015;18(11):pyv079.

160. Motta-Mena LB, Reade A, Mallory MJ, et al. An optogenetic gene expression system with rapid activation and deactivation kinetics. *Nat Chem Biol.* 2014;10(3):196-+.

161. Bugaj LJ, Choksi AT, Mesuda CK, Kane RS, Schaffer DV. Optogenetic protein clustering and signaling activation in mammalian cells. *Nat Methods.* 2013;10(3):249-252.

162. Wu YI, Frey D, Lungu OI, et al. A genetically encoded photoactivatable Rac controls the motility of living cells. *Nature.* 2009;461(7260):104-U111.

163. Levskaya A, Weiner OD, Lim WA, Voigt CA. Spatiotemporal control of cell signalling using a light-switchable protein interaction. *Nature.* 2009;461(7266):997-1001.

164. Tischer D, Weiner OD. Illuminating cell signalling with optogenetic tools. *Nat Rev Mol Cell Bio.* 2014;15(8):551-558.

165. Muller K, Engesser R, Schulz S, et al. Multi-chromatic control of mammalian gene expression and signaling. *Nucleic Acids Res.* 2013;41(12).

166. Endo M, Ozawa T. Strategies for development of optogenetic systems and their applications. *J Photoch Photobio C.* 2017;30:10-23.

167. Zhou XX, Chung HK, Lam AJ, Lin MZ. Optical control of protein activity by fluorescent protein domains. *Science.* 2012;338(6108):810-814.

168. Yu X, Liu H, Klejnot J, Lin C. The Cryptochrome Blue Light Receptors. *Arabidopsis Book.* 2010;8:e0135.

169. Chaves I, Pokorny R, Byrdin M, et al. The cryptochromes: blue light photoreceptors in plants and animals. *Annu Rev Plant Biol.* 2011;62:335-364.

170. Kennedy MJ, Hughes RM, Peteya LA, Schwartz JW, Ehlers MD, Tucker CL. Rapid blue-light-mediated induction of protein interactions in living cells. *Nat Methods.* 2010;7(12):973-U948.

171. Taslimi A, Vrana JD, Chen D, et al. An optimized optogenetic clustering tool for probing protein interaction and function. *Nat Commun.* 2014;5.

172. Taslimi A, Zoltowski B, Miranda JG, Pathak GP, Hughes RM, Tucker CL. Optimized second-generation CRY2-CIB dimerizers and photoactivatable Cre recombinase. *Nat Chem Biol.* 2016;12(6):425-U478.

173. Kennedy MJ, Hughes RM, Peteya LA, Schwartz JW, Ehlers MD, Tucker CL. Rapid blue-light-mediated induction of protein interactions in living cells. *Nat Methods.* 2010;7(12):973-975.

174. Muhlhauser WWD, Fischer A, Weber W, Radziwill G. Optogenetics - Bringing light into the darkness of mammalian signal transduction. *Bba-Mol Cell Res.* 2017;1864(2):280-292.

175. Yazawa M, Sadaghiani AM, Hsueh B, Dolmetsch RE. Induction of protein-protein interactions in live cells using light. *Nat Biotechnol.* 2009;27(10):941-U105.

176. Lungu OI, Hallett RA, Choi EJ, Aiken MJ, Hahn KM, Kuhlman B. Designing Photoswitchable Peptides Using the AsLOV2 Domain. *Chem Biol.* 2012;19(4):507-517.

177. Niopek D, Benzinger D, Roensch J, et al. Engineering light-inducible nuclear localization signals for precise spatiotemporal control of protein dynamics in living cells. *Nat Commun.* 2014;5.

178. Niopek D, Wehler P, Roensch J, Eils R, Di Ventura B. Optogenetic control of nuclear protein export. *Nat Commun.* 2016;7.

179. Yumerefendi H, Dickinson DJ, Wang H, et al. Control of Protein Activity and Cell Fate Specification via Light-Mediated Nuclear Translocation. *Plos One.* 2015;10(6).

180. van Bergeijk P, Adrian M, Hoogenraad CC, Kapitein LC. Optogenetic control of organelle transport and positioning. *Nature.* 2015;518(7537):111-+.

181. Strickland D, Lin Y, Wagner E, et al. TULIPs: tunable, light-controlled interacting protein tags for cell biology. *Nat Methods.* 2012;9(4):379-U392.

182. Guntas G, Hallett RA, Zimmerman SP, et al. Engineering an improved light-induced dimer (iLID) for controlling the localization and activity of signaling proteins. *P Natl Acad Sci USA.* 2015;112(1):112-117.

183. Kawano F, Suzuki H, Furuya A, Sato M. Engineered pairs of distinct photoswitches for optogenetic control of cellular proteins. *Nat Commun.* 2015;6.

184. Ryu MH, Moskvin OV, Siltberg-Liberles J, Gomelsky M. Natural and Engineered Photoactivated Nucleotidyl Cyclases for Optogenetic Applications. *J Biol Chem.* 2010;285(53):41501-41508.

185. Kaberniuk AA, Shemetov AA, Verkhusha VV. A bacterial phytochrome-based optogenetic system controllable with near-infrared light. *Nat Methods.* 2016;13(7):591-597.

186. Ryu MH, Kang IH, Nelson MD, et al. Engineering adenylate cyclases regulated by near-infrared window light. *Proc Natl Acad Sci U S A.* 2014;111(28):10167-10172.

187. Shimizu-Sato S, Huq E, Tepperman JM, Quail PH. A light-switchable gene promoter system. *Nat Biotechnol.* 2002;20(10):1041-1044.

188. Reichhart E, Ingles-Prieto A, Tichy AM, McKenzie C, Janovjak H. A Phytochrome Sensory Domain Permits Receptor Activation by Red Light. *Angew Chem Int Edit.* 2016;55(21):6339-6342.

189. Sawa M, Nusinow DA, Kay SA, Imaizumi T. FKF1 and GIGANTEA complex formation is required for day-length measurement in Arabidopsis. *Science.* 2007;318(5848):261-265.

190. Conrad KS, Bilwes AM, Crane BR. Light-Induced Subunit Dissociation by a Light-Oxygen-Voltage Domain Photoreceptor from Rhodobacter sphaeroides. *Biochemistry-Us.* 2013;52(2):378-391.

191. Zoltowski BD, Schwerdtfeger C, Widom J, et al. Conformational switching in the fungal light sensor vivid. *Science.* 2007;316(5827):1054-1057.

192. Kerruth S, Ataka K, Frey D, Schlichting I, Heberle J. Aureochrome 1 Illuminated: Structural Changes of a Transcription Factor Probed by Molecular Spectroscopy. *Plos One.* 2014;9(7).

193. Nash AI, McNulty R, Shillito ME, et al. Structural basis of photosensitivity in a bacterial light-oxygen-voltage/helix-turn-helix (LOV-HTH) DNA-binding protein. *P Natl Acad Sci USA.* 2011;108(23):9449-9454.

194. Losi A, Polverini E, Quest B, Gartner W. First evidence for phototropin-related blue-light receptors in prokaryotes. *Biophys J.* 2002;82(5):2627-2634.

195. Moglich A, Ayers RA, Moffat K. Design and Signaling Mechanism of Light-Regulated Histidine Kinases. *Journal of Molecular Biology.* 2009;385(5):1433-1444.

196. Schroder-Lang S, Schwarzel M, Seifert R, et al. Fast manipulation of cellular cAMP level by light in vivo. *Nat Methods.* 2007;4(1):39-42.

197. Stierl M, Stumpf P, Udwari D, et al. Light Modulation of Cellular cAMP by a Small Bacterial Photoactivated Adenylyl Cyclase, bPAC, of the Soil Bacterium Beggiatoa. *J Biol Chem.* 2011;286(2):1181-1188.

198. Tilbrook K, Arongaus AB, Binkert M, Heijde M, Yin R, Ulm R. The UVR8 UV-B Photoreceptor: Perception, Signaling and Response. *Arabidopsis Book.* 2013;11:e0164.

199. Crefcoeur RP, Yin R, Ulm R, Halazonetis TD. Ultraviolet-B-mediated induction of protein-protein interactions in mammalian cells. *Nat Commun.* 2013;4:1779.

200. Airan RD, Thompson KR, Fenno LE, Bernstein H, Deisseroth K. Temporally precise in vivo control of intracellular signalling. *Nature.* 2009;458(7241):1025-1029.

201. Karunarathne WK, Giri L, Kalyanaraman V, Gautam N. Optically triggering spatiotemporally confined GPCR activity in a cell and programming neurite initiation and extension. *Proc Natl Acad Sci U S A.* 2013;110(17):E1565-1574.

202. Li P, Rial D, Canas PM, et al. Optogenetic activation of intracellular adenosine A(2A) receptor signaling in the hippocampus is sufficient to trigger CREB phosphorylation and impair memory. *Mol Psychiatr.* 2015;20(11):1339-1349.

203. Koyanagi M, Terakita A. Diversity of animal opsin-based pigments and their optogenetic potential. *Bba-Bioenergetics.* 2014;1837(5):710-716.

204. Toettcher JE, Weiner OD, Lim WA. Using Optogenetics to Interrogate the Dynamic Control of Signal Transmission by the Ras/Erk Module. *Cell.* 2013;155(6):1422-1434.

205. Xu YK, Nan D, Fan JN, Bogan JS, Toomre D. Optogenetic activation reveals distinct roles of PIP3 and Akt in adipocyte insulin action. *J Cell Sci.* 2016;129(10):2085-2095.

206. Katsura Y, Kubota H, Kunida K, Kanno A, Kuroda S, Ozawa T. An optogenetic system for interrogating the temporal dynamics of Akt. *Sci Rep-Uk.* 2015;5.

207. Toettcher JE, Gong D, Lim WA, Weiner OD. Light-based feedback for controlling intracellular signaling dynamics. *Nat Methods.* 2011;8(10):837-U899.

208. Milias-Argeitis A, Summers S, Stewart-Ornstein J, et al. In silico feedback for in vivo regulation of a gene expression circuit. *Nat Biotechnol.* 2011;29(12):1114-1116.

209. Shimizu TS, Tu YH, Berg HC. A modular gradient-sensing network for chemotaxis in Escherichia coli revealed by responses to time-varying stimuli. *Mol Syst Biol.* 2010;6.

210. Shoval O, Goentoro L, Hart Y, Mayo A, Sontag E, Alon U. Fold-change detection and scalar symmetry of sensory input fields. *P Natl Acad Sci USA.* 2010;107(36):15995-16000.

211. Goentoro L, Shoval O, Kirschner MW, Alon U. The Incoherent Feedforward Loop Can Provide Fold-Change Detection in Gene Regulation. *Molecular Cell.* 2009;36(5):894-899.

212. Aoki K, Kumagai Y, Sakurai A, et al. Stochastic ERK Activation Induced by Noise and Cell-to-Cell Propagation Regulates Cell Density-Dependent Proliferation. *Molecular Cell.* 2013;52(4):529-540.

213. Wang XB, He L, Wu YI, Hahn KM, Montell DJ. Light-mediated activation reveals a key role for Rac in collective guidance of cell movement in vivo. *Nat Cell Biol.* 2010;12(6):591-U154.

214. Yoo SK, Deng Q, Cavnar PJ, Wu YI, Hahn KM, Huttenlocher A. Differential Regulation of Protrusion and Polarity by PI(3)K during Neutrophil Motility in Live Zebrafish. *Developmental Cell.* 2010;18(2):226-236.

215. Valon L, Etoc F, Remorino A, et al. Predictive Spatiotemporal Manipulation of Signaling Perturbations Using Optogenetics. *Biophys J.* 2015;109(9):1785-1797.

216. Behar M, Hoffmann A. Understanding the temporal codes of intra-cellular signals. *Curr Opin Genet Dev.* 2010;20(6):684-693.

217. Purvis JE, Lahav G. Encoding and Decoding Cellular Information through Signaling Dynamics. *Cell.* 2013;152(5):945-956.

218. Ong QX, Guo SL, Duan LT, Zhang K, Collier EA, Cui BX. The Timing of Raf/ERK and AKT Activation in Protecting PC12 Cells against Oxidative Stress. *Plos One.* 2016;11(4).

219. Zhang K, Duan LT, Ong QX, et al. Light-Mediated Kinetic Control Reveals the Temporal Effect of the Raf/MEK/ERK Pathway in PC12 Cell Neurite Outgrowth. *Plos One.* 2014;9(3).

220. Sako K, Pradhan SJ, Barone V, et al. Optogenetic Control of Nodal Signaling Reveals a Temporal Pattern of Nodal Signaling Regulating Cell Fate Specification during Gastrulation. *Cell Rep.* 2016;16(3):866-877.

221. Kim N, Kim JM, Lee M, Kim CY, Chang KY, Heo WD. Spatiotemporal Control of Fibroblast Growth Factor Receptor Signals by Blue Light. *Chem Biol.* 2014;21(7):903-912.

222. Shaner NC, Campbell RE, Steinbach PA, Giepmans BNG, Palmer AE, Tsien RY. Improved monomeric red, orange and yellow fluorescent proteins derived from Discosoma sp red fluorescent protein. *Nat Biotechnol.* 2004;22(12):1567-1572.

223. Shcherbakova DM, Verkhusha VV. Near-infrared fluorescent proteins for multicolor in vivo imaging. *Nat Methods.* 2013;10(8):751-+.

224. Duan LT, Che D, Zhang K, Ong QX, Guo SL, Cui BX. Optogenetic Control of Molecular Motors and Organelle Distributions in Cells. *Chem Biol.* 2015;22(5):671-682.

225. Denk W, Strickler JH, Webb WW. 2-Photon Laser Scanning Fluorescence Microscopy. *Science.* 1990;248(4951):73-76.

226. Helmchen F, Denk W. Deep tissue two-photon microscopy. *Nat Methods.* 2005;2(12):932-940.

227. Göppert-Mayer M. Über elementarakte mit zwei quantensprüngen. *Annalen der Physik.* 1931;401(3):273-294.

228. Li HY, Wang Y, Heap CR, et al. Dihydropyrrolopyrazole transforming growth factor-beta type I receptor kinase domain inhibitors: A novel benzimidazole series with selectivity versus transforming growth factor-beta type II receptor kinase and mixed lineage kinase-7. *J Med Chem.* 2006;49(6):2138-2142.

229. Nakao A, Afrakhte M, Moren A, et al. Identification of Smad7, a TGFbeta-inducible antagonist of TGF-beta signalling. *Nature.* 1997;389(6651):631-635.

230. Watanabe Y, Itoh S, Goto T, et al. TMEPAI, a transmembrane TGF-beta-inducible protein, sequesters Smad proteins from active participation in TGF-beta signaling. *Mol Cell.* 2010;37(1):123-134.

231. Dennler S, Itoh S, Vivien D, ten Dijke P, Huet S, Gauthier JM. Direct binding of Smad3 and Smad4 to critical TGF beta-inducible elements in the promoter of human plasminogen activator inhibitor-type 1 gene. *EMBO J.* 1998;17(11):3091-3100.

232. Sorre B, Warmflash A, Brivanlou AH, Siggia ED. Encoding of temporal signals by the TGF-beta pathway and implications for embryonic patterning. *Dev Cell.* 2014;30(3):334-342.

233. Vizan P, Miller DS, Gori I, Das D, Schmierer B, Hill CS. Controlling long-term signaling: receptor dynamics determine attenuation and refractory behavior of the TGF-beta pathway. *Sci Signal.* 2013;6(305):ra106.

234. Geng H, Lan RP, Wang GC, et al. Inhibition of Autoregulated TGF beta Signaling Simultaneously Enhances Proliferation and Differentiation of Kidney Epithelium and Promotes Repair Following Renal Ischemia. *Am J Pathol.* 2009;174(4):1291-1308.

235. Shi YA, Ryu DDY, Ballica R. Rheological Properties of Mammalian-Cell Culture Suspensions - Hybridoma and Hela-Cell Lines. *Biotechnol Bioeng.* 1993;41(7):745-754.

236. GeneCards. Weizmann Institute of Science; 1996-2018. https://www.genecards.org/.

237. Schaab C, Geiger T, Stoehr G, Cox J, Mann M. Analysis of High Accuracy, Quantitative Proteomics Data in the MaxQB Database. *Mol Cell Proteomics.* 2012;11(3).

238. Milo R. What is the total number of protein molecules per cell volume? A call to rethink some published values. *Bioessays.* 2013;35(12):1050-1055.

239. Schmierer B, Hill CS. Kinetic analysis of smad nucleocytoplasmic shuttling reveals a mechanism for transforming growth factor beta-dependent nuclear accumulation of Smads. *Mol Cell Biol.* 2005;25(22):9845-9858.

240. Schmierer B, Tournier AL, Bates PA, Hill CS. Mathematical modeling identifies Smad nucleocytoplasmic shuttling as a dynamic signal-interpreting system. *Proc Natl Acad Sci U S A.* 2008;105(18):6608-6613.

241. Zi Z, Klipp E. Constraint-based modeling and kinetic analysis of the Smad dependent TGF-beta signaling pathway. *PLoS ONE.* 2007;2(9):e936.

242. Zi Z. SBML-PET-MPI: a parallel parameter estimation tool for Systems Biology Markup Language based models. *Bioinformatics.* 2011;27(7):1028-1029.

243. Runarsson TP, Yao X. Stochastic ranking for constrained evolutionary optimization. *Ieee T Evolut Comput.* 2000;4(3):284-294.

244. Raue A, Kreutz C, Maiwald T, et al. Structural and practical identifiability analysis of partially observed dynamical models by exploiting the profile likelihood. *Bioinformatics.* 2009;25(15):1923-1929.

245. Press WH. *Numerical recipes in C : the art of scientific computing.* 2nd ed. Cambridge ; New York: Cambridge University Press; 1992.

246. Clarke DC, Brown ML, Erickson RA, Shi YG, Liu XD. Transforming Growth Factor beta Depletion Is the Primary Determinant of Smad Signaling Kinetics. *Mol Cell Biol.* 2009;29(9):2443-2455.

247. Massague J, Kelly B. Internalization of Transforming Growth-Factor-Beta and Its Receptor in Balb/C 3t3 Fibroblasts. *J Cell Physiol.* 1986;128(2):216-222.

248. Penheiter SG, Mitchell H, Garamszegi N, Edens M, Dore JJ, Jr., Leof EB. Internalization-dependent and -independent requirements for transforming growth factor beta receptor signaling via the Smad pathway. *Mol Cell Biol.* 2002;22(13):4750-4759.

249. Lu ZX, Murray JT, Luo WJ, et al. Transforming growth factor beta activates Smad2 in the absence of receptor endocytosis. *J Biol Chem.* 2002;277(33):29363-29368.

250. Erickson HP. Size and Shape of Protein Molecules at the Nanometer Level Determined by Sedimentation, Gel Filtration, and Electron Microscopy. *Biol Proced Online.* 2009;11(1):32-51.

251. Weizmann Institute of Science. GeneCards: TGFBR1 Gene. 1996-2018; v4.7.1 Build 10:https://www.genecards.org/cgi-bin/carddisp.pl?gene=TGFBR1&keywords=TGFBR1. Accessed 3 June, 2018.

252. Rys JP, DuForet CC, Monteiro DA, et al. Discrete spatial organization of TGF beta receptors couples receptor multimerization and signaling to cellular tension. *Elife.* 2015;4.

253. Nallet-Staub F, Yin XQ, Gilbert C, et al. Cell Density Sensing Alters TGF-beta Signaling in a Cell-Type-Specific Manner, Independent from Hippo Pathway Activation. *Developmental Cell.* 2015;32(5):640-651.

254. Narimatsu M, Samavarchi-Tehrani P, Varelas X, Wrana JL. Distinct polarity cues direct Taz/Yap and TGFbeta receptor localization to differentially control TGFbeta-induced Smad signaling. *Dev Cell.* 2015;32(5):652-656.

255. Vincent T, Neve EPA, Johnson JR, et al. A SNAIL1-SMAD3/4 transcriptional repressor complex promotes TGF-beta mediated epithelial-mesenchymal transition. *Nat Cell Biol.* 2009;11(8):943-U984.

256. Thuault S, Tan EJ, Peinado H, Cano A, Heldin CH, Moustakas A. HMGA2 and Smads Co-regulate SNAIL1 Expression during Induction of Epithelial-to-Mesenchymal Transition. *J Biol Chem.* 2008;283(48):33437-33446.

257. Bellomo C, Caja L, Moustakas A. Transforming growth factor beta as regulator of cancer stemness and metastasis. *Brit J Cancer.* 2016;115(7):761-769.

258. Lambert AW, Pattabiraman DR, Weinberg RA. Emerging Biological Principles of Metastasis. *Cell.* 2017;168(4):670-691.

259. Giese W, Milicic G, Schroder A, Klipp E. Spatial modeling of the membrane-cytosolic interface in protein kinase signal transduction. *Plos Comput Biol.* 2018;14(4).

260. Angermann BR, Klauschen F, Garcia AD, et al. Computational modeling of cellular signaling processes embedded into dynamic spatial contexts. *Nat Methods.* 2012;9(3):283-U295.

261. Neves SR, Tsokas P, Sarkar A, et al. Cell shape and negative links in regulatory motifs together control spatial information flow in signaling networks. *Cell.* 2008;133(4):666-680.

262. Brown GC, Kholodenko BN. Spatial gradients of cellular phospho-proteins. *Febs Lett.* 1999;457(3):452-454.

263. Peletier MA, Westerhoff HV, Kholodenko BN. Control of spatially heterogeneous and time-varying cellular reaction networks: a new summation law. *J Theor Biol.* 2003;225(4):477-487.

264. Hovis JK, Chou BR, Whitten K, Pfriem D, Pilecki N. Forward light scatter and visual acuity through scratched protective eyewear. *Clin Exp Optom.* 2014;97(2):140-146.

265. Piston DW, Fellers TJ, Davidson MW. Multiphoton Microscopy. https://www.microscopyu.com/techniques/multi-photon/multiphoton-microscopy, 2018.

266. Walker RG, Czepnik M, Goebel EJ, et al. Structural basis for potency differences between GDF8 and GDF11. *Bmc Biol.* 2017;15.

267. Andersson O, Reissmann E, Ibanez CF. Growth differentiation factor 11 signals through the transforming growth factor-beta receptor ALK5 to regionalize the anterior-posterior axis. *Embo Rep.* 2006;7(8):831-837.

268. Marquardt H, Lioubin MN, Ikeda T. Complete amino acid sequence of human transforming growth factor type beta 2. *J Biol Chem.* 1987;262(25):12127-12131.

269. Poniatowski LA, Wojdasiewicz P, Gasik R, Szukiewicz D. Transforming Growth Factor Beta Family: Insight into the Role of Growth Factors in Regulation of Fracture Healing Biology and Potential Clinical Applications. *Mediat Inflamm.* 2015.

270. Fujii D, Brissenden JE, Derynck R, Francke U. Transforming growth factor beta gene maps to human chromosome 19 long arm and to mouse chromosome 7. *Somat Cell Mol Genet.* 1986;12(3):281-288.

271. Barton DE, Foellmer BE, Du J, Tamm J, Derynck R, Francke U. Chromosomal mapping of genes for transforming growth factors beta 2 and beta 3 in man and mouse: dispersion of TGF-beta gene family. *Oncogene Res.* 1988;3(4):323-331.

272. ten Dijke P, Geurts van Kessel AH, Foulkes JG, Le Beau MM. Transforming growth factor type beta 3 maps to human chromosome 14, region q23-q24. *Oncogene.* 1988;3(6):721-724.

273. Cheifetz S, Hernandez H, Laiho M, Tendijke P, Iwata KK, Massague J. Distinct Transforming Growth-Factor-Beta (Tgf-Beta) Receptor Subsets as Determinants of Cellular Responsiveness to 3 Tgf-Beta Isoforms. *J Biol Chem.* 1990;265(33):20533-20538.

274. Jennings JC, Mohan S, Linkhart TA, Widstrom R, Baylink DJ. Comparison of the Biological Actions of Tgf Beta-1 and Tgf Beta-2 - Differential Activity in Endothelial-Cells. *J Cell Physiol.* 1988;137(1):167-172.

275. Li J, Foitzik K, Calautti E, Baden H, Doetschman T, Dotto GP. TGF-beta 3, but not TGF-beta 1, protects keratinocytes against 12-O-tetradecanoylphorbol-13-acetate-induced cell death in vitro and in vivo. *J Biol Chem.* 1999;274(7):4213-4219.

276. Uhlen M, Fagerberg L, Hallstrom BM, et al. Tissue-based map of the human proteome. *Science.* 2015;347(6220).

277. Kulkarni AB, Huh CG, Becker D, et al. Transforming Growth Factor-Beta-1 Null Mutation in Mice Causes Excessive Inflammatory Response and Early Death. *P Natl Acad Sci USA.* 1993;90(2):770-774.

278. Shull MM, Ormsby I, Kier AB, et al. Targeted Disruption of the Mouse Transforming Growth Factor-Beta-1 Gene Results in Multifocal Inflammatory Disease. *Nature.* 1992;359(6397):693-699.

279. Sanford LP, Ormsby I, GittenbergerdeGroot AC, et al. TGF beta 2 knockout mice have multiple developmental defects that are nonoverlapping with other TGF beta knockout phenotypes. *Development.* 1997;124(13):2659-2670.

280. Proetzel G, Pawlowski SA, Wiles MV, et al. Transforming Growth Factor-Beta-3 Is Required for Secondary Palate Fusion. *Nat Genet.* 1995;11(4):409-414.

281. Hall BE, Wankhade UD, Konkel JE, et al. Transforming Growth Factor-beta 3 (TGF-beta 3) Knock-in Ameliorates Inflammation Due to TGF-beta 1 Deficiency While Promoting Glucose Tolerance. *J Biol Chem.* 2013;288(44):32074-32092.

282. Yang LT, Kaartinen V. Tgfb1 expressed in the Tgfb3 locus partially rescues the cleft palate phenotype of Tgfb3 null mutants. *Dev Biol.* 2007;312(1):384-395.

283. Ratz M, Testa I, Hell SW, Jakobs S. CRISPR/Cas9-mediated endogenous protein tagging for RESOLFT super-resolution microscopy of living human cells. *Sci Rep-Uk.* 2015;5.

284. Mali P, Yang LH, Esvelt KM, et al. RNA-Guided Human Genome Engineering via Cas9. *Science.* 2013;339(6121):823-826.

285. Bugaj LJ, O'Donoghue GP, Lim WA. Interrogating cellular perception and decision making with optogenetic tools. *J Cell Biol.* 2017;216(1):25-28.

286. Tan EJ, Thuault S, Caja L, Carletti T, Heldin CH, Moustakas A. Regulation of Transcription Factor Twist Expression by the DNA Architectural Protein High Mobility Group A2 during Epithelial-to-Mesenchymal Transition. *J Biol Chem.* 2012;287(10):7134-7145.

287. Ozdamar B, Bose R, Barrios-Rodiles M, Wang HR, Zhang Y, Wrana JL. Regulation of the polarity protein Par6 by TGF beta receptors controls epithelial cell plasticity. *Science.* 2005;307(5715):1603-1609.

288. Viloria-Petit AM, David L, Jia JY, et al. A role for the TGF beta-Par6 polarity pathway in breast cancer progression. *P Natl Acad Sci USA.* 2009;106(33):14028-14033.

289. Hofmann TG, Stollberg N, Schmitz ML, Will H. HIPK2 regulates transforming growth factor-beta-induced c-Jun NH2-terminal kinase activation and apoptosis in human hepatoma cells. *Cancer Res.* 2003;63(23):8271-8277.

290. Yi JY, Shin I, Arteaga CL. Type I transforming growth factor beta receptor binds to and activates phosphatidylinositol 3-kinase. *J Biol Chem.* 2005;280(11):10870-10876.

291. Dumon N, Bakin AV, Arteaga CL. Autocrine transforming growth factor-beta signaling mediates smad-independent motility in human cancer cells. *J Biol Chem.* 2003;278(5):3275-3285.

292. Massague J. TGF beta in cancer. *Cell.* 2008;134(2):215-230.

293. Moustakas A, Heldin CH. Non-Smad TGF-beta signals. *J Cell Sci.* 2005;118(16):3573-3584.

294. Gradinaru V, Mogri M, Thompson KR, Henderson JM, Deisseroth K. Optical Deconstruction of Parkinsonian Neural Circuitry. *Science.* 2009;324(5925):354-359.

295. Wykes RC, Heeroma JH, Mantoan L, et al. Optogenetic and Potassium Channel Gene Therapy in a Rodent Model of Focal Neocortical Epilepsy. *Sci Transl Med.* 2012;4(161).

296. Krook-Magnuson E, Armstrong C, Oijala M, Soltesz I. On-demand optogenetic control of spontaneous seizures in temporal lobe epilepsy. *Nat Commun.* 2013;4.

297. Scharf R, Tsunematsu T, McAlinden N, Dawson MD, Sakata S, Mathieson K. Depth-specific optogenetic control in vivo with a scalable, high-density mu LED neural probe. *Sci Rep-Uk.* 2016;6.

298. Delbeke J, Hoffman L, Mols K, Braeken D, Prodanov D. And Then There Was Light: Perspectives of Optogenetics for Deep Brain Stimulation and Neuromodulation. *Front Neurosci-Switz.* 2017;11.

299. Hernandez VH, Gehrt A, Reuter K, et al. Optogenetic stimulation of the auditory pathway. *J Clin Invest.* 2014;124(3):1114-1129.

300. Laxpati NG, Mahmoudi B, Gutekunst CA, Newman JP, Zeller-Townson R, Gross RE. Real-time in vivo optogenetic neuromodulation and multielectrode electrophysiologic recording with NeuroRighter. *Front Neuroeng.* 2014;7:40.

301. Ye H, Daoud-El Baba M, Peng RW, Fussenegger M. A synthetic optogenetic transcription device enhances blood-glucose homeostasis in mice. *Science.* 2011;332(6037):1565-1568.

302. Bruegmann T, Malan D, Hesse M, et al. Optogenetic control of heart muscle in vitro and in vivo. *Nat Methods.* 2010;7(11):897-900.

303. Kim T, Folcher M, Doaud-El Baba M, Fussenegger M. A synthetic erectile optogenetic stimulator enabling blue-light-inducible penile erection. *Angew Chem Int Ed Engl.* 2015;54(20):5933-5938.

304. Folcher M, Oesterle S, Zwicky K, et al. Mind-controlled transgene expression by a wireless-powered optogenetic designer cell implant. *Nat Commun.* 2014;5:5392.

305. Allergan. RST-001 Phase I/II Trial for Advanced Retinitis Pigmentosa. 2015; https://clinicaltrials.gov/ct2/show/NCT02556736?term=optogenetics&rank=1.

306. Biologics G. Dose-escalation Study to Evaluate the Safety and Tolerability of GS030 in Subjects With Retinitis Pigmentosa (PIONEER). 2017; https://clinicaltrials.gov/ct2/show/NCT03326336.

307. Lee S, Park H, Kyung T, et al. Reversible protein inactivation by optogenetic trapping in cells. *Nat Methods.* 2014;11(6):633-+.

308. Carpenter AE, Jones TR, Lamprecht MR, et al. CellProfiler: image analysis software for identifying and quantifying cell phenotypes. *Genome Biol.* 2006;7(10).

309. Muller K, Zurbriggen MD, Weber W. Control of gene expression using a red- and far-red light-responsive bi-stable toggle switch. *Nat Protoc.* 2014;9(3):622-632.

310. Funahashi A, Matsuoka Y, Jouraku A, Kitano H, Kikuchi N. Celldesigner: A modeling tool for biochemical networks. *Proceedings of the 2006 Winter Simulation Conference, Vols 1-5.* 2006:1707-+.

List of Figures

List of Tables

Abbreviations

AMAM12	A disintegrin and metalloproteinase 12
AMH	Anti-Müllerian hormone
Arch	Archaerhodopsin-3
AsLOV2	*Avena sativa* LOV domain 2
BLUF	Blue light utilizing FAD
BMP	Bone morphogenetic proteins
BphP1	Bathy phytochrome1
BR	Bacteriorhodopsin
BV	Biliverdin ixα
CDK	Cyclin-dependent kinase
ChR2	Channelrhodopsin-2
CIB1	Cryptochromes-interacting basic helix-loop-helix 1
COP1	Constitutive photomorphogenesis protein 1
Co-Smad	Common partner Smad
Cph1	Cyanobacterial phytochrome 1
cPML	Cytoplasmic promeylocytic leukemia
CRY2	Cryptochrome 2
cytoTβRI	Cytoplasmic region of the TGFβ type I receptor
cytoTβRII	Cytoplasmic region of the TGFβ type II receptor
DAB2	Disabled-2
Dpp	Decapentaplegic
DUB	Deubiquitylase
EGF	Epidermal growth factor
EMT	Epithelial-to-mesenchymal transition
eNOS	Endothelial nitric oxide synthase
eNpHR	Enhanced halorhodopsin
ES	Embryonic stem
ETS1	E26 transformation-specific proto-Oncogene 1
FACS	Fluorescence activated cell sorting
FAD	Flavin adenine dinucleotide
FKBP12	FK506-binding protein
FKF1	Flacin-binding, Kelch repeat, F-box protein
FMN	Flavin mononucleotide
FOXO	Forkhead box O

FP	Fluorescent protein
FYVE	Fab1, YOTB/ZK632.12, Vac1 and EEA1
GDF	Growth and Differentiation Factor
GEF	Guanine nucleotide exchange factor
GI	Gigantea
Grb2	Growth factor receptor binding protein 2
GtR3	Rhodopsin-3
HDAC	Histone deacetylases
Hrs	Hepatocyte growth factor-regulated tyrosine kinase substrate
ICD	Intracellular domain
IL-6	Interleukin-6
iLID	Improved light inducible dimer
IR	Infra-red
IRES	Internal ribosome entry site
iRFP-Smad2	Smad2 tagged by iRFP682 (a near infrared FP)
I-Smad	Inhibitory Smad
LANS	Light-activated nuclear shuttle
LAP	Latency-associated polypeptide
LEXY	Light-inducible nuclear export system
LINuS	Light-inducible nuclear localization signal
LOV	Light-oxygen-voltage
LRC	Ligand-receptor-complex
LTBP1	Latent tgfβ-binding protein 1
MAPK	Mitogen-activated protein kinase
MH1	Mad homology 1
MYOD1	Myoblast determination protein 1
N2C	Nuclear-to-cytoplasmic
Ncap	N-terminal Cap
NGF	Nerve growth factor
NLS	Nuclear localization signal
NpHR	Halorhodopsin
ODE	Ordinary differential equation
optoHaCaT	HaCaT cells stably expressing the optoTGFβ system
optoHela	Hela cells stably expressing the optoTGFβ system
optoTGFβ	Light controllable TGFβ signaling
optoTβRI	Myr-cyto TβRI-CIBN
optoTβRII	cytoTβRII-CRY2PHR-dTomato
Par6	Partitioning defective 6 homolog

PAS	Per-arnt-sim
PCB	Phytococyanobilin
PHR	Photolyase homology region
PhyB	Phytochrome B
PIF	Phytochrome interacting factor
PKA	Protein kinase A
PKI	Protein kinase inhibitory
PM	Plasma membrane
PP1	Protein phosphatase 1
P-Smad2	Phosphorylated Smad2
PΦB	Phytochromobilin
qPCR	Quantitative PCR
R-Smad	Receptor regulated Smad
SAD	Smad4 activation domain
SARA	Smad anchor for receptor activation
SBML	Systems biology markup language
SEM	Standard errors of the mean
Shc	Src homology 2 domain containing
Smad	Sma- and Mad-related protein
TACE	TNF-alpha converting enzyme
TAK1	TGFβ activated kinase 1
TCPTP	The T cell protein tyrosine phosphatase
TGFβ	Transforming Growth Factor β
TIRFM	Total internal reflection fluorescent microscopy
TNF	Tumor necrosis factor
TRAF6	TNF (Tumor necrosis factor) receptor associated factor 6
Trk	Tropomyosin-related kinase
TULIPs	Tunable, light-controlled interacting protein tags
TβRI	TGFβ type I receptor
TβRII	TGFβ type II receptor
TβRs	TGFβ receptors (incl. TβRI and TβRII)
USP	Ubiquitin specific protease
UV	Ultraviolet
UVR8	UV-B resistance 8
VChR1	*Volvox* channelrhodopsin-1
Vps26	Retromer vacuolar protein sorting protein 26
VVD	Vivid

Acknowledgements

First of all, I would like to thank my PhD supervisor, Dr. Zhike Zi for giving me the opportunity to work in his lab and guiding me throughout the past four years of my research. I also want to thank Prof. Dr. Edda Klipp for her kind supports in finishing my PhD, and thank Prof. Dr. Nils Blüthgen for reviewing this thesis.

Next, many thanks go to my colleagues in the Zi lab, especially to Guoyu who helped me a lot in research as well as in daily life, and to Marjin and Susanne who gave me many advices on carrying out wet-lab experiments during the early stage of my PhD. I also would like to thank Difan for her assistance in running western blotting, and to Hongqing and Dan who provided a friendly working environment.

Furthermore, I would like to acknowledge our collaborators from the KAIST Institute, this work would never have been possible without their help. I also appreciate the technical assistance from the Microscopy facility in the Max Planck Institute for Molecular Genetics.

Last but not least, I would like to thank my dear family and wonderful friends. Especially, I want to express my deepest gratitude to my father and mother, they never stop giving me their unconditional and endless support and love.

Statement

Ich erkläre, dass ich die vorliegende Arbeit selbständig und nur unter Verwendung der angegebenen Hilfsmittel angefertigt habe.

Yuchao Li

Berlin, 21.07.2018